



Visually induced and spontaneous behavior in the zebrafish larva

Adrien Jouary

► **To cite this version:**

Adrien Jouary. Visually induced and spontaneous behavior in the zebrafish larva. *Neurons and Cognition [q-bio.NC]*. Université Pierre et Marie Curie - Paris VI, 2015. English. <NNT : 2015PA066605>. <tel-01391485>

HAL Id: tel-01391485

<https://tel.archives-ouvertes.fr/tel-01391485>

Submitted on 3 Nov 2016

HAL is a multi-disciplinary open access archive for the deposit and dissemination of scientific research documents, whether they are published or not. The documents may come from teaching and research institutions in France or abroad, or from public or private research centers.

L'archive ouverte pluridisciplinaire **HAL**, est destinée au dépôt et à la diffusion de documents scientifiques de niveau recherche, publiés ou non, émanant des établissements d'enseignement et de recherche français ou étrangers, des laboratoires publics ou privés.



**THÈSE DE DOCTORAT DE
L'UNIVERSITÉ PIERRE ET MARIE CURIE**

École doctorale Cerveau-Cognition-Comportement

Présentée par

Adrien Jouary

Pour obtenir le grade de

DOCTEUR de l'UNIVERSITÉ PIERRE ET MARIE CURIE

Sujet de la thèse :

**Comportement moteur induit visuellement et
spontané chez la larve du poisson zèbre**

Thèse soutenue le 9 octobre 2015

devant le jury composé de :

German SUMBRE	Directeur de thèse
José HALLOY	Rapporteur
Michael ORGER	Rapporteur
Georges DEBRÉGEAS	Examineur
Claire WYART	Examineur

Abstract

Behavior is often conceived as resulting from a stimulus-response association. Under this paradigm, understanding the nervous system is reduced to finding the relation between a sensory input and a motor output. Yet, in naturally behaving animals, motor actions influence sensory perceptions just as much as the other way around. Animals are continuously relying on sensory feedback to adjust motor commands. On the other hand, behavior is not only induced by the sensory environment, but can be generated by the brain's rich internal dynamics. My goal is to understand the sensory-motor dialogue by monitoring large brain regions, yet, with a single-neuron resolution. To tackle this question, I have used zebrafish larva to study visually induced and internally driven motor behaviors. Zebrafish larvae have a small and transparent body. These features enable using large-scale optical methods, such as selective plane illumination microscopy (SPIM), to record brain dynamics.

In order to study goal-driven navigation in conditions compatible with imaging, I developed a visual virtual reality system for zebrafish larva. The visual feedback can be chosen to be similar to what the animal experiences in natural conditions. Alternatively, alteration of the feedback can be used to study how the brain adapts to perturbations. For this purpose, I first generated a library of free-swimming behaviors from which I learned the relationship between the trajectory of the larva and the shape of its tail. Then, I used this technique to infer the intended displacements of head-fixed larvae. The visual environment was updated accordingly. In the virtual environment, larvae were capable of maintaining the proper speed and orientation in the presence of whole-field motion and produced fine changes in orientation and position required to capture virtual preys. I demonstrated the sensitivity of larvae to feedback by updating the visual world only after the discrete swimming episodes. This feedback perturbation induced a decay in the performance of prey capture behavior, suggesting that larvae are capable of integrating visual information during movements.

Behavior can also be induced by the internal dynamics of the brain. In the absence of salient sensory cues, zebrafish larva spontaneously produces stereotypical tail movements, similar to those produced during goal-driven navigation. After hav-

ing developed a new method to classify tail movements, I analyzed the sequence of spontaneously generated tail movements. The latter switched between period of quasi-rhythmic activity and long episodes of rest. Moreover, consecutive movements were more similar when executed at short time intervals (~ 10 s). In order to study how spontaneous decisions emerge, I coupled SPIM to tail movement analysis. Using dimensionality reduction, I identified clusters of neurons predicting the direction of spontaneous turn movements but not their timings. This Preliminary result suggests that distinct pathways could be responsible for the timing (when) and the selection (what) of spontaneous actions. Together, the results shed light on the role of feedback and internal dynamics in shaping behaviors and open the avenue for investigating complex sensorimotor process in simple systems.

Remerciements

Ces quatre années de thèse m'ont permis d'explorer un sujet qui m'a passionné, la neuroscience des systèmes. Je remercie tout d'abord German Sumbre de m'avoir initié à l'étude de ce petit poisson transparent, sa disponibilité et son attention ont été déterminantes dans l'aboutissement de ce travail. Le laboratoire aux expertises variées dans lequel j'ai travaillé m'a ouvert à l'ampleur des questions soulevées par ce petit cerveau. Poser les bonnes questions est un art subtil, les discussions que j'ai eu avec Sebastian Romano, Veronica Perez Schuster, Jonathan Boulanger-Weill, Selma Mehyaoui et Thomas Pietri ont grandement contribué à formuler les questions qui ont guidé mon travail. Je souhaite également remercier Mathieu Haudrechy, Sebastian, Alessia Candeo, Jonathan, Arthur Planul et Virginie Candat de m'avoir aidé à expérimenter avec le gel, les poissons, les lasers, les matrices de covariance et des neurones brillants.

Je remercie Gerard Paresys et Yvon Caribou pour leur aide concernant le hardware. Bilel Mokhtari, Phi-Phong Nguyen, Pierre Vincent ainsi qu'Auguste Genovesio pour l'informatique. Pour m'avoir initié à l'imagerie par nappe laser, je remercie le Laboratoire Jean Perrin et en particulier Raphaël Candelier.

Je profite également de cette tribune pour faire un big up à Raphaël, Yann, Maximilien, Loïc, Mehdi, Ugo, Alexis, Julien, Maayane, Sylvain Cajo, Anaïs, Jesse, Marine, Pierre-Marie, Gabriel, Thibault, Léa, Thalassa, Antton, Romain, Laura, Medjo, Paola, Adèle, Agathe, Alexandre Z, Alexandre G et Anne Claire¹. Je remercie tout particulièrement Anna pour son aide ces derniers mois et le temps passé avec elle. Finalement, ma famille, pour sa bienveillance et son soutien. Ma mère Carole et Christian, mon père Philippe et Marie, mes frères et sœur Camille, Lucas, Jean-Baptiste et François ainsi que mon cousin Cédric qui est pour moi un modèle de curiosité scientifique. Je remercie également Annemarie et Michel pour le beaufort et la bière.

La science ne se nourrit pas que d'inspiration, je suis reconnaissant à la fondation pour la recherche médicale d'avoir financé ma dernière année de doctorat.

¹Ainsi que Charlie

Table of contents

List of figures	ix
List of tables	xi
1 Introduction	1
1.1 Understanding behavior: the sensory-motor dialogue	1
1.2 Sensory feedback in the perception-action loop	4
1.2.1 Recording from behaving animals: Virtual reality in neuroscience	5
1.2.2 How real is virtual reality?	6
1.3 Internally driven behaviors	9
1.3.1 Motivation for action in absence of sensory stimulation	9
1.3.2 Neural basis of spontaneous behavior	11
1.4 Large-scale analysis of circuit dynamics underlying behavior in ze- brafish larva	17
1.4.1 The zebrafish as a model for systems neuroscience	17
1.4.2 Locomotion of zebrafish larva	20
1.4.3 Goal-driven behavior in the larval zebrafish	23
1.5 Main aims	28
2 A visual virtual reality system for the zebrafish larva	29
2.1 Introduction	29
2.2 Results	34
2.2.1 Prediction of the larva's trajectory from the kinematics of tail movements	34
2.2.2 Optomotor response in a two-dimensions visual virtual reality system	38
2.2.3 Prey-capture behavior in two-dimension visual virtual reality . .	40
2.2.4 Integration of visual information during tail bouts	43

2.3	Materials and methods	44
3	Internally driven behavior in zebrafish larvae	49
3.1	Introduction	49
3.2	Internally driven behaviors of zebrafish larva	51
3.2.1	Locomotor repertoire of zebrafish larva	51
3.2.2	Chaining of spontaneous motor actions	62
3.2.3	Supplementary Methods	67
3.3	Neuronal patterns predictive of spontaneous behaviors	72
3.3.1	Methods	72
3.4	Results	78
3.5	Supplementary Methods	86
4	Conclusions and perspectives	89
4.1	A visual virtual reality system for the zebrafish larva	89
4.2	Internally driven behaviors in zebrafish larva	91
4.3	Neural basis of internal decisions	93
	References	95

List of figures

1.1	Influence of the motor activity on the sensory system	5
1.2	Virtual Reality in neuroscience	6
1.3	Spatial navigation in VR.	8
1.4	Segregation of arousal between locomotor activity and sensory responsiveness according neuropeptides	13
1.5	Readiness Potential across taxa	15
1.6	Coarse brain anatomy of 6 dpf zebrafish larva	19
1.7	Circuit for graded locomotion in zebrafish larva	22
1.8	Flexibility of locomotor actions during prey capture	25
1.9	Phototaxis in zebrafish larva	27
2.1	Recording intention of movement in zebrafish larva	30
2.2	Quantification of tail movements	32
2.3	Prediction of trajectory from tail movements	36
2.4	Optomotor response in virtual reality	39
2.5	Prey-capture in virtual reality	42
2.6	Alteration of visual feedback during movement	45
3.1	Visually induced and spontaneous tail deflections	52
3.2	Quantification of tail bouts	53
3.3	Comparison of Feature and DTW-based similarity measurements	55
3.4	Continuum of tail kinematics	58
3.5	Classification of tail bouts.	60
3.6	Distribution of movements in induced and spontaneous conditions	62
3.7	Temporal chaining of tail movements	65
3.8	Memory in the chaining of movements	66
3.9	Alignment of tail deflection using DTWs	69
3.10	Scheme of the optical paths of the SPIM	74

3.11 Workflow for image preprocessing	75
3.12 Preprocessing of the fluorescence signal	77
3.13 Increase in activity prior to spontaneous movement	79
3.14 Predicting movement direction using DLDA	81
3.15 Specificity for the directionality of routine turns	84
3.16 Axial profile of the light sheet	86

List of tables

1.1	Animal models in neuroscience	18
1.2	Stereotypical tail movements	20
3.1	Optical Part	88

Nomenclature

Abbreviations	Descriptions
Bout	Discrete event of tail movement
DLDA	Direct Linear Discriminant Analysis
Dpf	Days post fertilization
DTW	Dynamic Time Warping
FKNN	Fuzzy K-Nearest Neighbor
IBI	Inter-bout-interval
NA	Numerical Aperture
NMLF	Nucleus of the Medial Longitudinal Fasciculus
OMR	Optomotor Response
PCA	Principal Component Analysis
ROI	Region of interest
Sem	Standard Error of the Mean
Sd	Standard Deviation
S/R	Stimulus/ Response
t-SNE	t-Distributed Stochastic Neighbor Embedding

The problem then is not this: How does the central nervous system effect any one, particular thing? It is rather: How does it do all the things that it can do, in their full complexity? What are the principles of organization?

John Von Neumann (1951). General and logical theory of automata

Chapter 1

Introduction

1.1 Understanding behavior: the sensory-motor dialogue

Deep neural networks are now capable of competing with primates in image recognition tasks (Cadieu et al., 2014). The architecture of artificial neural network reflects by fair means our understanding of the brain: an input-output system that builds complex associations from simple local operations (Bengio, 2009). After supervised learning, a chain of transformations in these networks associates an input to an appropriate output. The input provided to the network and its connectivity pattern deterministically specify the output. Early investigations on the brain circuitry were dominated by a similar idea: the reflex theory, where patterns of inputs delivered to the primary sensory neurons can be channeled to produce patterns of muscle activation. This theory relied on the observation that neurons are inert until an input is provided (Sherrington, 1906). This observation led Sherrington to claim, in 1906, that this was a general rule for the whole nervous system:

From the point of view of its office as the integrator of the animal mechanism, the whole function of the nervous system can be summed up in one world, conduction.

Under this scope, neural circuits can be seen primarily as input-output devices linking a sensory stimulation to an appropriate motor response. Reducing the coupling between sensory circuits, motor circuits and the environment to a causal mechanism between the stimulus and the response, greatly simplifies scientific investigation on animal behavior (Edelman, 2015). Under the input-ouput paradigm, behavior can be decomposed as a series of stimulus/response (S/R) associations.

The S/R assumption has provided neuroscience with a rich quantitative framework to understand the relation between neuronal activity and behavior. The methodology employed to investigate the neuronal causes of behavior can be grossly recapitulated by three successive steps (Clark et al., 2013). First is the need to characterize reproducible behavior. This is done by identifying environmental features that reliably trigger a motor response either by observing natural behavior, or, by training animals to perform a S/R association. Then, brain recording techniques are used to find neuronal correlates. Investigators identify circuits or neurons whose activity correlates with stimulus features, behavioral responses or cognitive states relevant for the behavior. Finally, the "causal" role of the identified circuit is demonstrated by showing its necessity and sufficiency for behavior. Suppression of its activity is used to demonstrate its necessity for eliciting the behavior. Direct optical or electrical stimulation of its activity establishes the sufficiency of the circuit to induce the behavior.

This connection between a circuit and a behavior is a useful constraint for the establishment of a model. However, it does not provide sufficient insight on how this function is carried out (Sompolinsky, 2014). By systematically repeating the same external sensory protocol in order to estimate the statistics of the animal response, studies often lead to the description of neurons in terms of their average preferred stimuli or actions. Indeed, the S/R paradigm is especially suited to understand both ends of the input-output computation: how does the tuning of sensory neurons encode stimulus properties (Hubel and Wiesel, 1959), and how does the activity of neurons in motor area shape the generation of complex movements (Ashe and Georgopoulos, 1994). Our current understanding of neuronal circuitry enables neuroscientists to decode visual environments from the activity of the primary visual cortex (Nishimoto et al., 2011), or to coordinate artificial prosthetics based on the dynamics of the primary motor cortex (Wessberg et al., 2000).

Behavioral theories conceive the organism as primarily reactive, driven by the sensory stimuli (Skinner, 1976). Other theories have emerged in neuroscience to overcome fundamental limitations of this reflexive view of the brain: cognitivism and embodiment. Cognitivism accounts for abstract mental states that are not directly coupled with action nor with environmental sensory stimulation but rather reflect the ongoing thought process (Raichle, 2010). Embodiment stresses the crucial role of the body and its actions to shape perception. In natural behaving conditions, the brain is not a passive receiver of sensory sensations but actively seeks information (Gover, 1996). The

behaviorist view, however is still dominant when considering "simple" animal models ¹. Nevertheless, in simple sensorimotor tasks, interactions with the environment cannot be decomposed into a sequence of distinct events that start with a discrete stimulus and end with a specific response. Actions are continuously modified through feedback control. Furthermore, animals continuously evaluate available actions and decide whether to pursue a given goal or to switch to an alternative. In my thesis project I have used two approaches to address the limitations of the stimulus/response framework:

1. **The influence between the sensory environment and motor actions is reciprocal.** The description of the environment as a set of external inputs does not account for the complex perception-action loop occurring in natural behavior. Even for simple sensorimotor tasks, sensory feedback resulting from action are critical to adjust motor commands in order to reach a goal. In the first part of this introduction, I will present virtual reality systems that provide a controlled sensory feedback allowing the study of goal-driven behavior in conditions compatible with brain functional imaging.
2. **Motor actions should not be considered only as a reaction to sensory stimuli.** In strong contradiction with the reflexive view of the brain, the energy budget associated with momentary demands of the environment could be as little as 1% of the total energy budget of the brain (Raichle, 2006), reflecting the major role of intrinsic activity. Previous studies have been dominated by research on neuronal activity and behaviors evoked by well controlled sensory stimuli. However, the brain's rich internal dynamics are capable of generating behavior even in the absence of sensory cues. In the second part of the introduction, I will present the ecological motivations for internally driven behaviors and I will review their underlying neuronal mechanisms.

¹In a recent paper, Buzsáki et al. (2015) considered a nervous system as "simple" when "the connection between output and input networks is direct and immediate". This definition of "simple animal" is reminiscent of Sherrington's view.

1.2 Sensory feedback in the perception-action loop

The nervous system is organized around goals that promote its fitness: finding a mate, escaping from predators or hunting preys. For an animal behaving naturally, motor actions influence the sensory system as much as the other way around.

Sensing is not a passive process. "Active sensing" is the process by which a sensory apparatus is positioned and modulated to enhance the animal's capacity to extract behaviorally relevant information (Gibson, 1962). This is obvious during tactile sensing: a rodent will rhythmically move its whisker. The sensation resulting from the bending of a whisker will be the result of a combination between the speed of the whisker and the tactile environment. Motor actions are thus actively driving sensations. A more widespread example of active sensing is eye movements. Eyes are not sensors waiting to receive external input but are continuously sampling the visual scene with systematic patterns of movement and fixation (MacEvoy et al., 2008). This rhythmic exploration resulting from eye movement has a crucial role in visual processing and perception (Schroeder et al., 2010).

The development of the visual system relies on proper motor feedbacks. In their classical study, Held and Hein (1963) showed the consequence of deprivation of active exploration on development. For 3 h a day and during 42 days, kittens were placed in the apparatus showed in **Figure 1.1.A**. One of them could freely move (A) while the other was passively exposed to identical visual and vestibular stimuli (P). When tested at the end of these experiments, the passive kittens (P) performed poorly in several visuo-motor tasks. This study provided evidence for a developmental process relying on the feedback of motor actions on sensory experience.

Motor actions influence sensory neurons even without the mediation of the environment or body. When changing from an immobile to flying state, visual motion sensitive neurons in the fly shift their tuning to higher velocities. **Figure 1.1.B** shows the tuning curve of a H1 speed-sensitive interneuron measured under two conditions: while the fly is not moving and during a flying state. In both cases, the visual stimuli are the same but the tuning of the neuron broadens toward high velocities during flight (Jung et al., 2011). A similar alteration of speed tuning in walking flies has also been reported (Chiappe et al., 2010).

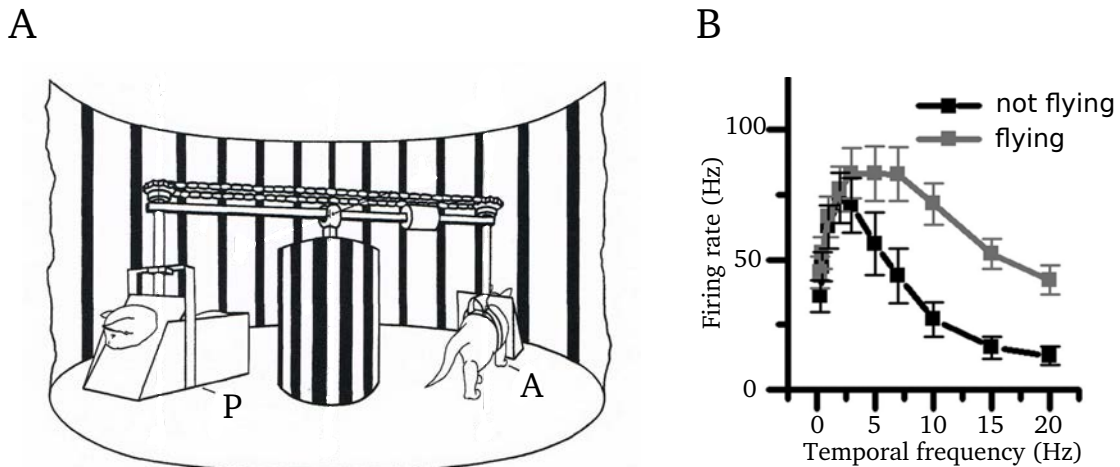


Fig. 1.1: **Influence of the motor activity on the sensory system**

(A) Illustration of the apparatus used to study the effect of motor feedback on the development of the sensorimotor system. Active (A) and passive (P) kittens have a similar sensory experience but (A) is freely moving in contrast to (P) that does not experience self-generated sensory change. The sensory experience of (P) is driven by (A). Adapted from Held and Hein (1963). (B) Temporal frequency tuning curves of the mean response of a H1 neurons in non-flying and flying flies (black and gray respectively). When the fly is flying, H1 neurons is tuned to higher temporal frequency. Adapted from Jung et al. (2011).

1.2.1 Recording from behaving animals: Virtual reality in neuroscience

We have seen how sensory feedback can affect brain activity during behavior. To study the neural basis of these behaviors, two options are available:

- The first is to record neuronal activity in freely moving animals. High resolution microscopy techniques are however difficult to adapt to moving animals. Methods can either measure temporally accurate signals from few neurons (e.g. bioluminescence marker (Naumann et al., 2010), head-attached electrode implants) or measure spatially defined signal with a poor temporal resolution (e.g. calcium integrator (Sohal et al., 2009)).
- An alternative solution is to use virtual reality (VR) in head-fixed conditions as shown in **Figure 1.2**. This method reproduces a subset of the sensory environment that the animal would sense while freely moving. In closed-loop VR, the stimuli are continuously updated according to the animal motor responses.

Virtual reality setups have two main advantages compared to monitoring neuronal activity in freely behaving conditions. In the first place, it is compatible with high-precision functional neuronal recordings given that the head needs to be restrained in all imaging techniques or intracellular recording. Secondly, feedback can be chosen to be similar to what the animal would experience in natural conditions or one can manipulate them to study how the brain adapts to perturbations. VR has been used for decades to study the neural basis of behavior and has been adapted to several animal models and different sensory modalities (Dombeck and Reiser (2012), Sofroniew et al. (2014)). By allowing spatial navigation, VR can be also used to investigate complex cognitive processes, for example, the maze running ability of rats allows the study of memory or decision making.

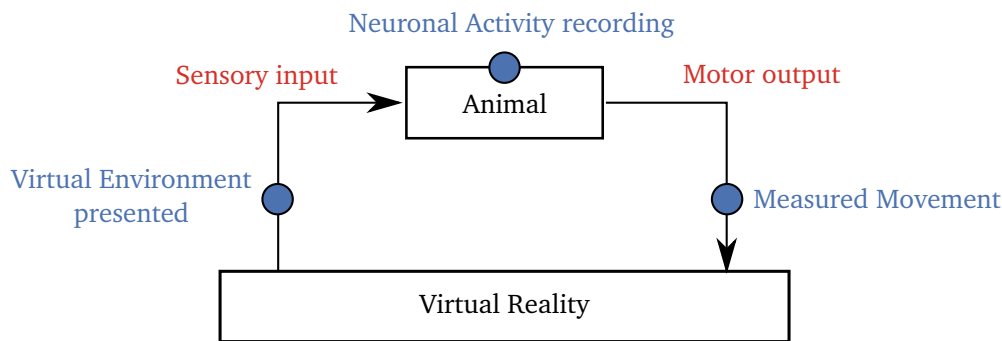


Fig. 1.2: **Virtual Reality in neuroscience.** Schematic view of a virtual reality behavioral experiment. The animal’s movements are measured and passed through instrumentation and computational stages in order to couple the movements with the sensory stimuli. Meanwhile, the neuronal activity can be monitored using functional imaging or electrophysiology.

1.2.2 How real is virtual reality?

How is spatial navigation experienced in VR, does it feel real? The answer may lay in the activity of neurons involved in representing space during virtual navigation. Even though birds can sense magnetic fields (Wu and Dickman, 2012), most animals are not equipped with position or orientation sensors. Position and orientation in space are inferred using a combination of external cues and path integration. In primates or rodents, neurons in the hippocampus become active during active exploration in specific locations of the environment. Those place-specific cells are called place cells, grid cells or border cells depending on the spatial pattern that they encode.

Early studies have shown that one dimensional place cells were found while a mouse was navigating along a virtual linear track (Dombeck et al., 2010). Extension of this setup to two dimension (2D) navigation failed to find place-specific cells. Only recently, an elegant setup allowed Aronov and Tank (2014) to monitor 2D place specific cells (**Figure 1.3.A,B**). In this experiment, the rodent was walking on a spherical treadmill. It could move forward by walking on the treadmill and turn by physically rotating its head. Although the head was restrained on one axis, it could still rotate, thus providing vestibular feedback absent in previous setups. The animal inferred its position in the 2D virtual environment through a combination of different sensory modalities: visual input from the display screen, vestibular input from the head movement and locomotor feedback. Providing only visual and locomotor feedback did not allow observing 2D place cells. This example illustrates how sensitive to feedback the neuronal representation of space is.

Insects are also capable of path integration (Collett et al., 2013). Recently, studies in VR of walking flies have shown the existence of head-direction cells combining self motion and external cues to represent their orientation with respect to the environment (Seelig and Jayaraman, 2015). The neuronal activity encodes the fly orientation using both visual landmarks and motor feedback. In darkness and in the absence of vestibular input, the orientation of the fly relative to the ball can be decoded from the population activity of neurons in the ellipsoid body. This shows their ability for path integration using only locomotor feedback (**Figure 1.3.C,D**).

The VR approach has been successfully applied to study behavior in combination with functional imaging. However, even simple behaviors can involve large networks distributed across different brain regions (Portugues et al., 2014). In rodent animal models, technological limitations prevent us from simultaneously monitoring extensive brain regions. Therefore, it can be advantageous to study a model system with a compact brain and a reasonably rich behavioral repertoire, which enables whole brain imaging with single-cell resolution such as the zebrafish larva (Ahrens and Engert, 2015).

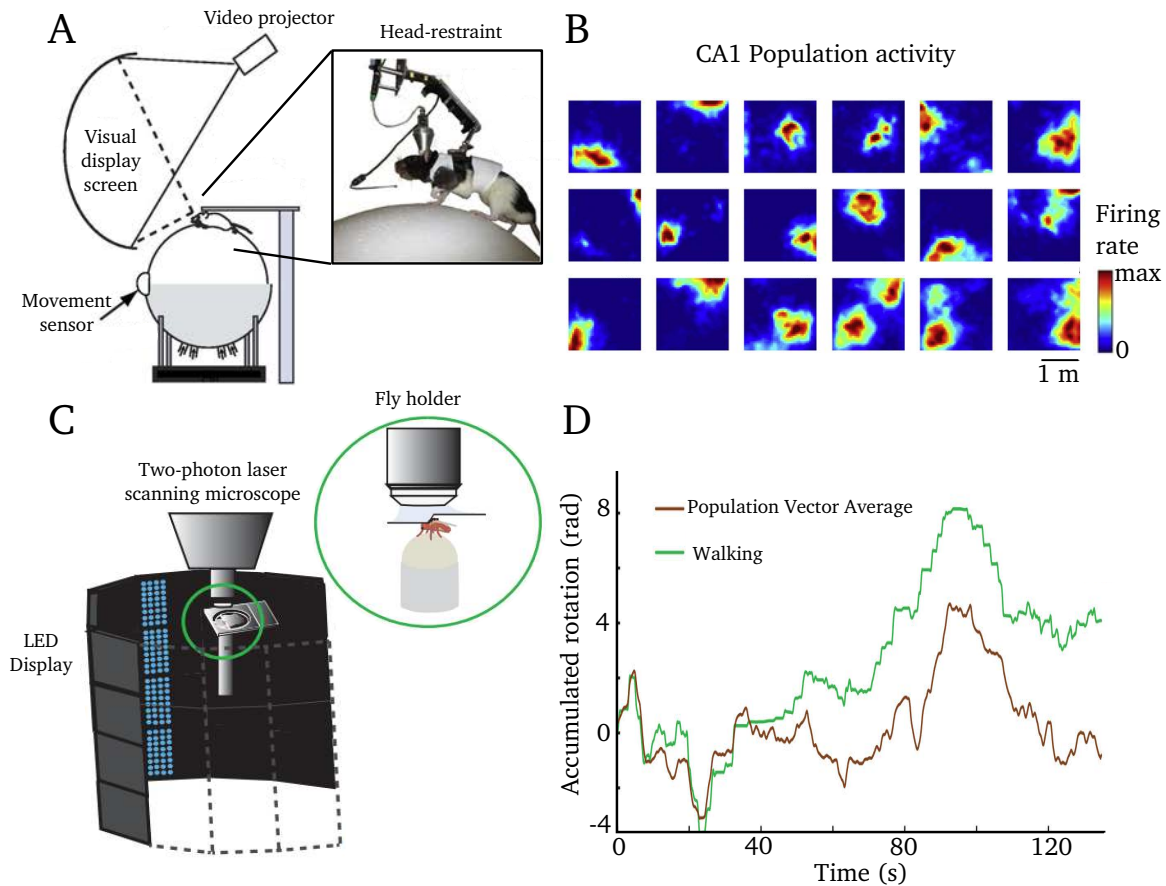


Fig. 1.3: **Spatial navigation in VR.** (A) Scheme of the setup used for rodent VR experiments. Mouse locomotion results in rotation of the trackball recorded by movement sensors. The visual scene is projected on a spherical screen surrounding the rodent. Head restraining the mouse allows recording neuronal activity. (B) Example of several rate maps recorded simultaneously from place cells in the hippocampus CA1 region. Neuron fire as a function of the animal position in the virtual environment consisting of a square area. Adapted from Aronov and Tank (2014). (C) Setup of the fly VR experiment and close-up on the fly on an air-floating ball. (D) Accumulated rotation of the ball while the fly is in total darkness (in green). A population vector average of neuron in the ellipsoid body (in brown) sufficed to predict the accumulated rotation. Adapted from Seelig and Jayaraman (2015).

1.3 Internally driven behaviors

1.3.1 Motivation for action in absence of sensory stimulation

Movement does not occur solely as a consequence of sensory stimulation. Even in the relative absence of stimuli, the brain's internal dynamics is capable of generating behavior. Hereafter, I will consider a behavior as being internally driven when it can not be linked to external stimulus. Internal drives such as hunger or fear can drive spontaneous movements even in the absence of external stimuli. But what happens if we consider a well-fed and comfortable animal with no obvious motivations? Although it is not trivial to determine the motivation underlying a spontaneous movement, we can consider several reasons why internally driven behaviors should not be considered as the output of a noisy system, with no biological relevance. Driving force of internally driven behaviors can be casted into two categories: extrinsic or intrinsic motivation (Gottlieb et al., 2013).

Extrinsic motivation for exploration

In extrinsically motivated contexts, behavior is a way to reach a biological goal e.g. finding food or potential mates. Foraging is an example of a natural decision-making process, widespread across taxa, from *C. elegans* (Calhoun and Hayden, 2015) to monkeys (Blanchard and Hayden (2014), Hayden et al. (2011)). In experience-studying foraging, the animal faces two possibilities: the default option (foreground) and the non-default option (background). For a sit-and-wait predator, the foreground decision is to keep waiting for possible prey, alternatively, the background option is to move to another location.

Neurons in the dorsal anterior cingulate cortex (dACC) of monkeys have been studied during foraging tasks. Firing rate in the dACC rose gradually when the animal chose the background option and reached a threshold during foreground. The rise and threshold were modulated by context (e.g. uncertainty about the background option) and internal drives (how desirable is the foreground option). The dACC neurons activity was consistent with an accumulation of evidence, and the level of its activity reflected the value of the background option (Hayden et al., 2011).

At the behavioral level, the Lévy-flight foraging hypothesis predicts that a predator should adopt search strategies known as Lévy-flights when prey is spatially sparse and distributed unpredictably. Lévy flight is a random walk in which the distance trav-

eled at each step follows a heavy tail distribution. In contrast with Brownian motion, Lévy-flights are less confined because of the small number of long walks (Viswanathan, 2010). Analysis of displacement, recorded from animal-attached GPS has shown that diverse marine predators: sharks, bony fish, sea turtles and penguins exhibit Lévy-walk-like behavior close to the theoretical optimum (Sims et al., 2008). Some individuals switched between Lévy and Brownian movement as they traversed different habitat types showing that they adapt their search strategy to the statistical patterns of the landscape (Humphries et al., 2010).

Foraging behavior is the result of a trade-off between exploiting immediate resources and exploring alternatives, a classic problem of reinforcement learning (Gottlieb et al., 2013). When an agent is engaged in a task aimed at maximizing extrinsic reward (e.g. food), seeking spontaneously for information represents an intermediate step in attaining a reward. As we will see, this contrasts with intrinsically motivated behavior where the exploration is the purpose in itself.

Intrinsic motivation for learning

Interestingly, in controlled environments, where food resources are always available and animals are over-trained to know where the food is, animals can still exhibit rich temporal and sequential behavioral dynamics (Jung et al., 2014). Under these conditions, the behaviors cannot simply be explained as an optimal strategy for exploiting available resources but may originate from an intrinsic drive for exploring.

In intrinsically motivated behaviors, information seeking is in itself the purpose, and it is not driven by imperatives of resource exploitation. In the sensorimotor domain, for instance, intrinsically motivated behavior could be used to acquire motor skills. The field of developmental robotics is aiming at designing of agents that can autonomously explore environments, without pre-programmed trajectories, but based solely on their intrinsic interest. Inspired from developmental psychology, the systems built were capable of learning the consequences of their motor actions and solve self-generated problems by maximizing the local learning progress (Gottlieb et al., 2013). Piaget described a sequence of progress occurring during child learning from sensorimotor to abstract reasoning stages (Piaget, 1972). The field of developmental robotics suggests that child learning is not necessarily a pre-programmed sequence, but may emerge through an intrinsically motivated learning.

Bird songs are a good example of intrinsically motivated behaviors. Male songbirds primarily aim at attracting mates. However, the zebra finche male also sings outside the breeding season. These songs were not aimed to any female, and thus they were defined as undirected songs (Kroodsma and Byers, 1991). Unlike sexually oriented songs, undirected songs are ignored by potential recipients and have no immediate effects on the conspecifics' behavior. Undirected songs show more variability than sexually oriented ones, suggesting that they could reflect a practicing exercise (Wellock, 2012). Their goal could be the retrieval of auditory information about their generated songs through feedback in order to improve it. Recent studies suggest that the rewarding mechanisms associated with undirected and sexually directed songs are different. Sexually oriented songs may be primarily reinforced by opioids released in neuronal circuits associated with the social context. In contrast, undirected songs are not effected by external rewards, but could be reinforced through opioids released in the ventral segmental area by the act of singing (Riters, 2012).

The goal of internally driven behavior is not to act on the environment but to retrieve information. The distinction between extrinsically and intrinsically motivated spontaneous behaviors is not trivial but illustrates that distinct motivations can underly internally driven behaviors. Beyond the nature of these motivations, the spontaneous decision-making processes rely on two questions: what and when. Which movement to choose and when to execute it. In the next section I will review investigations on the neuronal mechanisms involved in spontaneous movements.

1.3.2 Neural basis of spontaneous behavior

Looking at the same behavior in sensory-induced and spontaneous contexts, it is expected that the neuronal activity partially overlaps in both scenarios, at least at the level of the central pattern generators (CPGs) in the spinal cord. Under the S/R paradigm, it is tempting to consider that the pathways involved during sensory-based decision making can be activated by neuronal noise causing internally driven behavior. In this section, I will first review preliminary evidence indicating that spontaneously driven and sensory-induced decisions are controlled by partially non-overlapping pathways. Then, I will present the results on the neuronal mechanisms that specify the timing (when) and selection (what) of spontaneous actions.

Similarity between neuronal activity underlying internally driven and stimulus-induced behaviors

Fluctuations in the activation of sensory brain regions are insufficient to explain spontaneous movements. By recording motion-sensitive neurons in the fly optic lobes, Rosner et al. (2009) found that the variability was not sufficient to account for the variability in head movements. This raises the following questions: does a circuitry specific to spontaneous movements exist and affect the locomotor activity independently of any sensory stimulation? General arousal has been defined as promoting an increase in both locomotor activity and sensory responsiveness (Pfaff et al., 2008).

Experiments in rodents suggested that general arousal could account for 30% of the variance in activity measured in response to a wide variety of behavioral trial (Garey et al., 2003). Recent studies in zebrafish indicate that increase in locomotor activity and sensory responsiveness are not necessarily coupled. Woods et al. (2014) studied the influence of neuropeptides on the modulation of spontaneous locomotion and sensory responsiveness to several behaviors. Their study identified two neuropeptides, *Cart* and *Adcyap1b* that had no effect on spontaneous locomotor activity during night and day but affected the probability of inducing a behavioral response to both dark flash stimuli and tap stimuli (**Figure 1.4.A,B**). *Cck* generated the opposite effect, increasing the spontaneous activity without affecting sensory-induced responsiveness to the stimuli tested (**Figure 1.4.C**).

Arousal is thus partitioned into spontaneous locomotor activity and sensory responsiveness. The neuronal mechanisms responsible for this segregation are unknown, but this suggests that sensory evoked and spontaneous behavior could be controlled by partially different neuronal pathways, each affected differently by the neuropeptides mentioned.

When to move? Timing of spontaneous behavior

How does the brain spontaneously take the decision to execute a given action in the absence of environmental stimuli? By recording electroencephalogram signals before spontaneous decisions in humans, Kornhuber and Deecke first described, in 1964, a gradual buildup in activity starting ~ 1 s before a voluntary movement. In 1983, in a follow-up experiment, Libet asked subjects to report the time when they first felt the urge to move (**Figure 1.5.A**). Subject's conscious awareness of an intention to

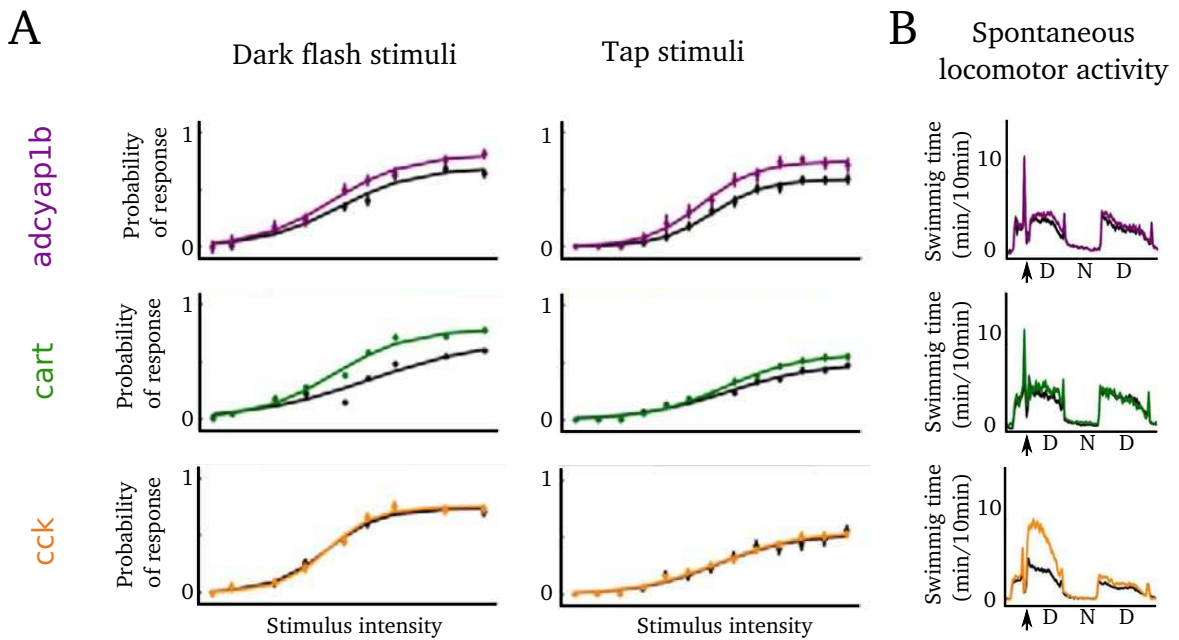


Fig. 1.4: **Segregation of arousal between locomotor activity and sensory responsiveness according to neuropeptides** (A) Neuropeptidic modulation of response to a dark-flash and tapping stimuli. Colored curves correspond to the induction of neuropeptide and black curves to wild-type siblings. Response probability \pm s.e.m is indicated for each stimulus intensity. Adcyap1b and cart increase the probability of response and decrease the stimulus threshold of detection for both dark-flash and tapping stimuli. Responsiveness of cck-expressing larvae show however indistinguishable from control. (B) Neuropeptidic modulations of locomotor activity. Swimming time is quantified by the time of swimming during a 10-minute window. The black arrows represent the heat-shock that induced the expression of neuropeptide. Spontaneous activity of larvae is monitored day (D) and night (N) after the heat-shock. Cck-expressing larvae showed an increase in locomotion following the heatshock contrasting with cart and adcyap1b expressing larvae that showed no significant variation. Adapted from Woods et al. (2014).

act occurs only 200 ms before the onset of a movement, which is much later than the onset of the readiness potential. The debate raised by this experiment is outside the scope of this thesis but this experiment is still unique in neuroscience in its philosophical implication. The idea that unconscious brain processes are the true initiators of voluntary acts inflicted a narcissistic blow to our notion of free-will. In humans, these results were confirmed using fMRI (Bode et al., 2011) and at the single neuron level in epileptic patients (Fried et al., 2011). **Figure 1.5.B** shows single-cell recording prior to self-initiated movement in the Supplementary Motor Area where electrical stimulations have been reported to induce an urge to move. Even though the report of the conscious time can only be studied in primates, readiness potential was found in other species as well.

In invertebrates, extracellular recordings from the crayfish descending motor pathway showed similar temporal dynamics before the onset of walking (**Figure 1.5.C,D**, Kagaya and Takahata (2010)). A recent study in the rat Secondary Motor Cortex (M2) showed interesting perspectives on possible mechanisms at the core of this gradual build-up in firing rate before movements (Murakami et al., 2014). In this experiment, rats had to choose between waiting for auditory cues to collect a big reward, or stop waiting to collect a small reward (**Figure 1.5.E**). The timing of the auditory cues was unpredictable. The study focused on trials where the rats decided to stop waiting for the auditory cues. Of the 385 neurons electrophysiologically recorded from M2, $\sim 10\%$ showed a "ramp-to-threshold" activity reminiscent of the readiness potential (**Figure 1.5.F**). The faster the ramping activity, the shorter was the time. Additionally, $\sim 20\%$ were identified as "transient neurons". Their firing rate was correlated with waiting time in a brief burst rather than a ramp (**Figure 1.5.F**). In the proposed model, a set of transiently active neurons served as inputs to integrator neurons displaying a ramping activity. This integration-to-bound model is similar to a decision model where a population of neurons accumulates evidences and generates an action when a threshold is crossed.

Probably due to the influence of Libet's experiments and its implication questioning the notion of free will, further studies have mainly focused on the timing of spontaneous movements. The literature is however scarce on the mechanisms underlying the selection of spontaneous actions.

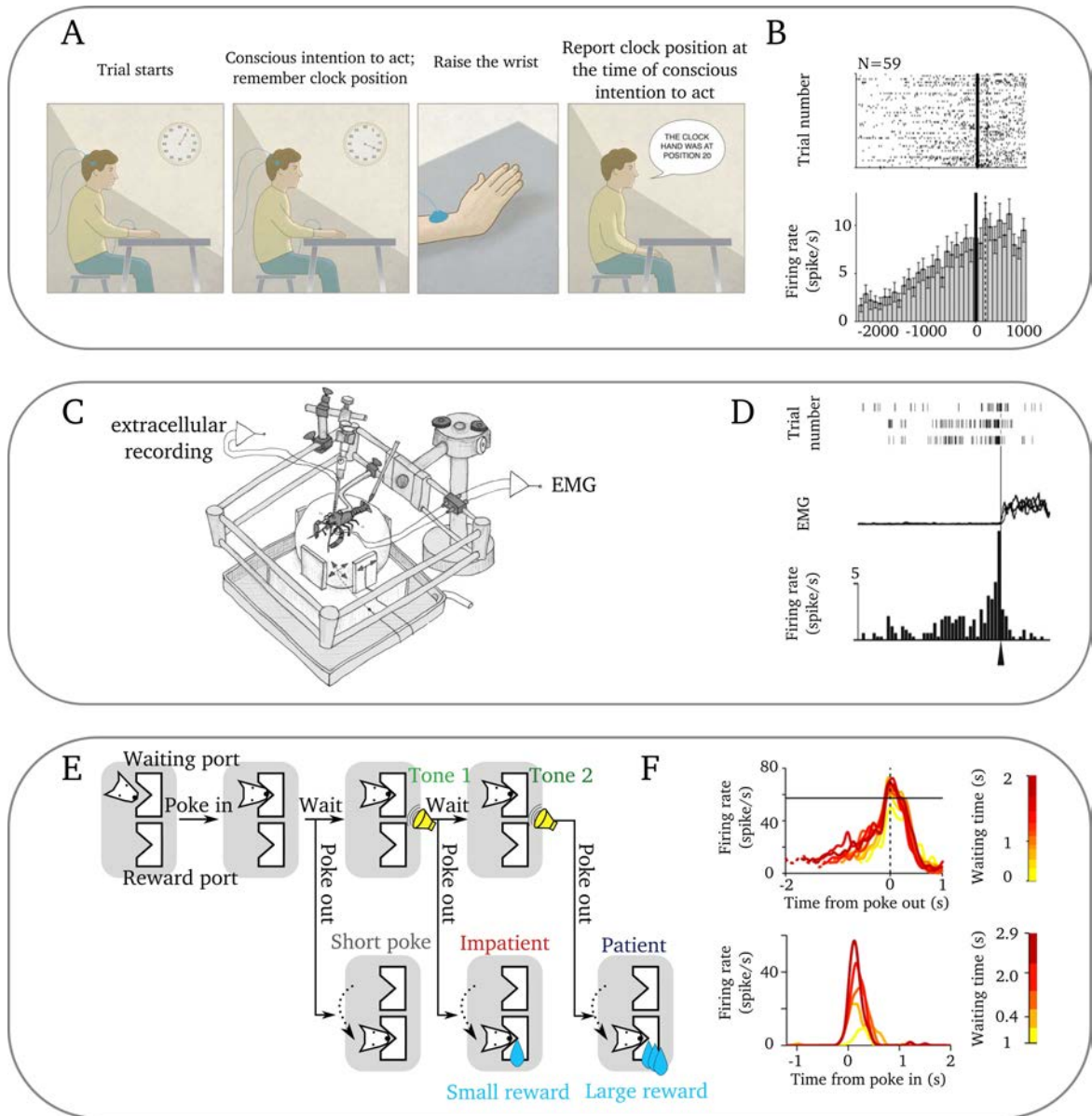


Fig. 1.5: Readiness Potential across taxa, legend next page

Fig. 1.5: (Previous page.) **(A)** Schematic description of the experimental paradigm of the Liber experiment. Subject is instructed to spontaneously flex his wrist at any time while looking at the clock-like display. After the movement, the subject had to report the time when he first became consciously aware of his intention. **(B)** Raster plot and histogram of a neuron recorded in the Supplementary Motor Area. Solid black lines indicate the time of the conscious decisions, dotted lines indicate the onset of movements. Adapted from Fried et al. (2011). **(C)** A spherical treadmill system used for extracellular recordings from the nervous system of a crayfish during walking. **(D)** Descending unit activity, with raster plot and trial averaged recordings from the circumesophageal commissure before the onset of spontaneous walking. Adapted from Kagaya and Takahata (2010). **(E)** Schematic diagram of trial events in the rat waiting task. In each trial, the rat was required to wait for tone 1 (T1) and moved to the reward port to obtain water. If the rat failed to wait for tone 1 (T1), there was no reward. If the rat waited for T1 but left before tone 2 (T2), a small reward was given. If the rat waited until T2, a large reward was provided. **(F)** The firing rate of two neurons recorded in M2. Upper panel: firing rate of a "ramp-to-threshold" neuron color-coded according to the length of the waiting time and aligned with the onset of the poke-out. Lower panel: firing rate of a "transient" neuron showing phasic activations at the beginning of the waiting period. The firing rate is positively correlated with the length of the waiting period of impatient trials. Adapted from (Murakami et al., 2014).

What to do? Selection of spontaneous action

The firing rate of "ramp-to-threshold" and "transient" neurons predict the timing of spontaneous actions. In order to find out if those neurons were action-specific or not, an extension of the nose-poke waiting task of **Figure 1.5.E** recorded the same neurons while the rat was performing a lever-press waiting time task. Murakami et al. (2014) found that among "transient" neurons, the percentage of lever-press predictive neurons among all the nose-poke predictive neurons was not more than among all neurons. Thus, neurons whose activity was correlated with the length of the waiting time period were also action-specific rather than being tied to a general preparation to any type of movement.

Alternatively, it is possible to consider that distinct paths specify the what and when of spontaneous movements. In crayfish, by looking at the direction of movement (forward-backward) in the experience in **Figure 1.5.C**, some descending units were found to be not-selective to the direction of movements. Interestingly, they were recruited ~ 4 s before the behavioral onset, the selective units followed them ~ 2.5 s later

(Kagaya and Takahata, 2010). The dissociation between the *when* and the *what* components of intentional decision is also supported by human experiments using fMRI. In a follow-up to Libet's experiment (Soon et al., 2008), subjects could freely choose between two options (e.g. right or left tap). While there are still some inconsistencies regarding the exact localization of these components (Serrien, 2010), they found that the region predictive of the choice of decision (*what*) was different from the region predictive of the timing of action (*when*). Interestingly, prediction concerning the type of movement can be made in advance to the prediction of the timing.

During internally driven behaviors, animals face a large set of possible actions and perform them in complex temporal patterns. Despite the advance in elucidating the mechanisms governing the when and the what of a decision, Libet-type experiments are subject to several shortcomings. First, experiments are usually structured in trials. Thus, the mechanisms observed could be more related to time estimation than to spontaneous behaviors. A striking example is the fact that populations of "transient" neurons in M2 are aligned with the beginning of the trial, not with the onset of the decision. Secondly, in order to have a well-controlled experimental setting, subjects have to be presented with a very limited set of alternatives (e.g. poke out or lever press). This situation is oversimplified compared to the vast action repertoire available in natural conditions. Finally, most neuronal recordings have been made in premotor or motor circuits, but the influence of other brain regions has not yet been investigated. Neuronal activities related to decision making are widely distributed (Cisek, 2012). By monitoring several brain regions, one can disentangle the dynamical properties of the circuits specifying the *what* and *when* of spontaneous motor decision. In the next section, I will present the zebrafish larva, an animal model that is ideally suited to study internally driven behaviors by overcoming these limitations.

1.4 Large-scale analysis of circuit dynamics underlying behavior in zebrafish larva

1.4.1 The zebrafish as a model for systems neuroscience

The brain complexity arises from the variety of levels of organization: from synaptic transmission to neuronal circuits and behavior. Each level of organization is attached to a specific discipline, from genetics to ecology. In this context, it is worthwhile to focus technological and scientific efforts on a restricted number of animal models,


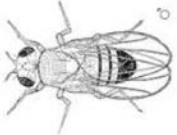



	Caenorhabditis Elegans	Drosophila Melanogaster	Zebrafish larva	Mouse	Rhesus macaque
					
Number of neurons	302	~135,000	~100,000	~71,000,000	~480,000,000

Table 1.1: **Animal models in neuroscience.** The last row indicates the estimated number of neurons. For Rhesus macaque, only cortical neurons are considered.

where our understanding will benefit from a multidisciplinary approach. Neuroscience uses several model organisms, each with different brain and behavioral complexities, illustrated in **Table 1.1**.

Zebrafish (*Danio rerio*) is a small gregarious teleost fish (~ 4 cm) originating from the south of Asia. They are easy to breed and have a fast reproduction cycle. Developmental and genetic studies have taken advantages of the transparency of their embryo since the late 1950s. Nowadays, a large library of transgenic and mutant fish is available, enabling us to target specific cell types or provide vertebrate models of human neurodevelopmental, neurological and neurodegenerative diseases (Deo and MacRae, 2011).

With the development of new optical methods and optogenetics, the zebrafish larva has recently become an appealing vertebrate model for systems neuroscience. Due to its small size and transparency, its brain activity is ideally accessible. State of the art optical methods including, two-Photon Scanning Microscopy, Selective Plane Illumination Microscopy, and Light-Field Microscopy have been successfully applied to simultaneously monitor the activity dynamics of large brain regions (**Figure 1.6**). Optogenetic sensors, such as GCaMP, a genetically encoded calcium indicator, can be expressed in selected populations of neurons. GCaMP changes its fluorescence properties in response to the binding of Ca^{2+} . The firing of neurons causes an increase in the intracellular calcium concentration resulting in rapid rises and decay in the fluorescence of GCaMP sensors.

Additionally, optogenetic actuators such as halorhodopsin or channelrhodopsin, can also be expressed. These light activated ion channels can induce or suppress

neuronal activity. This perturbation of neuronal activity can be useful to probe the causal role of neuronal activity in selected populations of neurons.

All these manipulations are commonly performed in an "all-optical" manner without the need for surgery, or anesthesia and just requires the larva to be head-restrained in agarose leaving the eyes and the tail free to move.

In order to understand behavior, it is necessary to understand the total action of the nervous system, as explained by D. Hebb in *The Organization of Behavior* (1949):

One can discover the properties of its various parts more or less in isolation; but it is a truism by now that the part may have properties that are not evident in isolation, and these are to be discovered only by study of the whole intact brain.

The ability to simultaneously monitor sensory and motor areas in a behaving animal make zebrafish an ideal model for the holistic approach on how the brain generates behavior (Ahrens and Engert, 2015).

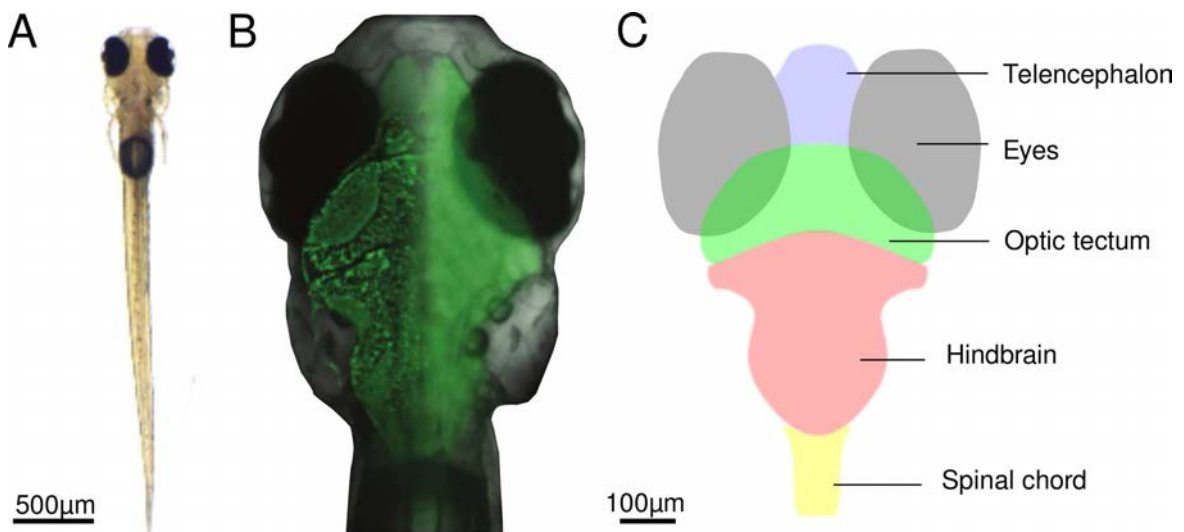


Fig. 1.6: Coarse brain anatomy of a 6 dpf zebrafish larva. (A) Bright-field image of a zebrafish larva. (B) Overlay of a bright-field image of the larva head with images of its brain acquired using two-photon microscopy (left part of the brain) and fluorescence imaging (right part of the brain). Note the spatial resolution on the left part obtained with a two-photon microscopy. Neurons are labeled with the green fluorescent calcium indicator GCaMP5G. Image reproduced from Fetcho (2012). (C) Schematic drawing of the larva's brain showed in B representing the main parts of the brain (telencephalon, optic tectum, hindbrain and spinal cord) and the eyes. The 100µm scale bar is common for B and C.




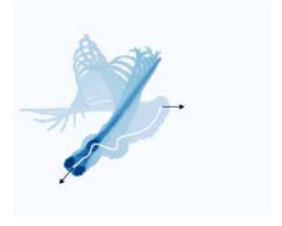
Slow scoot	J turn	Routine turn	C bend
			
Low degree of bending and tail beat frequency. Yaw angle smaller than 3° .	Fine reorientation tuning associated with prey capture. A prominent bend occurs at the caudal portion of the tail.	Slow-speed turn with a large bend angle resulting in reorientation of the larva. The bend is mostly unilateral.	High-velocity turn of short duration. Rely on the Mauthner cells.

Table 1.2: **Stereotypical tail movements.** Each column represents a typical tail movement and its characteristics. The middle column shows the superimposition of image of the larva during the tail bout. The trajectory of the head is shown by a white line, the black arrows represent the head orientation at the beginning and end of the bout.

1.4.2 Locomotion of zebrafish larva

The locomotor repertoire of zebrafish larva

The zebrafish larva propels itself through a sub-carangiform pattern of body undulations. The oscillations of the tail are coordinated with pectoral fins movements. At the larval stage, zebrafish locomotor patterns are characterized by swimming episodes intermingled with non-swimming episodes called "beat and glide". The discrete segments formed by the beat and glide swim in larvae are called tail bout, the range of durations of tail bouts is 80-400 ms, the range of tail beat frequency is 30-100 Hz (Buss and Drapeau, 2001). The quantification of behaviors is greatly facilitated because of the discrete nature of locomotion. Zebrafish larvae exhibit a variety of tail bouts: they include slow scoot (also called forward swim), routine turn, J turn or C bend illustrated in **Table 1.2**. These categories were described according to the tail movements as well as the kinematics of the trajectories (Mirat et al. (2013), Borla et al. (2002), Budick and O'Malley (2000)). Because they are defined by the properties of the trajectory, this categorization is not suited for the head-fixed conditions, where the trajectories are unknown.

The natural segmentation of movement events associated with a reasonably stereotyped locomotor repertoire is ideally suited for large-scale characterization of zebrafish behavior.

Neural basis of locomotion

Due to its limited locomotor repertoire and optical accessibility, zebrafish offers the opportunity to dissect the circuits involved in the generation of movements.

Within the spinal cord, activation of neurons follows a dorso-ventral organization. Ventral spinal interneurons and motor neurons are activated during slow-swimming regimes, and more dorsal neurons are recruited as the velocity of locomotion increases. Menelaou and McLean (2012) suggested that a continuous variation of the group of interneuron cell types, produces a smooth shift in the locomotor speed. Some interneurons within the spinal cord are specific to a category of movement. Optogenetic stimulation of Kolmer-Agduhr cells generated spontaneous slow scoots, whereas activation of Rohon-Beard touch sensitive cells triggered C-bends (Wyart et al., 2009).

The spinal cord receives descending glutamatergic inputs from the reticulospinal cells (RS), causing the tail to oscillate. This population is composed of less than 300 neurons located in the hindbrain and mid-brain (**Figure 1.7.A**). The most iconical is the Mauthner cell, a large neuron implicated in short latency escape responses. Apart from the Mauthner cells, a large part of RS neurons is multifunctional.

Individual RS neurons can be active during multiple types of locomotor behavior. The nucleus of the longitudinal fasciculus (nMLF) has been implicated in prey capture and responses to whole field motion. Ablation of two pairs of identified cells within the nMLF, MeLc and MeLr impaired prey capture as well as the ability to modulate speed in response to whole-field motion (Gahtan et al. (2005), Severi et al. (2014)). Electrical activation of the nMLF induced scoot movements whose duration and speed are modulated by the strength of the stimulation (**Figure 1.7.B**).

A small portion of cells are involved in turning, and the ventromedial spinal projection neurons (vSPNs) bias forward scoot to asymmetrical movement under different behavioral contexts (Huang et al. (2013), Orger et al. (2008)). Their activity is direction specific and graded by the amount of turning (**Figure 1.7.C**). Ablation of these cells decreased the number of turns but also increased the proportion of forward swim movements, consistent with the idea that these cells bias the kinematic of scoots in a

graded fashion.

The upstream circuitry that leads to the selective activation of these descending control neurons can be investigated by studying the neuronal activity in sensory evoked locomotion.

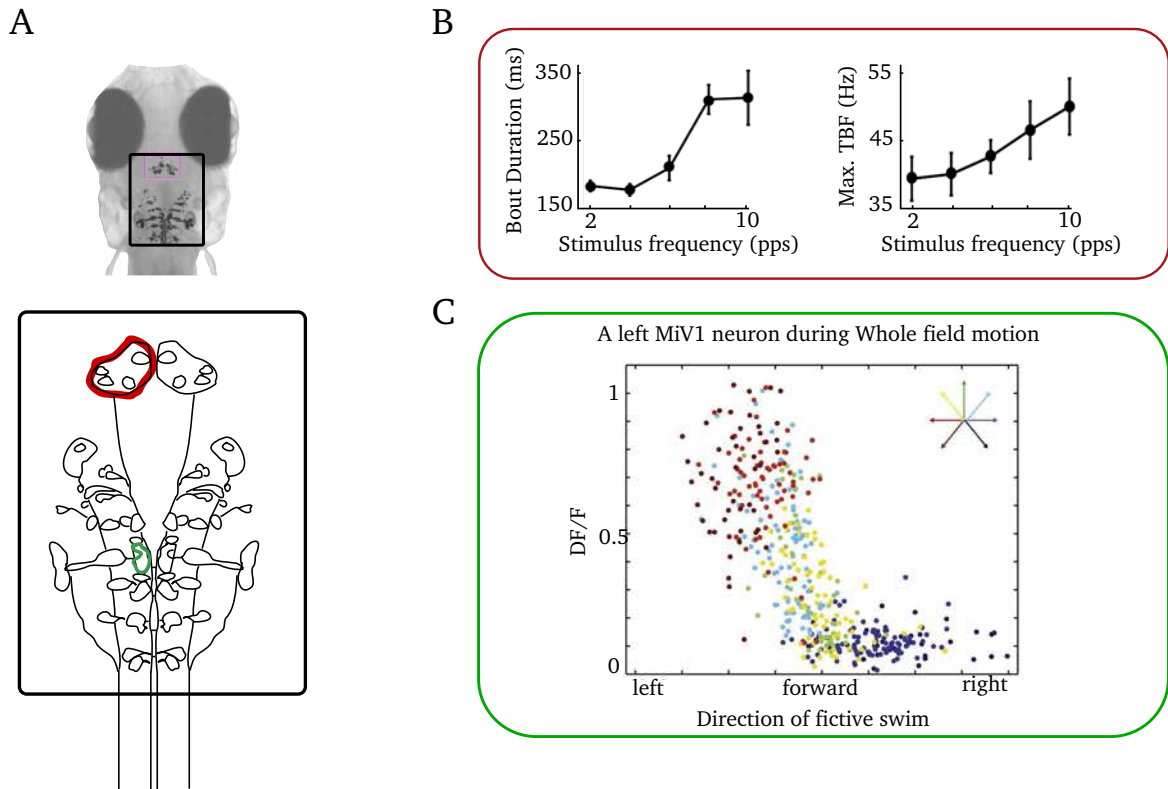


Fig. 1.7: Circuit for graded locomotion in zebrafish larva. (A) Head of a zebrafish larva. The RS circuits are located in the rectangle. Inset shows a scheme of the RS neurons. (B) Average bout duration and maximal tail beat frequency per bout recorded in response to electrical stimulation of the nMLF circuit. Adapted from Severi et al. (2014). (C) Fluorescent calcium response (DF/F) of a MiV1 neuron as a function of swimming direction. Each dot represents a bout and the color indicates the direction of the visual stimuli used to elicit the swim. Adapted from Huang et al. (2013). The color of the bounding box of (B) and (C) match the respective location of the cells in (A).

1.4.3 Goal-driven behavior in the larval zebrafish

Typical habitat of zebrafish consists of shallow and clear water with slow moving streams. Zebrafish are commonly found in ephemeral pools or rice paddles. They are omnivorous, consuming insects, zooplankton and algae (Parichy, 2015). By 6dpf, the vitellus lipids reserves are consumed and the larva needs to catch prey. This vulnerability results in a mortality rate as high as 50% due to starvation at 12 dpf (Bardach et al., 1972). This illustrates the ecological pressure which induced a rapid and early development of functional sensory-motor circuits.

Compared to rodents or primates whose behaviors have been comprehensively evaluated and defined (Shettleworth, 2010), the description of zebrafish behavioral repertoire is still a developing field of research (Kalueff et al., 2013). Field observations of zebrafish larvae behaviors are surprisingly rare. Most of what we know about their behavior has been inferred from experimental studies in laboratory environments. The simplest forms of goal-directed behavior are taxis. During taxis behavior, an animal will try to reach a desired location in the environment. The location can be chosen according to different properties, light in the case of phototaxis, chemical compositions for chemotaxis or prey for telotaxis. I will focus on visually induced taxis in zebrafish larva.

The optomotor response

The optomotor response (OMR) is common to fish and insects, animals that could be carried away by air or water streams. OMR designates a form of visual taxis whereby animals follow the whole-field motion. This could allow larva to avoid being carried downstream by the current. When presented with a whole-field moving stimulus, fish will turn and swim in the direction of perceived motion thus maintaining a stable image of the world on the retina and thus a stable position with respect to their visual environment.

OMR can be reliably evoked from 5 dpf and is maintained throughout adulthood. Thanks to the reliability of its responses, OMR has been widely used to conduct large scale genetic screens (Muto et al., 2005), study the psychophysics of vision (Orger and Baier, 2005), reveal the reticulospinal circuitry controlling movements (Orger et al. (2008), Severi et al. (2014)), confirm the cerebellum's role in processing discrepancies between perceived and expected sensory feedback (Ahrens et al., 2012a) and to implicate the dorsal raphe in different states of arousal (Yokogawa et al., 2012).

The prey-capture behavior

Four days after fertilization, zebrafish starts hunting potential food. This behavior is critical for survival and relies on several decision-making processes. The first step is the visual recognition. Larvae rely mostly on vision to capture prey, as demonstrated by the dramatic decrease in the number of prey eaten in the dark (Gahtan et al., 2005). Small moving dots (4° diameters) will elicit specific locomotor and oculomotor movements intended to position the larva in front of its prey (**Figure 1.8.A,B**), on the contrary, big dots will elicit turns away from the stimulus (Bianco et al., 2011a). After recognition, the larva will initiate a bout to bring the paramecia in front of it. Successive bouts will bring the paramecia progressively closer (**Figure 1.8.C**). The capture itself will occur via suction or biting depending on the relative position of the prey (Patterson et al., 2013). Prey capture is a highly flexible behavior, zebrafish can bias the speed, intensity and directionality of their movements based on visual cues. **Figure 1.8** shows how the direction of movements is gradually adjusted to the relative position of the prey.

Semmelhack et al. (2015) found that AF7 (arborization field 7) displayed an increase in activity specific to the detection of prey-like stimuli. Neurons in AF7 receives input from the retina and project to the optic tectum (OT, AF10), nMLF and the hindbrain. The OT is the largest recipient of retinal projections, it presents a complex layered structure with a retinotopic organization. The OT respond to a wide variety of stimuli (Gabriel et al. (2012), Muto et al. (2013)).

By presenting a battery of visual stimuli with different features (direction, speed, polarity of contrast and size), Bianco and Engert (2015) found that neurons in the OT showed a non-linear mixing of selectivity for different features relevant for prey detection. A different set of neurons in the OT anticipated eye convergence indicative of prey detection.

Although the neuronal circuits underlying detection of prey have been revealed, little is known about the neuronal activity during the approach nor the computations underlying the decision to pursue or not a prey.

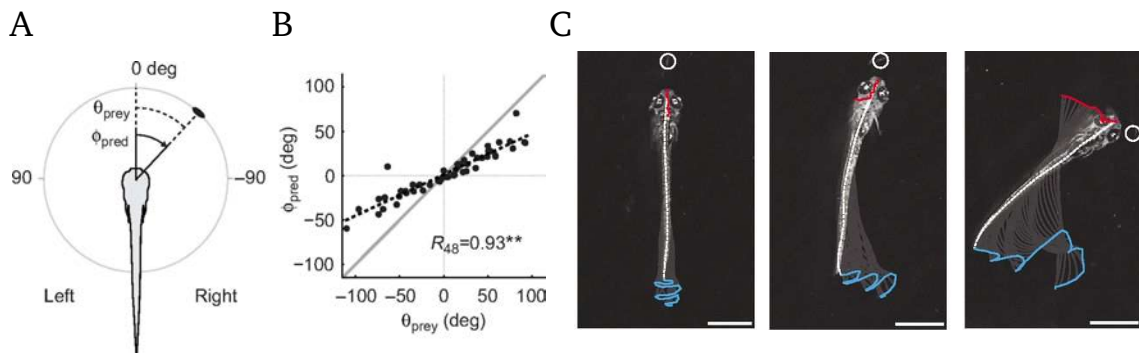


Fig. 1.8: **Flexibility of locomotor actions during prey capture.** (A) Diagram illustrating the prey azimuth θ_{prey} and the corresponding turn angle ϕ_{pred} . (B) Scatter plot of the orientation of the initial turn as a function of the prey azimuth. Larvae performed gradual turn but consistently underestimated prey location. The information about the prey location is reliably transposed into a corresponding motor command. (C) Frames from high-speed video illustrating differences in the directionality of movements following the initial orientation turn. The red and blue curves represent the position of the head and the caudal part the tail respectively. The white dot indicates the location of the paramecia. The larva continuously adjusts its trajectory to the prey location during the prey capture sequence. Adapted from Patterson et al. (2013).

Phototaxis

Phototaxis is the ability of an organism to move toward (positive phototaxis) or away (negative phototaxis) from a light source. Phototactic responses are observed across taxa, from bacteria and plants to vertebrates. This basic form of goal-directed behavior is also present in the zebrafish larva (**Figure 1.9.A,B**).

Using fine behavioral characterizations of wild-type and mutant larvae, the latter showing a selective disruption of the retinal ON or OFF pathways, Burgess et al. (2010) showed that two distinct retinal pathways are driving phototaxis. ON retinal ganglion cells are active following an increase in light intensity. They control the rate of approach by activating forward scoots. The OFF pathway, sensitive to the decay in lighting deploys contralateral turns. A simple input-output relationship would thus be enough to account for the trajectory of the larva toward the light (**Figure 1.9.C**).

Recent behavioral studies have shown a form of phototaxis performed by larvae in absence of a spatial gradient (Chen and Engert, 2014). In this setup, the presence of a larva inside a virtual border (circle) caused the whole field to be illuminated, and when the larva stepped out of this border, the light was turned off (**Figure 1.9.D**). After swimming out of the circle, the larva was capable of returning to the illuminated area in a directed manner (**Figure 1.9.D**). To explain this rudimentary form of path integration, the authors employed two hypotheses : 1) A mechanism similar to the ON/OFF pathways, where the larva preferentially performs turns (respectively forward scoots) following an illumination intensity decay (respectively increase) (**Figure 1.9.E**). But this explanation is not sufficient to account for the ability of larvae to return inside the virtual border by performing an efficient turn 70% of the time (**Figure 1.9.F**). 2) The mechanisms employed to explain the efficiency of turn relied on the larva's ability to integrate some information about its recent swimming history (over ~ 7 s).

Building a robot performing phototaxis is straightforward, it just requires to connect two light detectors with contralateral wheels. Unlike this simple mechanisms, the detailed analysis of phototaxis behavior in larval zebrafish sheds light on the complex navigation strategy at play that cannot be trivially reduced to successive mapping between light intensity and motor commands.

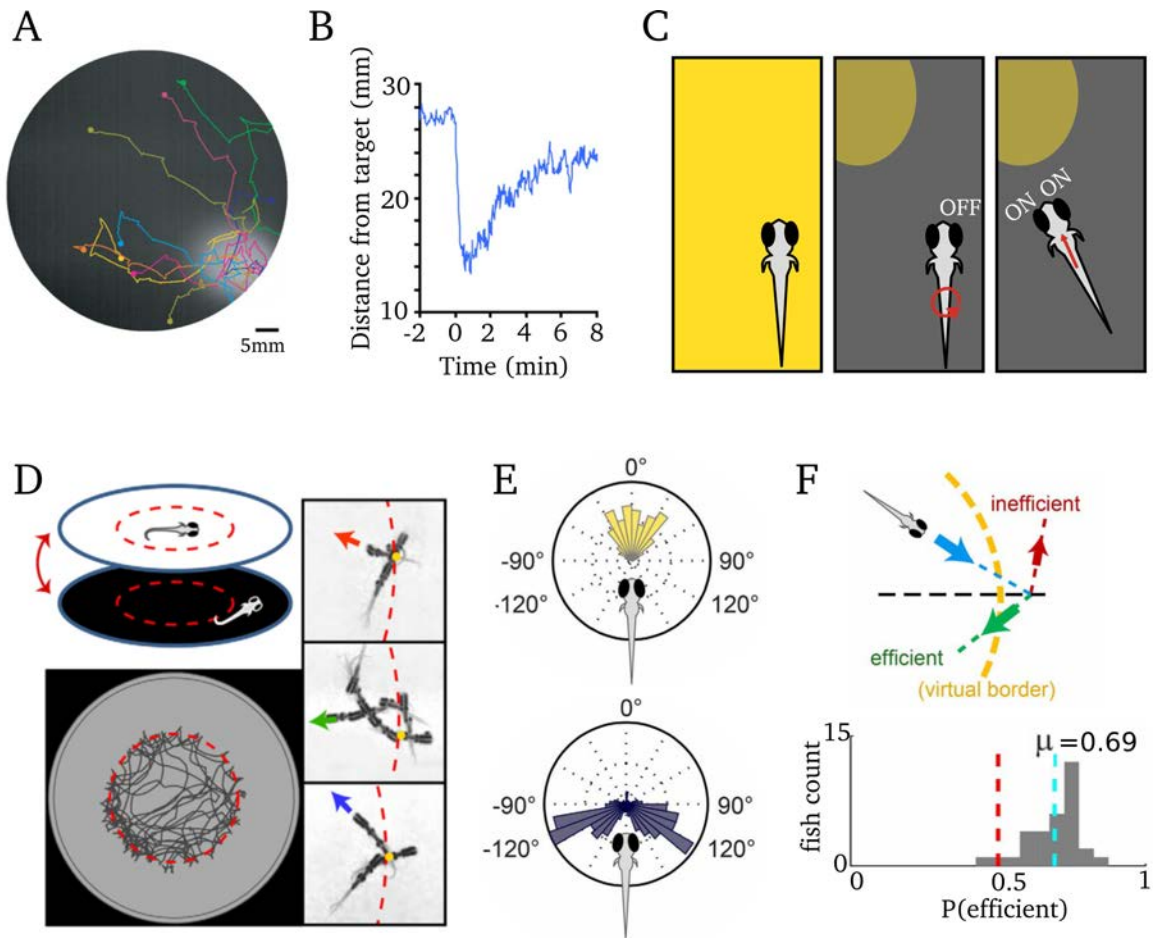


Fig. 1.9: **Phototaxis in zebrafish larva.** (A) Scheme showing the phototaxis behavior, larvae are maintained under uniform illumination and tested for phototaxis by changing to a dark field with a light spot. The trajectories of nine larvae in this essay are superimposed. (B) Mean larval distance to the target at 0.5 s intervals. (C) Scheme of the mechanisms required for the larvae to perform phototaxis. The retinal OFF pathway activates turn in the contralateral direction following a decrease in light intensity. The retinal ON pathway activates forward swim following an increase in light intensity. (D) Upper panel: Scheme of temporal phototaxis, the uniform illumination is turned off when the fish exits the virtual circle (red dashed line) and turned on again when the fish returns. Lower panel: trajectory of a larva during the essay. On the right: a close up view of the trajectory segments close to the border. (E) Turning-angle distributions from on larva. Upper panel: all turns in light. Lower panel: the first turn after Light-to-dark transition. (F) Upper panel: illustration of "efficient" vs "inefficient" turns. In order to return to the light, the direction shown by the green arrow is more efficient than the red arrow. Lower panel: histogram of the per-fish "efficiency", the red dashed line marks the 50/50 probability, the dashed cyan line marks the mean of the distribution. Adapted from Burgess et al. (2010) and Chen and Engert (2014).

1.5 Main aims

Most investigations on brain functions have focused on local circuits and S/R associations (Sompolinsky, 2014). However, this framework is limited for understanding behaviors that cannot be decomposed as a series of input-output association. The zebrafish model provides the opportunity to study neuronal activity simultaneously from multiple brain regions. This advantage may help to shed light on the complex, non-linear and contextual effects underlying brain functions during behavior.

In the first part of this manuscript, I presented a method for VR in zebrafish larva. This flexible behavioral paradigm enables the study of the chaining of locomotor patterns underlying different goal-directed tasks: the optomotor response and prey tracking. I also demonstrated how the timing of the visual feedback resulting from motor actions is critical for the success of prey capture.

Experiments on spontaneous actions provide animals with restricted behavioral options. This approach does not account for the decision-making process underlying the complex temporal pattern of spontaneous actions occurring in natural behaviors such as foraging. Zebrafish larva spontaneously generates movements in the absence of sensory stimulation. Taking advantages of its small locomotor repertoire, I first quantitatively described the complex temporal patterns of spontaneous tail bouts. Then, using selective plane microscopy, I monitored the neuronal activity from large portions of the zebrafish brain preceding the onset of spontaneous movements. Preliminary results indicate that the selection of spontaneous locomotor action and their timing are specified by different population of neurons.

Being virtually killed by virtual laser in virtual space is just as effective as the real thing, because you are as dead as you think you are.

Douglas Adams (1992). Mostly Harmless

Chapter 2

A visual virtual reality system for the zebrafish larva

2.1 Introduction

The use of VR in zebrafish larva gives the opportunity to shed light on the role of sensory feedback during goal-directed behaviors. Moreover, the combination of VR with functional imaging would be useful to learn about the dialogue between the sensory and motor circuits.

In walking animals, leg movements can be measured using a spherical treadmill in head-fixed preparations (**Figure 1.3**). On the contrary, obtaining a readout of the displacement intended by the tail movements of a zebrafish larva is not a straightforward task. I developed a method to relate the tail movement kinematics to the intended displacements of the larva, in a visual virtual environment, where the larva can perform goal directed behavior. Recent works have used virtual reality in zebrafish larva (Portugues and Engert (2011), Ahrens et al. (2012b), Ahrens et al. (2013a), Vladimirov et al. (2014), Trivedi and Bollmann (2013)).

Two options were used to record motor activity illustrated in **Figure 2.1**. The first option is to use "fictive swim", which involves recording in a bundle of motor neuron axons (Ahrens et al. (2012b), Ahrens et al. (2013a), Vladimirov et al. (2014)). Larvae turn using asymmetric tail oscillations. Therefore, the direction of the intended movement was obtained by comparing the intensity of the signal recorded from both sides of the tail. This method enabled larva to perform phototaxis and optomotor response in a virtual 2D environment. The alternative is to monitor the tail movements, when the larva is head-embedded in low melting point agarose using a high-speed

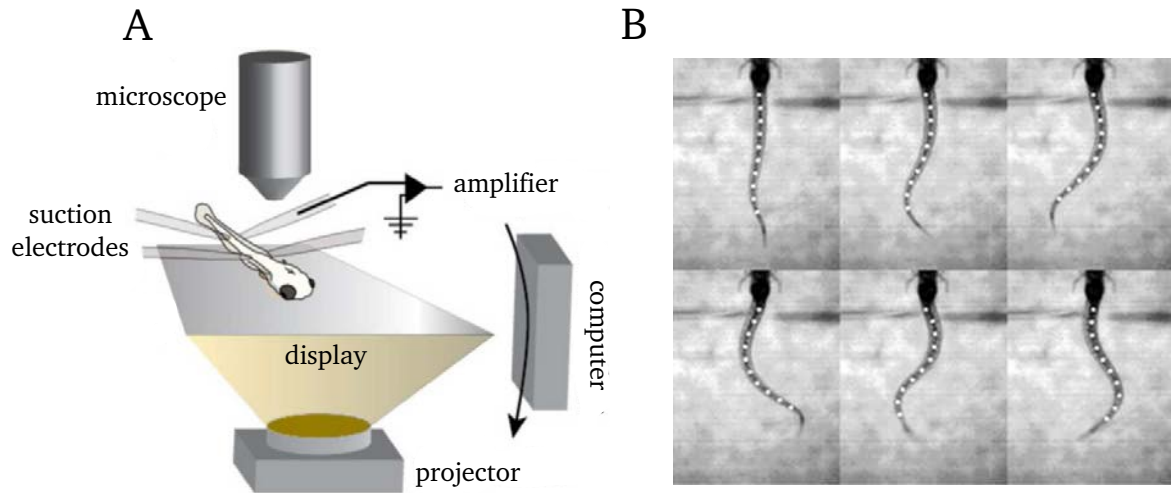


Fig. 2.1: **Recording intention of movement in zebrafish larva.** (A) "Fictive swim" setup. The larva is paralyzed and suspended using pipettes, the suction electrodes record activity from motor neuron axons in both side. Adapted from Ahrens et al. (2013a). (B) Six frames showing the automated reconstruction of the tail of a larva head-embedded in agarose. Adapted from Portuges and Engert (2011).

camera. This preparation was used to study motor adaptation during navigation in a linear track where the larva could only move forward (Portugues and Engert, 2011).

There are several advantages of inferring the larva's motion directly from the tail movement's kinematic rather than using "fictive swim". Firstly, due to the variation in the positioning of the electrodes, fictive swim readout must be calibrated regularly. Head-embedding larvae in agarose while leaving the tail free to move is simpler and straightforward. Secondly, recording tail movements allows for post-hoc analysis that cannot be computed in real time such as categorization of movements (Semmelhack et al., 2015), or fine tracking of tail kinematics (Patterson et al., 2013). Finally, zebrafish swim is composed of discrete episodes of propulsion interleaved with periods of inactivity, the use of the fictive swim method requires setting a threshold on motor nerve electrical activity. A drawback of letting the tail move is that the head fixation exerted mechanical constraint during movement which are absent in freely swimming larva. Additionally, the "fictive swim" method is advantageous because the paralysis allows for more stable recording of the brain activity.

In order to relate the tail kinematics to the intended displacements of the larva, I monitored freely swimming larvae and extracted the relationship between tail movement and change in orientation and position. I then used this relationship in head-restrained larvae. While monitoring their tail movements and computing, in real

time, the intentional displacement in order to update to the visual environment displayed around the larva. I demonstrate that this method enables the larva to interact meaningfully with its visual environment in different behavioral contexts. The larva maintained the proper speed and orientation in presence of whole-field motion and produces fine changes in orientation and position required to capture virtual preys. I also illustrated how alteration of the sensory feedback can be used to investigate neuronal process underlying navigation.

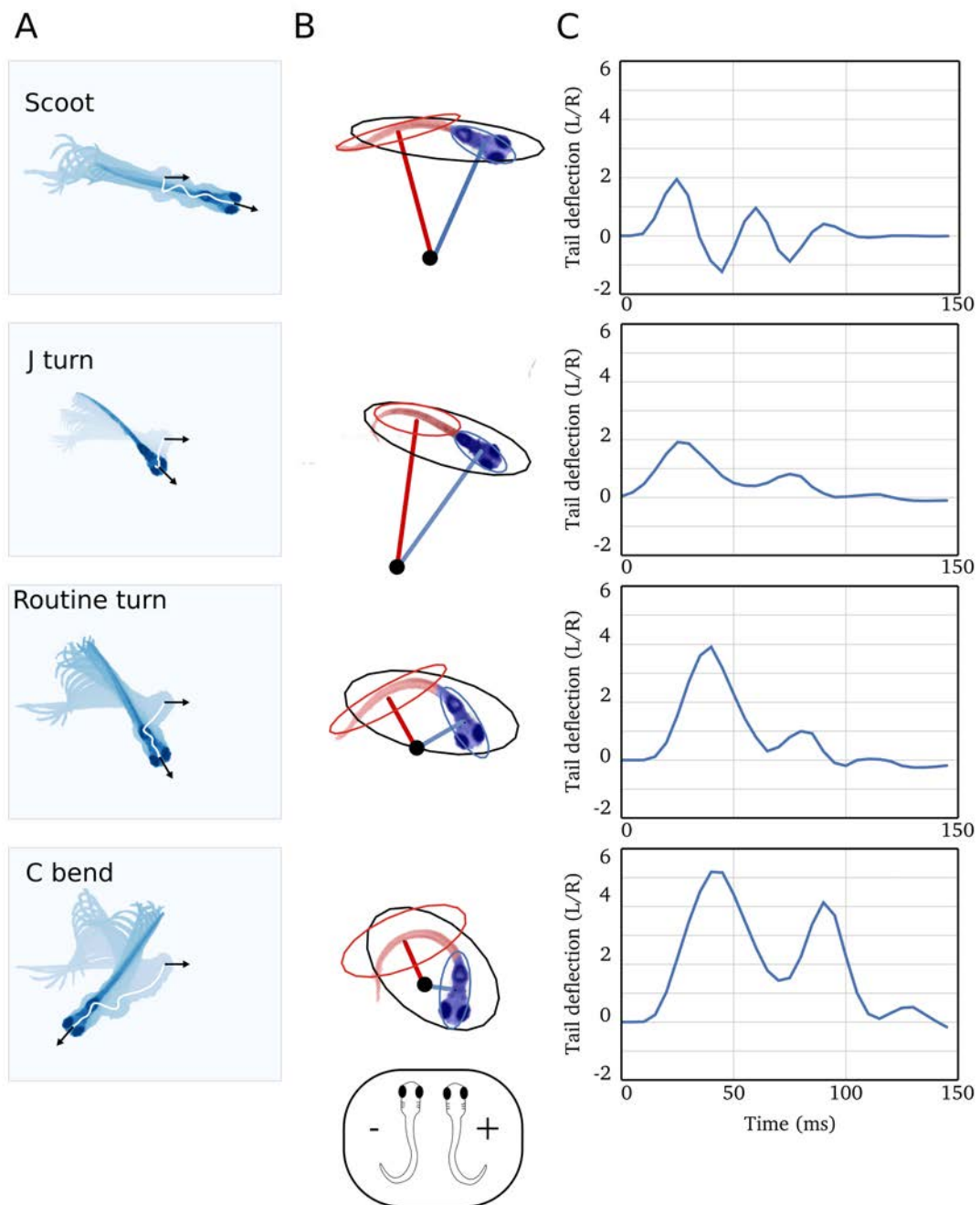


Fig. 2.2:]
Quantification of tail movements], legend next page

Fig. 2.2: (Previous page.) Each row depicts a movement from different category. **(A)** Superimposition of image of the larvae during a tail bout. The trajectory of the head is shown by a white line, the black arrows represent the head orientation at the beginning and end of the bout. **(B)** Illustration of the image processing method on a characteristic snapshot of the movement in **(A)**, an ellipse is fitted on the binarized larva (in black). Pixels are split in two groups according to the small axis of the black ellipse: pixel shown in red or blue overlaid on the larva. On those two groups of pixels, an ellipse is fitted (red and blue ellipse) and the corresponding small axis are drawn in red and blue line. The center of curvature (black dot) is defined as the intersection between the small axis. From this point the deflection is defined as the inverse of the average distance between all the pixel in the fish and the center of curvature ($1/R$). The result is multiplied by the length of the fish at rest L_0 in order to obtain a dimensionless value. The sign of the deflection is computed according to the convention indicated in the inset. **(C)** Deflection of the tail associated with each movement.

2.2 Results

2.2.1 Prediction of the larva's trajectory from the kinematics of tail movements

Zebrafish larvae navigate by producing discrete stereotypical tail movements called swim bouts. Larvae do not track moving gratings faster than 10 Hz (Rinner et al., 2005), this indicates that a refresh rate of 60 Hz from a video projector is sufficient to accommodate the temporal acuity of zebrafish vision. The typical frequency of oscillations of the tail during a bout in restrained larvae is 20 to 30 Hz (Severi et al., 2014). In order to provide a real-time feedback, the tail kinematics should be filmed at high acquisition rates (above 200 Hz), and the processing of the acquired images must be computed in just a few milliseconds. The Reynold's number of swimming larvae is between 50 and 900 Re, which puts them in a transitional flow regime (McHenry and Lauder, 2005), thus neither inertial nor viscous forces can be neglected. Approximations in flow regime could enable to compute, in real time, the thrust generated by the tail movements of an adult fish (Bergmann and Iollo, 2011). However, computing the thrust in transitional flow regime is so far unachievable.

To predict trajectories from tail kinematics, I used a data-driven approach to learn the relationship between tail movements and fish kinematics in the horizontal plane. I recorded the displacement and tail kinematics from freely swimming larvae in shallow water to generate a large library of movements. Paramecia were also introduced to induce the larvae to generate prey-capture behaviors (5% of the library). Our library of movements consisted of ~ 300 tail bouts from 6-8 days post fertilization wild-type larvae. The shape of the tail was quantified by computing the tail deflection using a method developed by Raphael Candelier. **Figure 2.2** shows the time series of the tail deflection associated with stereotypical movements. This quantification of tail kinematics was fast ($\sim 1\text{ms}/\text{frames}$ with 100 px square image in C++), and it resulted in a low-noise, smooth and oscillating times series. To describe the change in orientation and position of the larva in the swimming plane, I have used 3 parameters: axial, lateral and yaw speed (**Figure 2.3.A**). **Figure 2.3.C** shows the kinematic parameters for freely swimming larvae associated with 4 different types of movements. Kinematic parameters were chosen to be smooth oscillating time series during swim bouts.

To identify the relation between the oscillating tail deflections and changes in orientation and position, I used an auto-regressive model with external input (ARX

Model, Ljung (1998)). This technique can predict the value of a kinematic parameter (axial, lateral or yaw speed) using a linear combination of both the past value of the kinematic parameters and the past and current values of the tail deflection (**Figure 2.3.B**). Thus, a simple regression is needed to fit the relationship between the tail deflection and the resulting trajectories.

To assess our model, I predicted the trajectories in the test dataset of free-swimming larvae using only the tail deflection. The resulting trajectories were then compared to the actual trajectories of the larva. **Figure 2.3.C** shows that the trajectories resulting from different categories of tail movements can be fitted using the same model. Errors accumulate such that the trajectory predicted from the tail deflection diverges from the observed trajectory but the overall kinematics were similar.

The quality of the predictions of the final orientation and position after a tail bout is shown in **Figure 2.3.D**. I computed the error between predicted and observed path using bootstrap between a test and a train dataset. The error in the prediction of the direction of movements had a standard deviation of 19.41° (**Figure 2.3.D.ii**), a similar standard deviation of 23.41° was observed in the prediction of the change in the larva's head direction (**Figure 2.3.D.i**). The difference between the predicted and observed amplitude of the movement had a standard deviation of 0.3 mm which represent 1/10 of the body length of the larva (**Figure 2.3.D.iii**).

To create the visual VR system, I head restrained the larvae in a drop of low-melting agarose and place in a recording chamber (see Material and Methods). The tail movements were then filmed with a high-speed camera at a frame rate of 200 Hz. Using the ARX model, I inferred the changes in kinematic parameters resulting from tail movements. This was used to update in real time the patterned visual stimuli displayed around or below the larva using a pico-projector. I used a custom program in C++ using OpenCV to process images and OpenGL to display the visual environment.

Due to the flexibility of this method, I was able to study different types of visual behaviors. All the routines required for the analysis of the library of movements and the generation of the ARX model were computed in an IPython Notebook to reproduce the data analysis and they could be adapted to the need of specific experimental paradigms. As a proof of principle, I tested the VR system using two different visual behaviors: The optomotor response and prey-capture behavior.

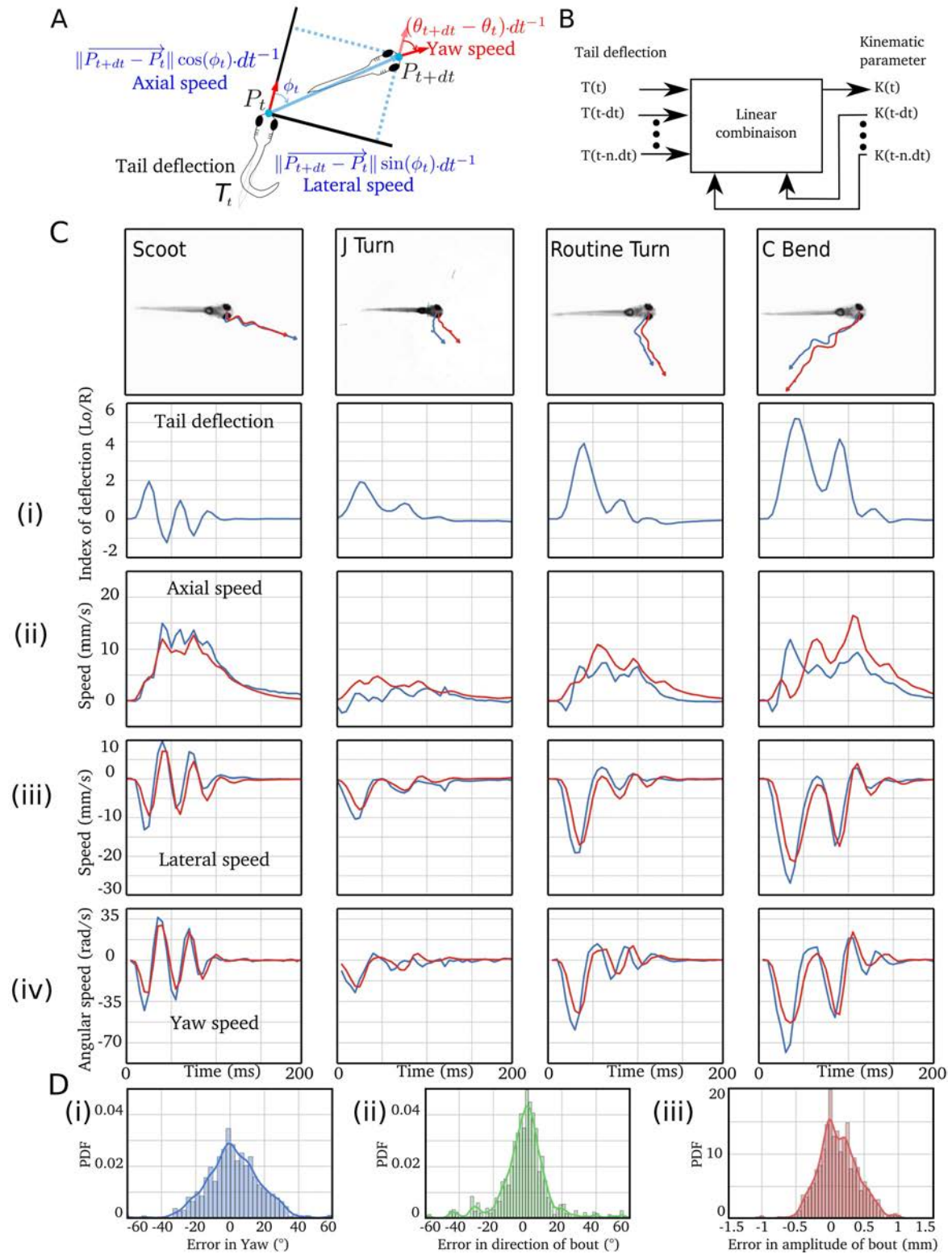


Fig. 2.3: Prediction of trajectory from tail movements, legend next page

Fig. 2.3: (Previous page.) **(A)** Parametrization of the displacement of the larva in the horizontal plane. Only 3 parameters are required to describe the trajectory: the axial, lateral and yaw speed. **(B)** Illustration of the Auto-regressive Model with External Input. Each of the three parameters of trajectory is computed using the tail deflection. Each of the kinematic parameters at time t , $K(t)$ is computed using a linear combination of its past values: $K(t - dt)$, $K(t - 2.dt)$, ..., $K(t - n.dt)$ and the present and past values of the tail deflection: $T(t)$, $T(t - dt)$, ..., $T(t - n.dt)$. See Material and Methods for details. **(C)** Four examples of trajectory and the associated kinematic parameters observed (in blue) and predicted from the different tail movements (in red). **(i)** Tail deflection corresponding to different categories of movement. **(ii)** Axial speed observed (blue) and predicted (red). **(iii)** Lateral speed observed (blue) and predicted (red). **(iv)** Yaw angle observed (blue) and predicted (red). **(D)** Distribution of the prediction error in the position and orientation resulting from a tail bout. **(i)** Error in the prediction of the change in head orientation. **(ii)** Error in the prediction of the direction of movement. **(iii)** Error in the prediction of the amplitude of a tail bout. The results presented in **(C)** and **(D)** were taken from the test dataset.

2.2.2 Optomotor response in a two-dimensions visual virtual reality system

The optomotor response, a visual component of rheotaxis, is a highly reproducible behavior in zebrafish larva. Presenting a moving grating below the larva elicits a movement in the same direction. I tested whether larvae were capable of orienting towards and follow a moving grating stimulus in the VR.

The speed of the grating (1 cm/s) and its spatial period (1 cm) were chosen according to previous studies (Portugues and Engert (2011), Ahrens et al. (2013a)). At the beginning of each trial, I randomly chose the angle between the initial orientation of the grid movement and the head direction of the larva (between -180° and 180°). During the stimulation, the speed and orientation of the grid was updated according to the tail movements of the larva. The stability of the trajectories in the VR was improved by applying a gain of 3 to the axial speed. Each experiment consisted of 120 trials, each trial was split into periods of visual stimulation of 6s and resting periods of 20s.

Using this paradigm, we found that when the whole-field motion was aligned with the larvae, they displayed a shorted response time before the first bout (**Figure 2.4.F**). During the stimulation, larvae maintain an average speed of 0.15 cm/s in the direction of the grid. They produced on average 3 bouts per trial (3.26, N=549, from 9 larvae) and the average bout duration was ~ 300 ms (0.313ms, N=1783, from 9 larvae), which is consistent with previous report (Severi et al., 2014).

As expected, the distribution of the angles between the larva and the grating's direction decreased with time (**Figure 2.4.C,D**). Successive bouts brought the head angle of the larva to an average deviation of 20° with the grid (**Figure 2.4.G**). Considering that the larva is aligned with the motion if the difference between the angle of its head and the angle of the grid motion is lower than 30° (the deviation observed in free swimming OMR, Ahrens et al. (2013a)). The proportion of aligned larva increased by two folds during the 6 s trial (from 28.2° to 51.6° , N=546, from 9 larvae, **Figure 2.4.E,H**).

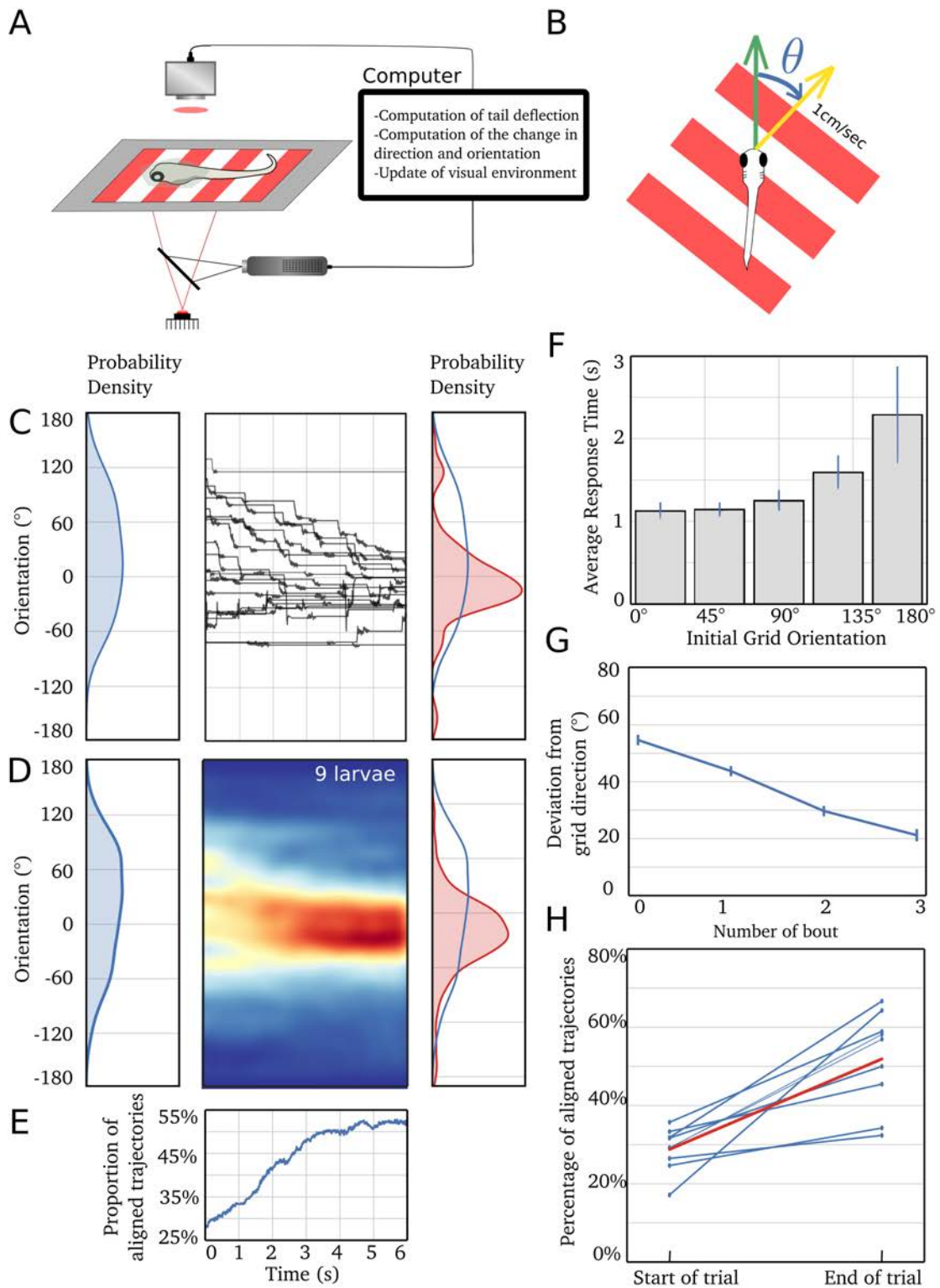


Fig. 2.4: Optomotor response in virtual reality, legend next page.

Fig. 2.4: (Previous page.) **(A)** Scheme of the experimental setup. The tail is imaged using the combination of a high speed camera, an IR LED and a high-pass filter to filter out the visual stimulation. A projector is used to display the moving grid on a diffusive screen placed 0.5 below the larva. The larva is head-embedded in low-melting agarose at the bottom of a petri-dish, the tail is free to move. **(B)** The grid is moving at 1 cm/s, the angle of the grid motion (Yellow arrow) relative to the heading direction of the larva (green arrow) is θ . **(C)** Center panel: example of angular trajectory for one larva. Left panel: Initial distribution of θ for the same larva. Right panel: Final distribution of θ . **(D)** Initial distribution of θ for all larvae. Center panel: color-coded density of θ as a function of time for the 6s trials. Right panel: Final distribution of θ for all larvae. **(E)** Proportion of fish aligned with the grid ($|\theta| < 30^\circ$) as a function of time during the trial. The time scale is common to (C), (D) and (E). **(F)** Histogram of response time as a function of the initial orientation of the θ , error bars indicate the s.e.m. **(G)** Average of the deviation $|\theta|$ for successive bouts, the error bars indicate the s.e.m. **(H)** Average percentage of trajectory aligned with the grid ($\theta \in [-30^\circ, 30^\circ]$) at the beginning and end of trial for each larva. In all panels, only the trials where the larva initiated at least one tail bout were considered.

2.2.3 Prey-capture behavior in two-dimension visual virtual reality

Zebrafish larvae begin to hunt paramecia after 5 days post fertilization, just two days after hatching. This visually driven behavior is crucial for their survival. After detecting a prey, the larva orients itself towards the prey and uses forward scoots and J turns. The larva executes a capture maneuver and swallows its prey when the paramecia is closer than $400 \mu m$.

Under head-restrained conditions, the larvae could perform orienting and pursuit maneuvers toward the pseudo-paramecia in a visual virtual environment (**Figure 2.5.A,B**). Each trial mimicked a situation where a $100 \mu m$ paramecia appears 1.5 mm away from the larva. In this configuration, the apparent angle of the paramecia (diameter of 4°) was presented to optimally elicit a prey-capture behavior (Bianco and Engert (2015), Semmelhack et al. (2015)).

At the beginning of each trial, we projected on the circular screen a 4° circular black spot moving on a white background at an angular speed of $\pm 90^\circ/s$ along the azimuthal plane. The angular velocity of $90^\circ/s$ is not consistent with the speed of moving paramecia ($\sim 100 \mu m/s$) at a distance of 1.5 mm from the larva, but it has been

shown to be optimal to elicit prey capture (Semmelhack et al., 2015). It is possible that this optimal speed results from the relative velocity between the larva and the paramecia when the larva is actively foraging. Right after the onset of the larva's first tail bout, the angular speed of the prey in the virtual environment was set to $0^\circ/s$ and the change in size and position of the black circle projected on the screen were computed according to the predicted trajectory of the larva. **Figure 2.5.B** illustrates the experimental design. If the larva oriented itself toward the virtual paramecium, the circle projected then reached the center of the field of view of the larva and its radius increased as the larva swam in its direction. We considered that a larva captured the virtual prey if its trajectory in the virtual environment was closer than $400 \mu m$ from the virtual prey (the corresponding apparent angle of the virtual prey would have a diameter of 15°).

Each experiment consisted of 250 trials, with each trial ending after a successful capture or when the angle between the head angle and the virtual paramecium exceeded 90° . We found that larvae produced at least a tail movement in 14% of the trials (13.8%, $N=6750$, from 27 larvae), which is consistent with previous reports (Bianco et al. (2011b), Bianco and Engert (2015)). For trials where the larva initiated a tail movement, larvae were able to capture the virtual preys on average 16% of the time, and up to 40% for the best performing larvae (**Figure 2.5.E**). By shuffling the trajectories with respect to the position of the prey as a control, we showed that random trajectories could reach the final target with a 5% change (**Figure 2.5.E**). We could also reproduce previously described characteristic of prey-capture behaviors in freely swimming larvae. Larvae preferentially initiate the first tail bout when the prey was in a field of view of $\pm 30^\circ$ (**Figure 2.5.F**). The larvae performed in average 3.6 bouts ($N=99$ successful trials, from 27 larvae) to capture the virtual prey. The trajectory of larvae in the virtual environment were graded according to the azimuthal position of the virtual prey (**Figure 2.5.C,D**).

As observed in freely swimming larvae, the bouts coarsely bring the paramecia in front of the larva and successive smaller correcting bouts bring the paramecia progressively closer (**Figure 2.5.G**, Patterson et al. (2013)). Bout durations were on average 180ms (182ms, $N=1358$ from 27 larvae) which was significantly lower than for OMR (0.313ms). Moreover, successful virtual prey captures were associated with an increase in eye convergence during the first two bouts (**Figure 2.5.H**), as reported in freely swimming conditions (Trivedi and Bollmann, 2013).

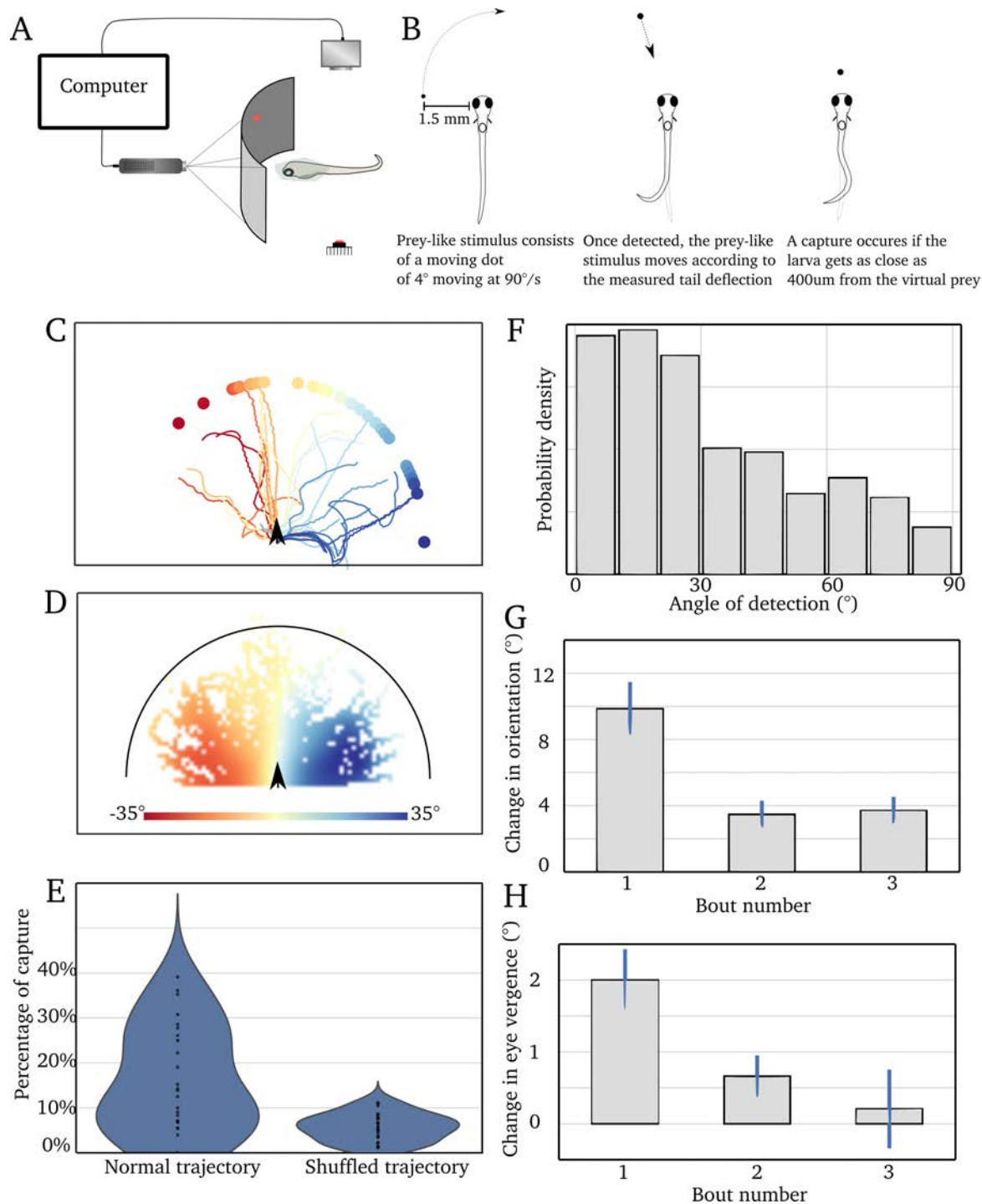


Fig. 2.5: Prey-capture in virtual reality, legend next page.

Fig. 2.5: (Previous page.) **(A)** Scheme of the experimental setup. The larva is positioned on an elevated stage surrounded by a cylindrical screen covering a field of view of 180° centered around the larva's head direction. The tail is imaged using the combination of a high speed camera, an IR LED. Two projectors are used to project the virtual prey, each covering a field of view of 90° . **(B)** Presentation of the virtual environment presented in each trial. The virtual prey of 4° appears from either side of the larva with an angular speed of $90^\circ/s$. After the onset of the first tail bout, the angular speed of the virtual prey is set to $0^\circ/s$ and the position of the virtual larva in the screen is updated according to the tail movements. A trial is successful if the larva approach the paramecium closer than $400\mu m$ in the virtual environment. **(C)** Trajectory of a larva in the virtual environment, the individual trajectory in each trial are color-coded according to the angle of the prey at the onset of the first tail bout. **(D)** Overlay of the trajectory of the 27 larvae in all trials. Each bin of the mesh grid is color-coded according to the average position of the larva for the trajectory in the bin. The dynamic range is reduced to $[-35^\circ, 35^\circ]$ in order to show the gradation of trajectory according to the position of the paramecia. In (C) and (D) the black arrows indicate the initial position of larvae. **(E)** Violin plot of the percentage of trials that resulted in a capture. Only the trials where larva executed at least one tail bout were considered. Right: Each dot shows the performance of individual larva. Left: The performance obtained by shuffling the angular positions of the virtual prey. **(F)** Histogram of the angle of the prey at the onset of the first trial. **(G)** Change in head orientation for the first three bouts. **(H)** Change in eye vergence occurring before each of the first three bouts. In (G) and (H), only the trial where larvae performed at least three bouts were considered. Error bar indicate the s.e.m.

2.2.4 Integration of visual information during tail bouts

In absence of vestibular input, external landmarks can provide a feedback on the result of a motor action by comparing the visual scene before and after a movement. An alternative strategy is to have a continuous update on the action rather than a discrete one by integrating the angular speed of the visual environment during the movement. Computing the cumulative rotation would, however require the visual system to integrate over large angular displacements while the amplitude of oscillations of the head can reach velocities of up to $4000^\circ/s$ during a turn (**Figure 2.3.C.iv**). Previous studies have reported that the larva is less sensitive to sensory feedback during movement, and uses visual feedback in-between swim bouts to compare the observed and the expected position (Trivedi and Bollmann, 2013). To test whether visual feedback is not used by the larva during swimming, I altered the visual feedback provided during the movements. We thus performed experiments in which the feedback

was updated only at the end of the bout, when the speed was smaller than 0.2 mm/s (**Figure 2.6.A**). In comparison to trials in which visual feedback was provided in real time, the delay resulted in longer bout durations of 200ms (199.3ms, N=668, from 27 larvae, **Figure 2.6.C,D**). This subtle change in the visual feedback also decreased by half the percentage of capture (**Figure 2.6.B**). Overall, these findings suggest that the zebrafish larva is capable of integrating visual information during movements. These results demonstrate the sensitivity of the zebrafish larva to visual feedback provided during movement.

2.3 Materials and methods

Zebrafish preparation

Experiments were performed on 6-8 dpf larvae of a transgenic Nacre line. Embryos were collected and raised at 28°C in E3 embryo medium, larvae were kept under a 14/10 h on/off cycles and fed with paramecia after 5 dpf. All experiments were approved by *Le Comité d'Éthique pour l'Expérimentation Animal Charles Darwin (Ce5/2009/027)*. For VR experiments, larvae were embedded in low-melting agarose (2%) dorsal side up in the center of the chamber. After the agarose had set, the chamber was filled with embryo medium. For OMR experiment, the agarose around the tail was removed up to the swim bladder using a scalpel, for prey-capture experiments, the eyes were also freed from agarose.

Imaging of zebrafish movements

An IR LED (850 nm, IR dragon optic, Osram) was used to illuminate the larvae. For imaging the eye and tail movements, I used a high-speed camera (200 frames per seconds, M3 MotionScope, Redlake) mounted on a microscope (PZMIII-BS, World Precision Instrument). The setup was placed on an anti-vibration table (Kinetic System vibraplane, 2212). In freely swimming larva, the position and orientation of the larva was computed by detection the eyes that present a distinct contrast in Nacre larva. The tail movement were quantified using the method presented in **Figure 2.2**. Quantification of the eye vergence was done by fitting an ellipse on each eye and computing the difference between angle associated with each ellipse.

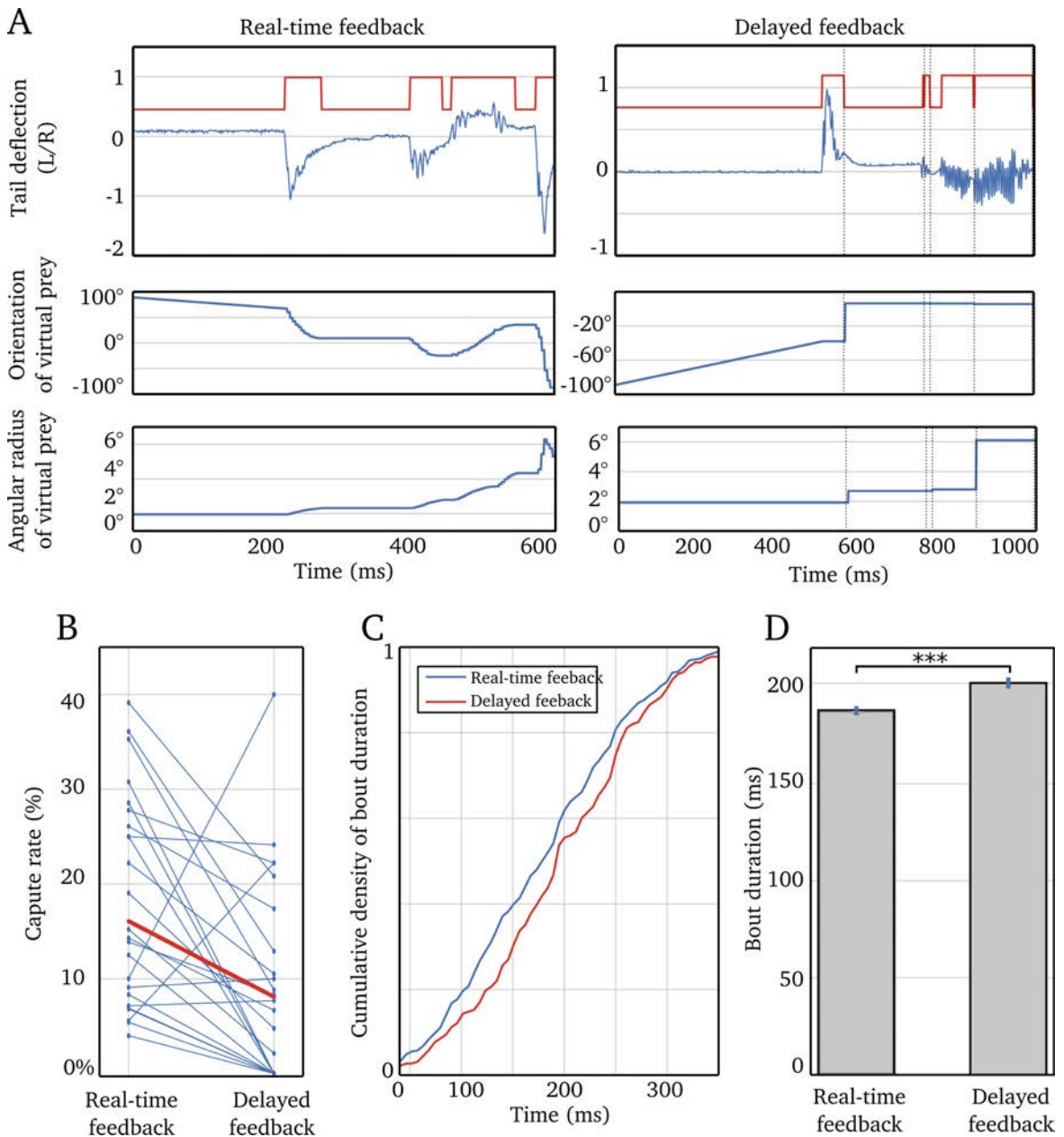


Fig. 2.6: **Alteration of visual feedback during movement.** (A) Tail deflection and corresponding visual feedback: angular position and size of the virtual prey. Left panel: the feedback are continuously updated during the tail movements (the red curve). Right panel: the feedback are delayed until the end of a bout (time indicated by the vertical dashed line). The red square-form curve indicate the detection of tail bouts. (B) Percentage of trials leading to a capture for all 27 larvae, in real-time (left) and delayed (right) feedback conditions. (C) Cumulative distribution for real-time (blue) and delayed (red) feedback. (D) Average bout duration with real-time and delayed feedback. The error bar indicate the s.e.m. A Mann-Whitney test was used to compare the distribution of bouts duration in both conditions ($p \approx 8.10^{-6}$).

Visual stimulation

A pico-projector (refresh rate of 60 Hz, P4x, Aaxa) was used for the visual stimulation projected on the diffusive screen ($N^{\circ}216$, White diffusion, Rosco Cinegel). For the OMR VR, the larva was immobilized at the center of a petri dish. Stimuli consisted of a square wave grating with a spatial period of 1cm at the maximal contrast projected on a screen placed 5mm below the larva. For prey-capture experiments, the larva was positioned on an elevated stage within a cylindrical chamber of 5 cm diameters. The cylinder was covered with a diffusive screen. Two projectors placed at 45° relative to the larva's head direction were used to project the visual environment. The position of the projector was chosen to minimize the deformation when projecting a checkerboard.

Autoregressive Model with External Input

The Autoregressive Model with External Input is a time-domain system identification model which has the following structure:

$$\sum_{k=0}^N a_k y(n-k) = \sum_{k=0}^N b_k x(n-k) + e(n)$$

In our case, y represent the output kinematic parameters (axial, lateral or yaw speed), x is the input tail deflection and e is the error. The choice $a_0 = 1$ ensures that the resulting system is causal. The vector of the unknown parameters we seek to identify is:

$$\Theta = [a_1, a_2, \dots, a_N, b_0, \dots, b_M]^T$$

We start by observing a system at rest. An input signal $x(n)$ is fed into the system, and the output $y(n)$ is observed for the interval $0 \leq n \leq K$.

$$\begin{aligned} y(0) &= b_0 x(0) + e(0) \\ y(1) &= b_0 x(1) + b_1 x(0) - a_1 y(0) + e(1) \\ &\vdots \\ y(n) &= \sum_{k=0}^N b_k x(n-k) - \sum_{k=1}^N a_k x(n-k) + e(n) \\ &\vdots \\ y(K) &= \sum_{k=0}^N b_k x(K-k) - \sum_{k=1}^N a_k x(K-k) + e(K) \end{aligned}$$

All these equations can be written as a large matrix equation:

$$D\Theta = Y - E$$

Avec:

$$D = \begin{bmatrix} 0 & 0 & \dots & 0 & x(0) & 0 & \dots & 0 \\ -y(0) & 0 & \dots & 0 & x(1) & x(0) & \dots & 0 \\ \vdots & \vdots & \vdots & \vdots & \vdots & \vdots & \vdots & \vdots \\ -y(n-1) & -y(n-2) & \dots & -y(n-N) & x(n) & x(n-1) & \dots & x(n-M) \\ \vdots & \vdots & \vdots & \vdots & \vdots & \vdots & \vdots & \vdots \\ -y(K-1) & -y(K-2) & \dots & -y(K-N) & x(K) & x(K-1) & \dots & x(K-M) \end{bmatrix}$$

$$Y = [y(0), y(1), \dots, y(n), \dots, y(K)]^T$$

$$E = [e(0), e(1), \dots, e(n), \dots, e(K)]^T$$

Thus, the solution for θ is obtained by a linear regression that minimize the norm of the error vector. For the lateral and yaw speed we chose $N = 7$, $M = 7$, the input x was the tail deflection. For the axial speed, because this kinematic parameter was mostly taking positive value, we used the absolute value of the tail deflection as the input x with $N = 20$ and $M = 7$. The parameters N and M were chosen to maximize the goodness of fit. The value obtain for the goodness of fit were $R_{Lateral}^2 = 0.67$, $R_{Axial}^2 = 0.79$ and $R_{Yaw}^2 = 0.72$.

Under carefully controlled experimental circumstances, an animal will behave as it damned well pleases.

The Harvard Law of Animal Behavior

Never send a human to do a machine's job.

Agent Smith (~ 2199). The Matrix

Chapter 3

Internally driven behavior in zebrafish larvae

3.1 Introduction

In natural conditions, internal decision processes will select the type of action to perform and the timing to execute it. From human daily tasks (e.g. e-mail communication) to animal foraging, the timing of internally driven actions follows complex temporal patterns at multiple time scale rather than being simply a uniform or rhythmic succession (Proekt et al. (2012), Goh and Barabási (2008), Sorribes et al. (2011)). Experiments on internally driven behaviors are usually structured along trials, in each trial the subject is free to choose the timing of a predefined action (for example poke out or press a button). The small set of actions available in these studies is not representative of the large repertoire of possible actions in unconstrained conditions. Moreover, the trial-structure of these experiments does not permit the study of the mechanisms responsible for the generation of complex temporal structures. Here, I aim at understanding the process governing the timing and selection of motor actions in absence of sensory stimuli.

Zebrafish is an ideal animal model to study internally-driven behaviors and the underlying mechanisms predicting them. In the absence of salient sensory cues, the zebrafish larva spontaneously produces tail movements. Their limited locomotor repertoire allows studying the natural action-selection process without imposing restrictions on the actions available. Moreover, their optical accessibility and small size is ideal for the study of how endogenous neuronal activity shapes behavior.

In the optic tectum of the zebrafish and, despite the absence of retinal drive, spontaneous activity is topographically organized in compact assemblies of functionally similar neurons showing all-or-nothing activations patterns (Romano et al., 2015). Using optic fiber to activate neurons in larva expressing Channelrhodopsin, Fajardo et al. (2013) showed that activation of neurons in the anterior-ventral optic tectum induced J-Turn tail bouts.

In the hindbrain, neurons involved in the control of swimming have been found to present spontaneous oscillation where bilaterally clustered neurons oscillate in opposition of phase with a typical period of ~ 20 s (Ahrens et al., 2013b). Optically evoked activity in larva expressing Channelrhodopsin in V2a neurons was sufficient to trigger tail movement (Kimura et al., 2013). Electrical activation of neuron in nMLF triggers tail movements with oscillation depending on the strength of the electrical stimulation (**Figure 1.7.B**, Severi et al. (2014)).

Despite these pathways from the midbrain and hindbrain to the spinal cord, several mechanisms could explain how spontaneous neuronal activity does not systematically trigger a movement. A first hypothesis would be that spontaneous activity lies below some spinal activation threshold in absence of movements. Another possibility could be that spontaneous activity is nullified by an inhibitory gate, as it was shown for the brainstem oculomotor system (Evinger et al., 1982). In zebrafish, activity in hypothalamic dopaminergic neurons can increase the excitability of Mauthner neurons in response to auditory stimuli (Mu et al., 2012). Projection of dopaminergic neurons from the caudal hypothalamus to the hindbrain could play a similar role in gating spontaneous behavior. Finally, a study of cortical activity in the primary motor cortex and dorsal premotor areas has revealed that, while the animal is not moving, motor cortical activity cancels out at the level of the population (Kaufman et al., 2014). In this case, distinct patterns of collective activity control the communication with the muscles and between brain areas.

In order to study the internal decision process underlying spontaneous locomotor actions, I first quantified the temporal and sequential dynamics of tail movement. In the second part, using Selective Plane Illumination Microscopy that enables monitoring neuronal activity from very large neuronal circuits from different brain regions, I recorded and analyzed neuronal activity prior to the onset of spontaneous movements.

3.2 Internally driven behaviors of zebrafish larva

In order to study the neuronal basis of internally driven behaviors, I first investigated the organization of spontaneous behavior. After quantifying their kinematics, I developed a method for classifying tail movements. This allowed me to study the chaining of events during spontaneous behavior.

For this purpose, the behavior of 25 head-restrained larvae was monitored for a period of 4h. During the first hour, visual stimulations consisting of whole-field motion or dark flashes were presented in order to observe visually induced behavior. For the last 3h, a homogeneous non-patterned illumination was projected below the larva (**Figure 3.1**). This experiment enabled me to collect 16000 individual bout movements.

3.2.1 Locomotor repertoire of zebrafish larva

I developed an automatic method to quantify the locomotor repertoire of head-restrained zebrafish larva, which allowed me to study the temporal structure of internally driven locomotor action.

Quantification of tail movements

Quantifying locomotor action requires choosing an appropriate level for the movement's description, between the most detailed analysis of muscle activations to the simple binary detection of movements. In order to quantify the variety of spontaneously generated movements, I needed to estimate how similar or different two movements were. To that end, I computed both the curvature along the tail and the deflection index. The method to compute the deflection index is presented in **Figure 2.2**. In order to compute the curvature, I adapted the technique presented in Huang et al. (2013). To find the "skeleton" of the larva's body, I calculated the barycenter of the larva's image along a circle weighted by the pixel's intensity. The first circle was centered to a position between the eyes. By iteration, the skeleton of the fish was obtained (**Figure 3.2.A**). A cubic spline was fitted along the skeleton and the curvature was computed along this curve. Both techniques were implemented in real time in C++ in order to reduce the amount of post-processing analysis.

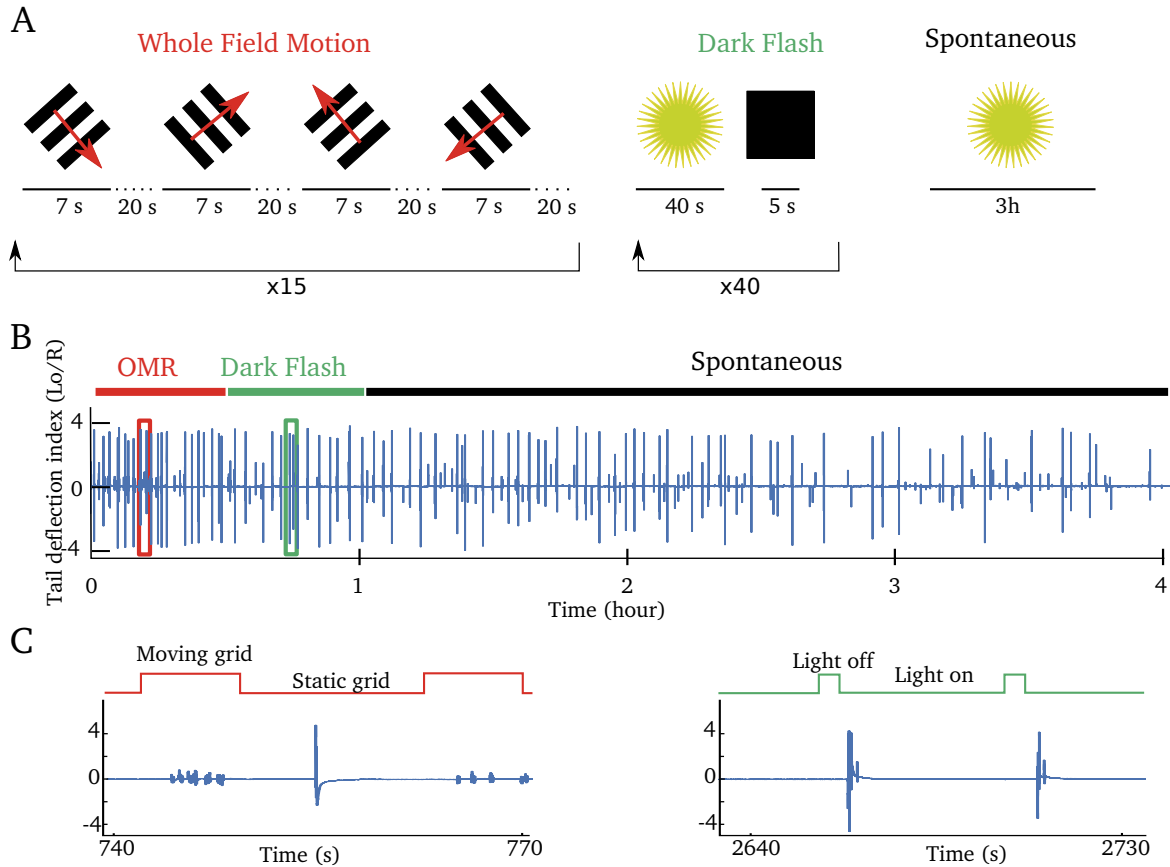


Fig. 3.1: **Visually induced and spontaneous tail deflections.** (A) The experimental paradigm showing periods of visual stimulation and absence of stimulation. Visual stimuli were presented below the larva during the first hour. The first stimuli consisted of 15 repetitions of whole-field motion at -45° , $+45^\circ$, 135° and 225° angles relative to the head axis. Dark flash stimuli consisted of a sudden change in the background illumination from brightness to darkness, it was repeated 40 times. Then the visual background was left constant for 3h. (B) Example of tail deflection recorded during the experiment for one larva. The tail was active in both spontaneous and induced conditions. (C) Left panel: zoom in the red rectangle of (B). Right panel: zoom in the green rectangle of (B) during the transition from "light off" to "light on". Amplitude of the tail deflection were different for both stimuli.

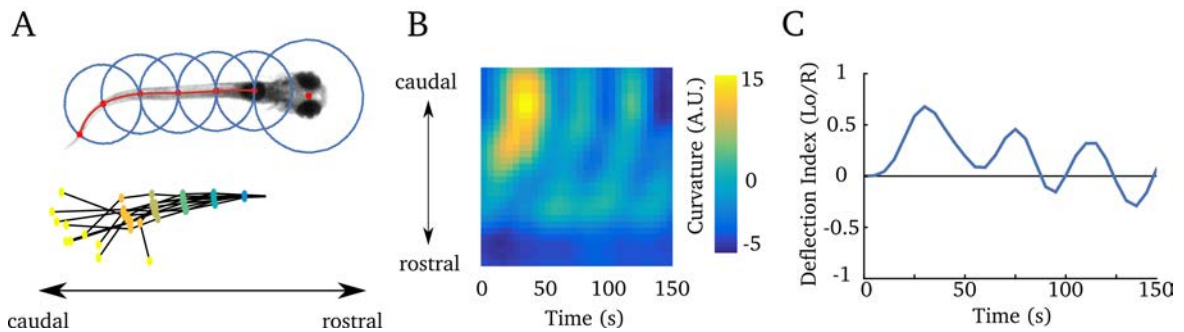


Fig. 3.2: **Quantification of tail bouts.** (A) Upper panel: A larva is overlaid on the circles used to compute the skeleton of the larva's body. The first center was placed between the two eyes. Successive centers were computed as a barycenter of pixel intensity on the successive circles. Lower panel: example of the positions of the skeleton during a tail bout. Each skeleton represents a different time point during a bout. The color dots represent the center of the circles in (A). (B) Evolution of the tail curvature during a bout. At each time point, the curvature was computed according to a cubic spline fitted along the skeleton. (C) Deflection index along time. The same tail bout was used for the 3 panels.

Similarity between tail movements

Using the curvature and deflection index, I established a measure of similarity between movements. A similarity measure was necessary to find categories of movements. I benchmarked two alternative measures: feature and distance based similarity.

The feature-based description of a tail movement added heterogeneous measurements: tail bending, amplitude and change in orientation. In head-fixed larva, the features can only use the time series of the tail curvature. Each bout was described by a high-dimensional vector of these features. Its dimensionality was then reduced using principal component analysis (see Supplementary methods for details and **Figure 3.3.A**).

The distance-based approach uses Dynamic Time Warping (DTW) to compare the time series of tail deflection. DTW is a similarity measure between time series that is robust to small deformation of the time series. In contrast, with euclidean distance, the main advantages of DTW is that it recognized similar shapes, even when the time series present signal transformation such as shifting or scaling (see Supplementary methods for details and **Figure 3.3.A**).

Figure 3.3.B shows the nearest neighbors using both methods for three reference tail bouts. Despite the fact that the DTW neighbors were computed using the deflection index alone, it was sufficient to recover neighbors that shared similar curvatures. The distance obtained from features of the curvature and the similarity based on DTW of the deflection index had a correlation of 0.77. Thus, I chose to use DTW to measure similarity because it is more direct and does not rely on an arbitrary choice of the different bout's features. I then performed cluster analysis in order to define different movement categories.

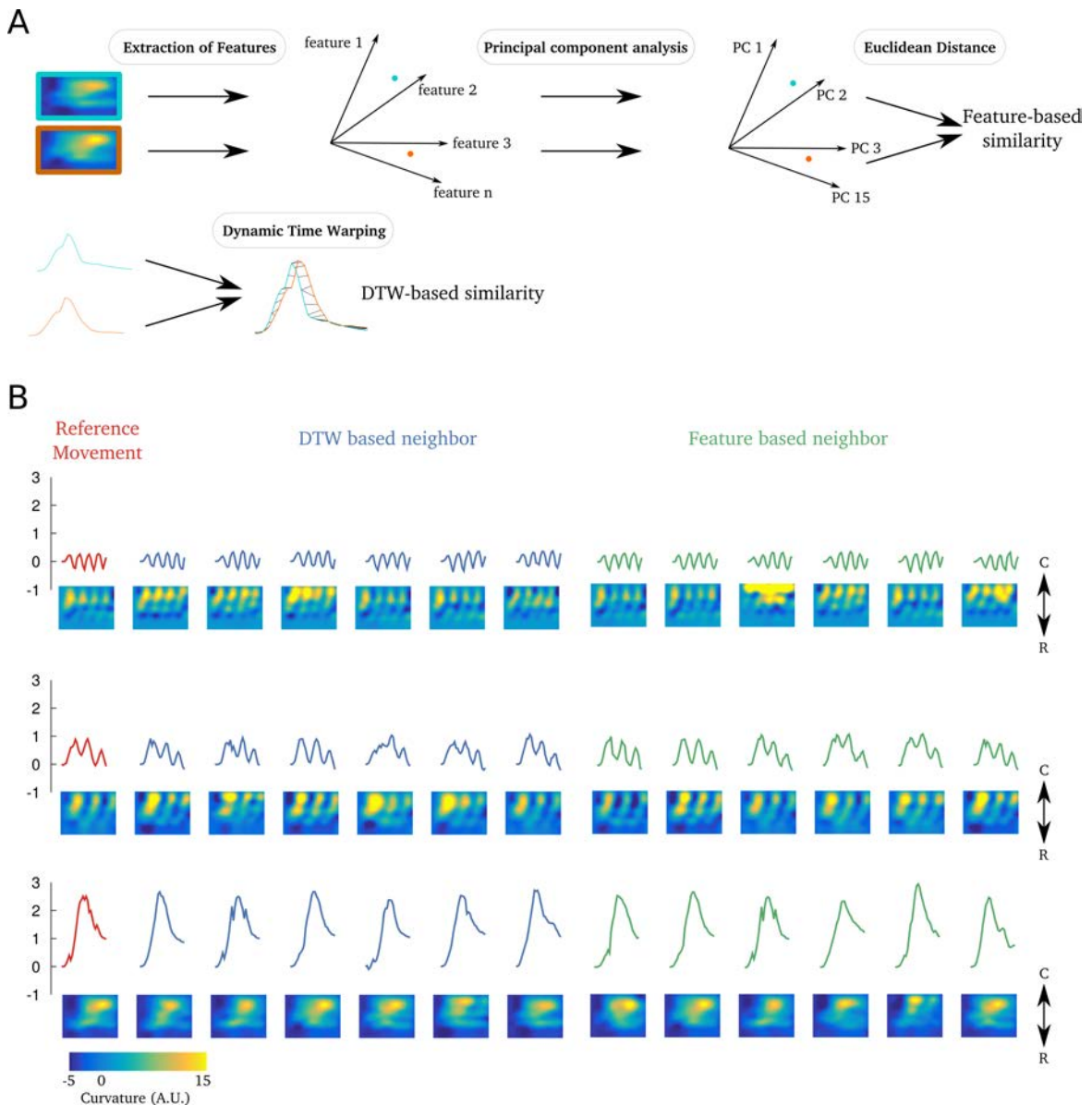


Fig. 3.3: Comparison of Feature and DTW-based similarity measurements. (A) Scheme of the procedure used to compute the feature and DTW similarity measurements. Upper panel: feature vectors were extracted from the curvature matrix using the procedure described in Supp Methods, after a projection of the feature vectors on the 15 principal components with the highest variance. The euclidean distance in the principal components' subspace was finally computed. Lower panel: the dynamic time warping was computed from the deflection index of the tail using the algorithm described in Supplementary methods. (B) Each rows shows the nearest neighbor of three reference movements (in red) computed using features-based distance (in blue) and DTW similarity (in green). In each row, individual tail bouts were represented using the tail deflection index and the corresponding tail curvature (below). Arrows indicate the caudo-rostral axis. The colorbar is common to all curvatures.

Classification of tail movements

The goal of clusterization is to find groups of movements that are more similar with each other than to those in other groups. Each tail deflection index was duplicated to its opposite in order to obtain a symmetric library of movements. **Figure 3.4.B** shows the t-distributed stochastic neighbor embedding (t-SNE) of all tail movements recorded. This method embedded high-dimensional data into a two dimensional representation where each point corresponds to a tail movement (see Supplementary Methods for details). The axis in the t-SNE embedding should not be interpreted, but the local distances between points in 2D reflect the similarity between the movements that they represent. Thus, neighboring points correspond to similar tail movements.

This visualization did not reveal clearly isolated groups of points or density local maxima, but rather a continuum between tail movements (**Figure 3.4.B,C**). Unsupervised classification methods, such as k-mean or density based clustering (Rodriguez and Laio, 2014) isolated a cluster formed by forward scoot, but failed to find the other categories of movement. Therefore, I used supervised clustering to define categories.

Supervised techniques infer the category of a movement using a set of manually labeled movements (Keller et al., 1985). I chose 8 categories: scoot (symmetric), asymmetric scoot (positive or negative), routine turn (positive or negative), C bend (positive or negative) and burst (symmetric). J turns (**Table 1.2**) were associated with asymmetric scoots or routine turns depending on their amplitude. Escapes were grouped along with bursts.

In order to account for the continuity between categories, I used a soft-clustering algorithm: the fuzzy K-nearest neighbor (see Supplementary Methods for details). Using soft-clustering, a movement can belong to more than one cluster, thus it is defined according to a set of membership levels. For each movement, the membership level associated with a category can be interpreted as the probability that the movement belongs to this category. The category of a movement was attributed according to the highest membership value.

This method resulted in an accuracy in classification of the movements of 82% estimated using cross-validation. Cross-validation consisted in iteratively removing the manually labeled tail bouts of one larva (the test set) and comparing its label to the label inferred from the remaining library of tail bouts (the training set). **Figure 3.5.A** shows the misclassification matrix, errors in classification occurred mostly between neighboring clusters, e.g. scoot movements were unlikely to be classified as a

burst. Moreover, the maximal value of the membership was lower for misclassified movements than for well classified ones (**Figure 3.5.B**). Thus, errors in classification occurred mostly when there was an ambiguity between the membership levels. I then colored movements in the t-SNE according to their membership, the geometry of the 2D embedding was nicely represented by the membership (**Figure 3.5.C**). It should be noted that the representation obtained by t-SNE was not used for the classification but only for visualization purpose. The classification relied only on the distance matrix obtained using DTW (**Figure 3.4.A**).

I used cluster analysis in order to get a parsimonious description of locomotor actions. The categories chosen are known to represent the action of distinct group of neurons or different behavioral context (see **1.4.2**). In contrast with previous studies (Mirat et al. (2013), Budick and O'Malley (2000)), this method does not rely on the trajectory of the larva and can therefore be applied to study movements performed in conditions compatible with brain imaging.

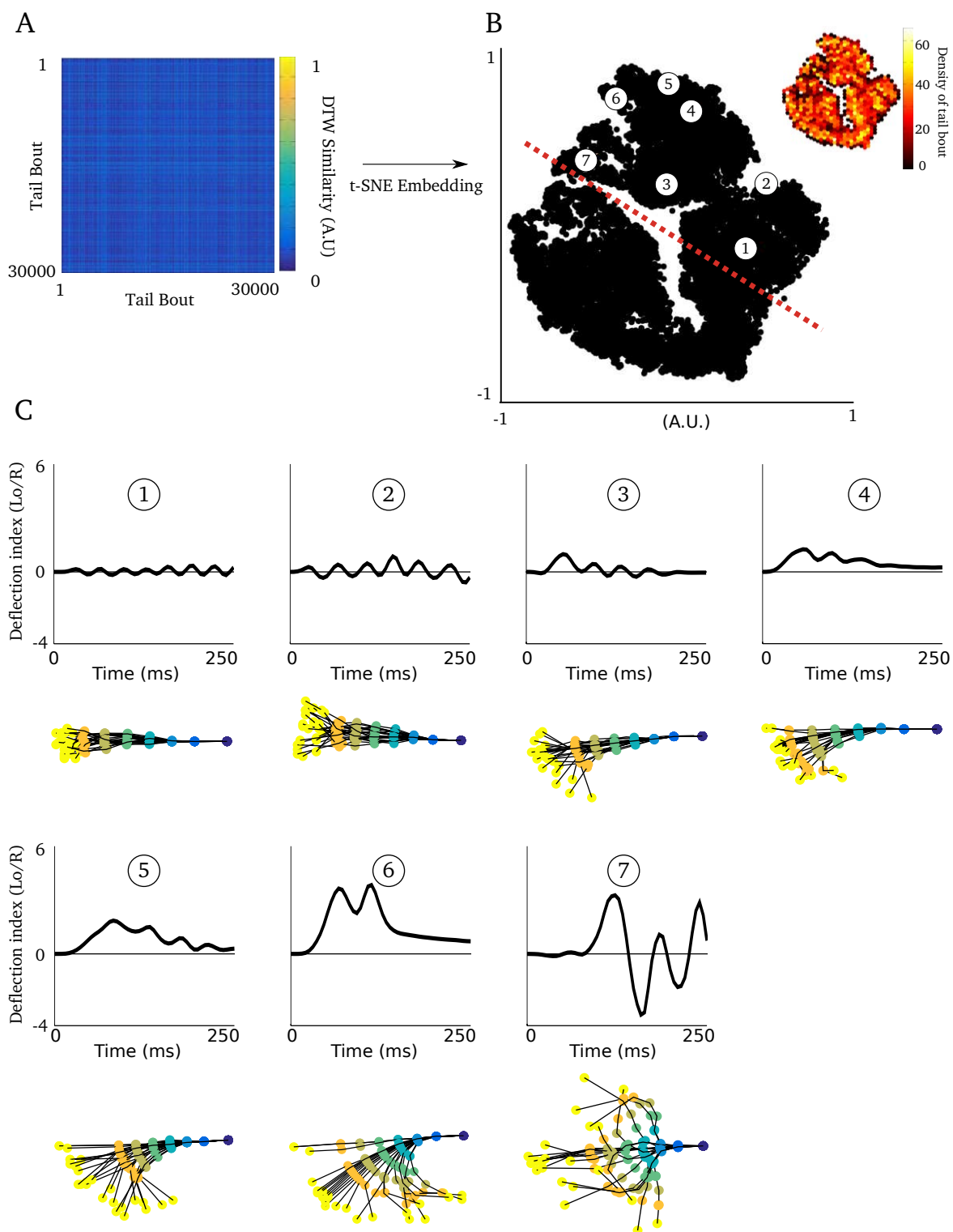


Fig. 3.4: Continuum of tail kinematics, legend next page

Fig. 3.4: (Previous page.) **(A)** Distance matrix computed on the library of evoked and spontaneous tail bouts. **(B)** t-SNE embedding of the distance matrix. Each dot represents a tail movement. The red dashed line indicates the approximate position of the axis corresponding to the symmetry between movements with opposite tail deflection indexes. Inset shows the density computed in hexagonal bins. Note that the density is homogeneous along all regions of the graph, suggesting that in head-restrained conditions, the repertoire of the larva's tail movements can not be classified in discrete movement types, but is rather follows a continuum. **(C)** Illustration of the continuum between tail movements for a selection of 7 different tail bouts, a symmetric version could be found in the other side of the dashed axis. The deflection index (top) as well as the corresponding skeleton (bottom) are displayed. The position of the tail bouts in the t-SNE embedding is shown by an indexed circle.

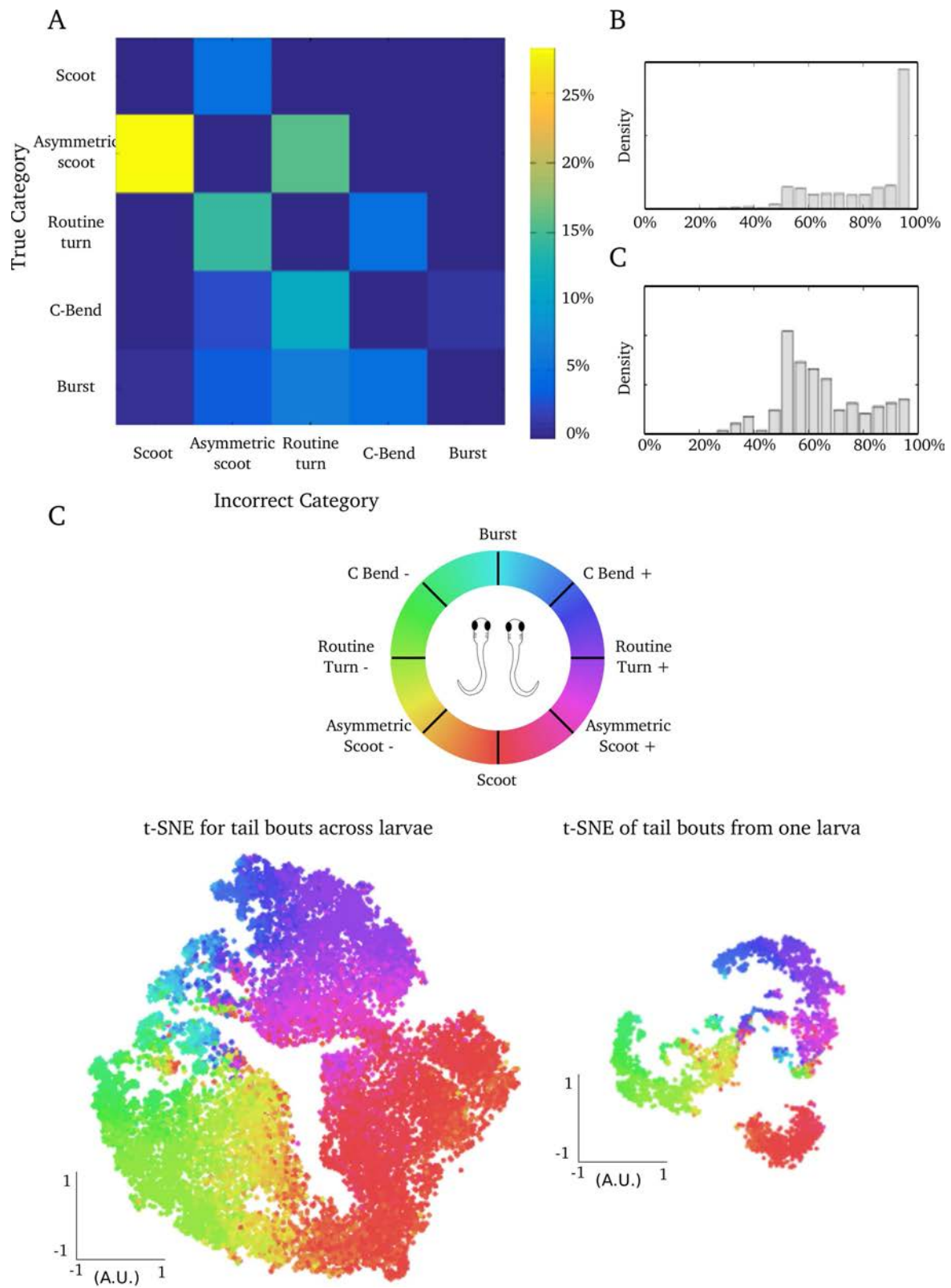


Fig. 3.5: Classification of tail bouts., legend next page

Fig. 3.5: (Previous page.) **(A)** The misclassification matrix is a contingency table of the error in classification obtained during cross-validation. Rows represent the true category (defined by user) and columns represent the categories that were erroneously attributed during cross-validation. High values are centered around the diagonal indicating that error occurred primarily between neighboring categories, especially between scoots and asymmetric scoots. **(B)** Upper panel: Distribution of the maximum level of membership for movements in the test set. Lower panel: Distribution of the maximum level of membership for movements in the test set that were misclassified. Errors in classification were associated with more uniform level of membership suggesting ambiguity. **(C)** Movements in the t-SNE embedding graph were color-coded according to their membership to the different categories. Each of the 8 category of movements was associated with an angle (top). For each movement, the average angle weighted by its membership values was computed and associated with the hue of its color (shown in the circular HSV colormap). The convention for the laterality is indicated by the larva's scheme corresponding to positive or negative deflection indexes. Bottom left: t-SNE computed from the entire library of tail bouts. Bottom right: t-SNE computed for only one larva. The axis in both embedding graphs were different but displayed similar structures.

Distribution of movements according to evoked or spontaneous conditions

In order to confirm that the choice of categories was relevant to study the behavioral repertoire, I analyzed how stimulus biased the distribution of movements across categories (**Figure 3.6**). Compared to spontaneous movements, whole-field motion in the caudo-rostral direction induced a large majority of scoot movements. In comparison, the proportion of scoot movements was smaller when the grid moved in the rostro-caudal direction. Finally, dark flashes induced a proportion of C bends 2.5 times higher than during spontaneous behaviors, consistent with previous reports (Burgess and Granato, 2007).

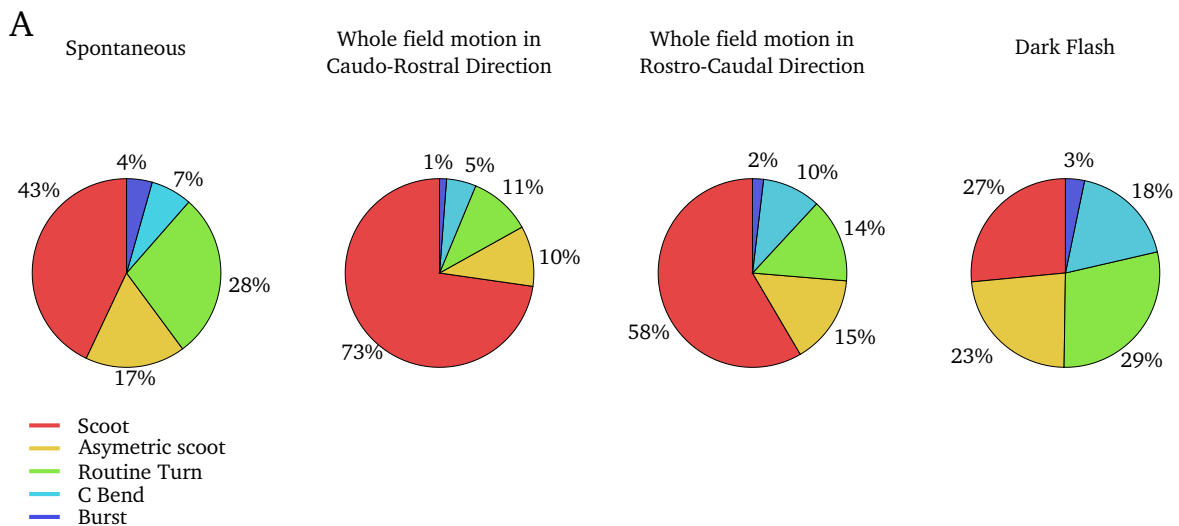


Fig. 3.6: Distribution of movements in induced and spontaneous conditions. Each column shows a pie chart of the distribution between categories of movements in spontaneous or sensory evoked conditions.

3.2.2 Chaining of spontaneous motor actions

When to act? Bursts and heavy-tail temporal dynamics

In the case of a regular process where the probability of occurrence of an event is constant across time and events occur independently from each other, a Poisson process parametrized by a single value describe the uniform probability of having an event during a given time interval. In this case, the probability distribution of the waiting time between one event and the next follows an exponential distribution. I performed a detailed analysis of the temporal distribution of spontaneous tail movements. These distributions showed that rather than regular, the timing of events was

non-homogeneous. I observed two deviations from a homogeneous Poisson process: a heavy-tail distribution and a bias for increased activity after an event.

Figure 3.7.A displays the distribution of inter-bout intervals (IBI). The IBI is the time different between the offset of a tail movement and the onset of the next movement. The distribution showed a clear deviation from Poissonian behavior (**Figure 3.7.B**). For long IBI, the distribution appeared to follow a Weibull distribution. The Weibull distribution corresponds to a stretched exponential distribution whose expression is:

$$P(\tau) = \frac{u}{\tau_0} \left(\frac{\tau}{\tau_0}\right)^{u-1} \exp\left(-\left(\frac{\tau}{\tau_0}\right)^u\right)$$

Two parameters characterize the Weibull distribution, the scale τ_0 and the shape u . The scale parametrizes the characteristic decay time. The shape parameter describes the degree of burstiness. Poissonian processes have a shape value $u = 1$. $u < 1$ is a hallmark of heavy-tail distributions. For each larva, the IBI distribution was correctly fitted by a Weibull distribution (Goodness of fit $R^2=0.8$ (mean) ± 0.2 (s.d)). All larva displayed a heavy-tail distribution with $u=0.53$ (mean) ± 0.12 (s.d).

In order to study the occurrence of tail movements over short IBI, I computed the hazard rate:

$$h(t) = \lim_{dt \rightarrow 0} \frac{\mathbb{P}(t < IBI < t + dt | IBI < t)}{dt} = \frac{\mathbb{P}(t < IBI < t + dt)}{dt \cdot \mathbb{P}(IBI < t)}$$

The hazard or failure rate is commonly used in demography or risk analysis, it gives a natural way to interpret the chance of occurrence of an event. For exponentially distributed waiting time in an homogeneous Poisson process, the failure rate is constant. For a Weibull distribution, the hazard rate is a monotonic function:

$$h(t) = \frac{u}{\tau_0} \left(\frac{t}{\tau_0}\right)^{u-1}$$

Figure 3.6.C displays the hazard rate computed for the IBI which shows a peak around 3s. The location of the peak was 2.95s (mean) ± 1.91 s (s.d). However, 10% of the larvae did not display a local maximum in the hazard function. The maximum near zero indicates a bias for IBI of a few seconds.

The temporal dynamics of spontaneous tail movements displayed a bimodal divergence from a homogeneous Poisson process: a heavy-tail regime with long periods of inactivity and a rhythmic succession between movements at short time intervals. This burstiness could be induced by different underlying processes. For example, it

could represent a model that combines multiple Poissonian processes with different timescales or interactions induced by intrinsic correlations between successive IBI. In order to test whether successive intervals of time were correlated, I computed the autocorrelation of the IBI. The autocorrelation decayed rapidly and did not exhibit any significant oscillatory behavior. A simple measure of the memory was shown by the correlation coefficient of successive IBI time values. I measured a correlation of 0.044 (mean) ± 0.153 (s.d). Thus, successive IBIs were, to a large degree, independent. To further describe internally driven behaviors, I characterized the influence of the categories of movement on the chaining between events.

What to do? Memory in the chaining of locomotor actions

The distribution of movements was highly biased, scoot and asymmetric scoots accounted for 60% of the movements, routine turns represented 28% and C bends and bursts accounted for 14% (**Figure 3.8.A**). Individual larvae showed different biases toward movements of either large or small amplitude (the s.d of the percentage of scoot across larva was $\sim 20\%$). The low percentage of bursts and C bends indicated that, on average, larvae were not trying to escape from agarose but rather generated spontaneous natural-like tail movements. **Figure 3.8.B** shows the chaining between consecutive movements according to their category for one larva. The similarity between consecutive movements as a function of the IBI is shown in **Figure 3.8.D,E**. Consecutive movements were more likely to be similar if the IBI was shorter than ~ 10 s (**Figure 3.8.E**). Similarly, **Figure 3.8.D** shows that consecutive movements were more likely to have a similar laterality if they were chained within less than 10s than for longer IBIs ($p=0.93 \cdot 10^{-3}$ using a Mann-Whitney test). The effect of chaining was not uniform across categories (**Figure 3.8.E**), short IBIs were more likely to result in small movements (scoots or asymmetric scoots) than large movements (routine turns, C bends or bursts).

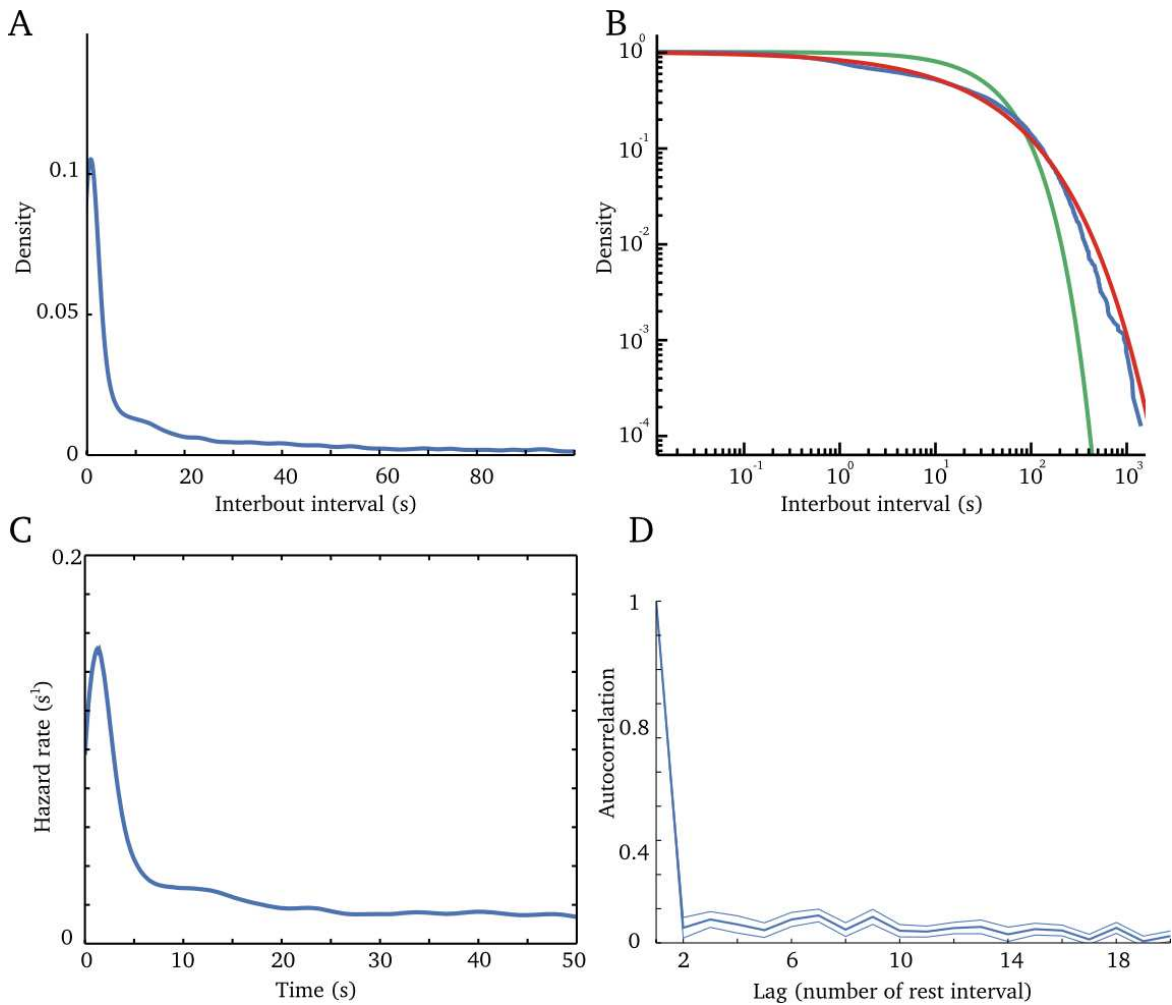


Fig. 3.7: **Temporal chaining of tail movements.** (A) Distribution of IBI pooled across larvae. (B) Same distribution as (A) in log-log scale (blue). Green curves shows the exponential fit of the IBI that follows a Poissonian process. The red curve shows the Weibull fit of the IBI. (C) Hazard rate of IBI pooled across larvae as a function of time. It would be constant for a Poissonian process and monotonically increasing or decreasing for a Weibull distribution. (D) Autocorrelation of IBI (\pm s.e.m.). The rapid decay indicates the independence of successive resting times.

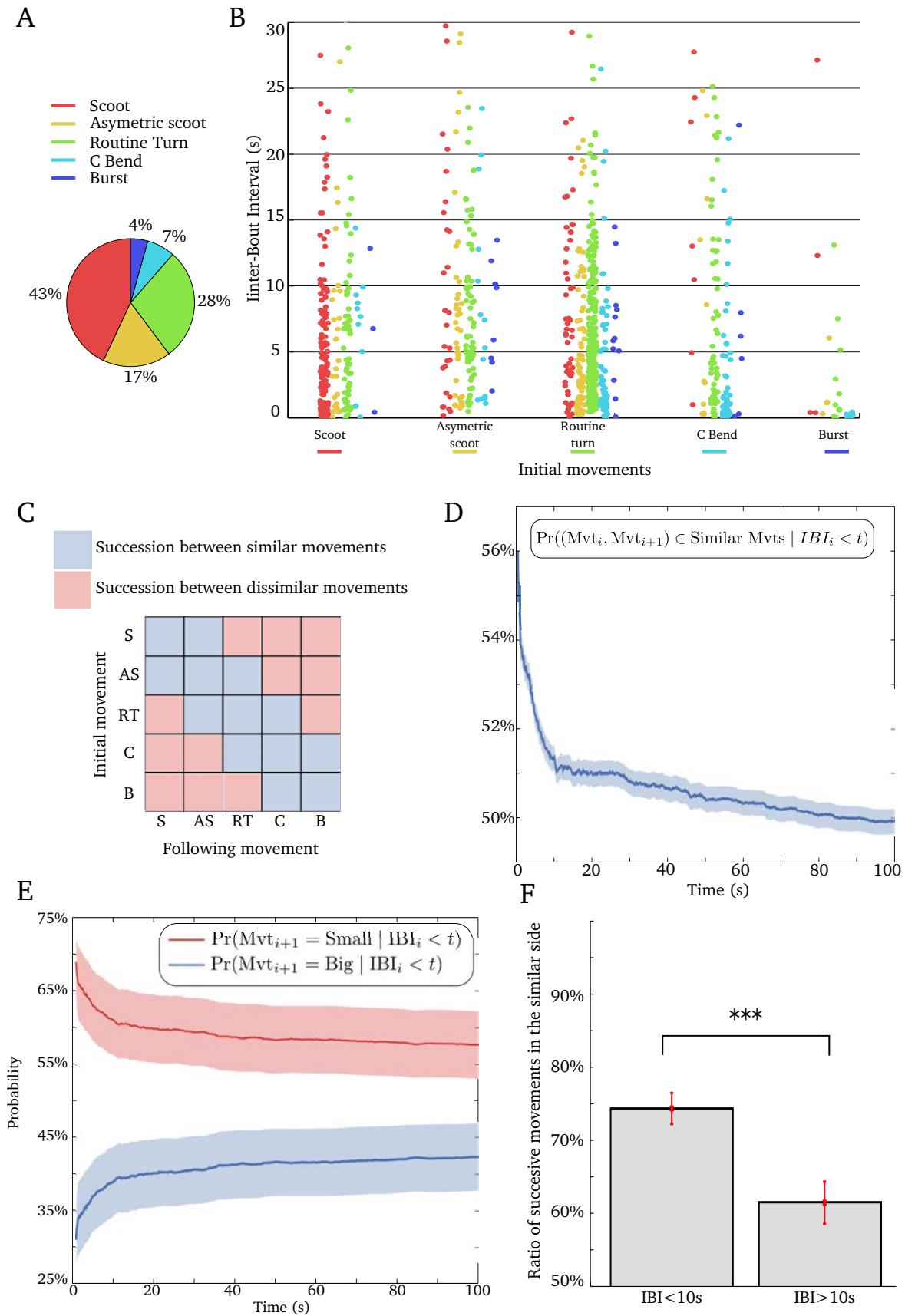


Fig. 3.8: Memory in the chaining of movements, legend next page

Fig. 3.8: (Previous page.) **(A)** Percentage of the different categories of movements during spontaneous behavior. **(B)** Chaining of movements for one larva. Each of the five columns represent an initial movement, each sub-column corresponds to the category of the following movement. For example, cyan points in the first column represent transitions from scoots to C bends. The vertical position of a point represents the IBI between the initial movement and the following. A random jitter was added in the horizontal direction for visualization purpose. Successive movements were likely to belong to similar categories. **(C)** Matrix indicating what was defined as a transition between similar or dissimilar movements. **(D)** The graph represents the probability that a transition occurred between similar movements knowing that the IBI was shorter than a given value (more formally the equation on top). It displayed a decay during the first 10s. Shadings indicates the s.e.m. **(E)** Small movements represent scoots and asymmetric scoots. Large tail deflection movements involve routine turns, C bends and bursts. The ratio of small movements (red curve) over large ones (blue curve) was higher for short IBIs. The shading indicates the s.e.m. **(F)** For IBIs shorter than 10s, the movements have a 74% chance to be toward similar directions. For IBIs longer than 10s, this ratio was 61%. This probability was not 50% because larvae often displayed a bias towards one direction. The error bars correspond to the s.e.m.

3.2.3 Supplementary Methods

Feature Extraction

To compute the feature of the curvature matrix of a tail bout, I concatenated features from the time series of the curvature along the tail's length. Each time series represented the curvature at a specific location of the tail, I computed statistical moments up to the 4th order, maximum, minimum, number of peaks, number of zero crossing and Fourier coefficients. After this, a PCA was applied and only the subspace corresponding to the 15 largest components was kept.

Dynamic Time Warping

The DTW algorithm has earned its popularity by being an efficient similarity measurement for time series in areas such as data mining (Keogh and Pazzani, 2000), gesture recognition (Gavrila et al., 1995) or speech processing (Juang and Rabiner, 1993). DTW reduces the distance between the time series by warping the time axis. Given two tail bouts for which the tail deflection index were $X = (x_1, x_2, \dots, x_N)$ and $Y = (y_1, y_2, \dots, y_N)$ with $N = 30$ corresponding to a bout duration $T=150\text{ms}$ and a sampling frequency $F_s=200\text{ Hz}$. DTW yield an optimal solution in $O(N^2)$ time.

The algorithm starts by building the distance matrix $C \in \mathbb{R}^{N \times N}$ representing all pairwise distances between X and Y (**Figure 3.9.A**). Once the cost matrix is built, the algorithm aims at finding the lowest energy path in the matrix (**Figure 3.9.A**). The alignment path built by DTW was a sequence of points $p = (p_1, p_2, \dots, p_K)$ with $p_l = (n_i, m_j) \in [1 : N]^2$ for $l \in [1 : K]$ which satisfied the following criteria:

- Boundary condition: $p_1 = (1, 1)$ and $p_K = (N, N)$. The starting and ending points of the path must be the first and last points of the sequences.
- Monotonicity condition: $n_1 < n_2 < \dots < n_K$ and $m_1 < m_2 < \dots < m_K$. This condition preserves the time-ordering of the points.
- Step-size condition: $p_{l+1} - p_l \in \{(1, 1), (1, 0), (0, 1)\}$. This criteria limits the shifts in time from large jumps.

DTW uses dynamic programming to find the path of minimal cost p^* :

$$DTW(X_{1:N}, Y_{1:N}) = C_p^*(X, Y) = \min(C_p(X, Y) | p \text{ is a warping path})$$

The optimal path p^* is computed in reverse order of the index, starting with $p_L = (N, N)$. Supposing that $p_l = (n, m)$ has been computed. In the case where $(n, m) = (1, 1)$, one must have $l = 1$ and the algorithm is complete. Otherwise,

$$p_{l-1} = \begin{cases} (1, m-1) & \text{if } n = 1 \\ (n-1, 1) & \text{if } m = 1 \\ \operatorname{argmin}\{DTW(X_{1:n-1}, Y_{1:m-1}), DTW(X_{1:n-1}, Y_{1:m}), DTW(X_{1:n}, Y_{1:m-1})\} & \text{otherwise} \end{cases}$$

It should be noted that DTW is a similarity measure or a pseudo-metric. Unlike the euclidean distance, it does not verify triangular inequality required for metric.

Fuzzy k-nearest neighbor classification (FKNN):

The k-nearest neighbor is the simplest non-parametric classification method (Derrac et al., 2014). A class is assigned according to the most common class among its k-nearest neighbors. In FKNN, a membership level u_i is assigned to a tail movement x using the following formulation:

$$u_i(x) = \frac{\sum_{j=1}^k \frac{u_{ij}}{D(x, x_j)^4}}{\sum_{j=1}^k \frac{1}{D(x, x_j)^4}}$$

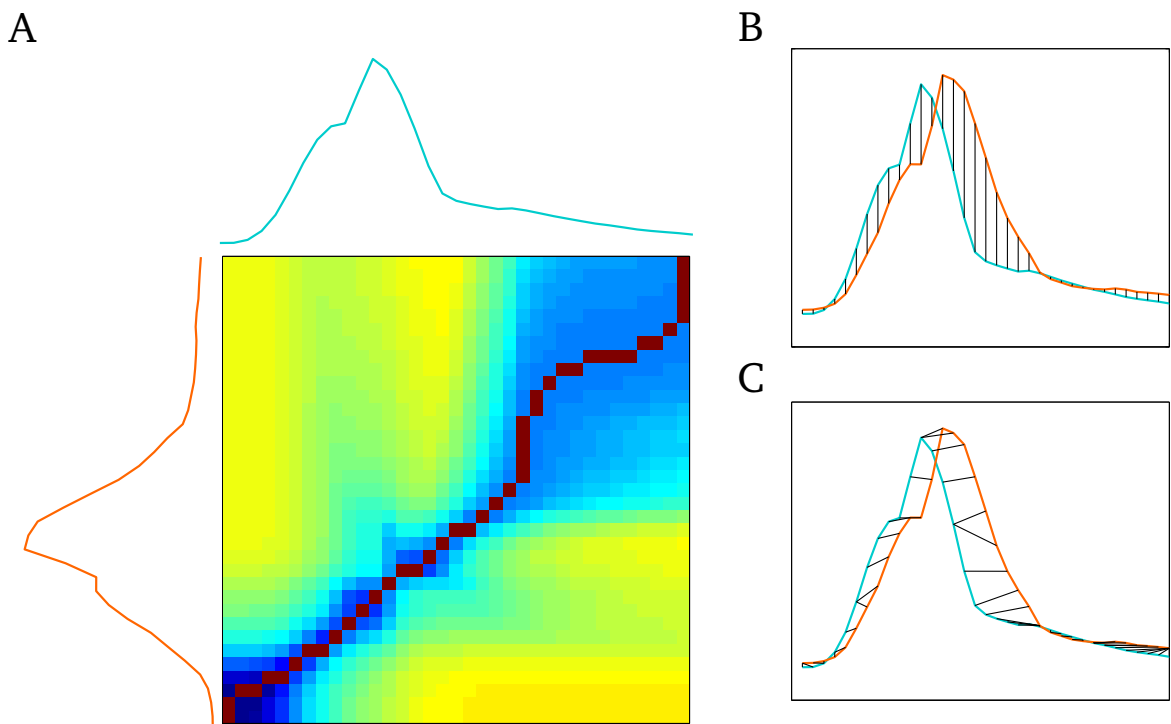


Fig. 3.9: **Alignment of tail deflection using DTW.** (A) Cost matrix for the time series of two tail deflection indexes in cyan and orange. The optimal alignment path is shown in red. (B) An example of measurement of the euclidean distance for the two time series of tail deflection in (A). The comparison point by point is unable to recover the similarity between the two time series because of the small temporal offset. (C) Optimal time alignment of the two sequences is shown in black.

where $i = 1, 2, \dots, 5$ corresponds respectively to the category : Scoot, Asymmetric Scoot, Routine Turn, C Bend, Burst. x_j are the tail bouts in the library of user-defined labeled tail bouts (containing ~ 800 tail bouts). The distance D is the DTW distance. The factor 4 is used to weight the similarities and was found to minimize the error in classification. We only consider the $K = 10$ first neighbors. The u_{ij} terms represent the membership degree of the movement x_j from the training set to the class i . They are defined as:

$$u_{ij}(x_k) = \begin{cases} 0.51 + \frac{n_j}{K} \cdot 0.49 & \text{if } i = j \\ \frac{n_j}{K} \cdot 0.49 & \text{if } j \neq i \end{cases}$$

The value n_j is the number of neighbors which belong to the j -th class. Thus even tail movements that were manually labeled have a fuzzy membership to account for error during the manual labeling. Note that the sum of memberships u_i is equal to 1 making the interpretation as a probability straightforward. The direction (or bias) of movements belonging to asymmetric categories : Asymmetric Scoot, Routine Turn and C Bend was defined by the sign of $\sum_{t=1}^N x(t)^3$.

t-Distributed Stochastic Neighbor Embedding

Dimensionality reduction techniques such as PCA, multi-dimensional scaling or Isomap minimize the deformation of large distances (Cox and Cox (2000), Roweis and Saul (2000)). Similarity measurements such as DTW are more relevant at the level of the local neighborhood. I chose t-SNE for visualization because it aims at minimizing local distortions (Van der Maaten and Hinton, 2008). For t-SNE, the conserved invariants are related to the Markov transition probabilities of a random walk performed on the dataset. Specifically, it defines the probability of transition from a tail movement x_i to another x_j , $p_{j|i}$, to be proportional to a Gaussian kernel of the distance between them:

$$\begin{cases} p_{j|i} = \frac{\exp(-d(x_i, x_j)^2/(2\sigma_i^2))}{\sum_{k \neq i} \exp(-d(x_i, x_k)^2/(2\sigma_i^2))} \\ p_{i|i} = 0 \end{cases}$$

Each σ_i is set such that all points have the same transition entropy : $H_i = \sum_j p_{j|i} \log p_{j|i} = 5$. This parameter can be interpreted as controlling the number of neighbors considered, similar to K in the FKNN. Then, t-SNE places the points in the 2D euclidean space where the transition probabilities $q_{j|i}$ are as similar to $p_{j|i}$ as possible. $q_{j|i}$ is chosen, for technical reason, to be proportional to a Cauchy (or Student-t) kernel of

the distance between points in the 2D space. This algorithm results in an embedding that minimizes local distortions. $p_{j|i}$ with small values corresponding to dissimilar tail movements will impose little constraints on the embedding. The complexity of the method in $O(N^2)$ restricts its applications to datasets that contain no more 10 000 points. I used the Matlab implementation provided by the authors of the algorithm.

3.3 Neuronal patterns predictive of spontaneous behaviors

3.3.1 Methods

Understanding the neuronal mechanisms underlying internally driven behaviors requires recording the neuronal activity preceding many spontaneous movements. In the absence of external stimuli, a larva produces on average 80 tail bouts per hour. Therefore, I needed to monitor behavior and neuronal activity over long periods of time. Moreover, to study the involvement of different brain circuits in the generation of internal decision, it was necessary to monitor spontaneously dynamics of large neuronal circuits from different brain regions. For this reason, I used Selective Plane Microscopy (SPIM) in combination with transgenic zebrafish larvae expressing pan-neuronally the genetically encoded calcium indicator GCaMP5, to record neuronal activity. I performed preliminary experiments in the *Laboratoire Jean Perrin*. I later built a custom SPIM in my laboratory and performed additional experiments. The methods and preliminary results described in this thesis concern the latter.

Recording neuronal activity using SPIM

SPIM possess several advantages over point scanning microscopy techniques (Panier et al. (2013), Ahrens et al. (2013b)). The low numerical aperture (NA) of the excitation beam causes less photodamage than for typical high-NA beams used in point-scanning microscopy. Moreover, SPIM records signal simultaneously from different points. Thus, collecting the same signal requires a weaker laser power used than for point-scanning microscopy. This allowed me to record neuronal activity for up to 6h with little phototoxicity (**Figure 3.12.A**). Additionally, SPIM gives the ability to record from all cells in the same brain section without decreasing the temporal sampling. Unlike two-photon microscopy, I used a visible blue laser (488nm) to probe the calcium sensor, this blue light could modulate the decision making but this modulation would be constant during the experiment and thus would not provide salient sensory cues. SPIM is subject to a trade-off between temporal and spatial sampling. Brain-wide imaging can only be obtained at low sampling frequency (0.5 Hz for a $200\mu m$ vertical stack). In order to study the temporal dynamics of the neuronal activity prior to spontaneous movement, I chose to record from a single coronal section of the brain at 10Hz. The methods presented could be easily extended to a larger number of plane.

Zebrafish larva

I used larva with genetically encoded calcium indicator GCaMP5G (Akerboom et al., 2012) under the control of the pan-neuronal HuC promoter. This transgenic line was developed by Jonathan Boulanger-Weill, a PhD student in the lab. Embryos husbandry was similar to the VR experiments. All experiments were approved by *Le Comité d'Éthique pour l'Expérimentation Animal Charles Darwin (Ce5/2009/027)*.

Selective plane illumination microscopy

I built a custom SPIM which allows monitoring simultaneously neuronal activity at cellular resolution across the brain (**Figure 3.10**). For this purpose, the larva were placed dorsal-side up, head-fixed in agarose. Once solidified, the agarose around the tail was removed, letting it free to move. Visual stimuli were projected on a screen placed below the recording chamber, a small hole in the screen allowed imaging of the locomotor activity of the larva.

Processing of the acquired fluorescence images

16-bits images were acquired with the Hamamatsu Orca Flash 4.0 sCMOS at a rate of 10Hz. Typical image had 800x900 pixels and the 6h recording resulted in $\sim 300GB$ size datasets per experiment. Routine operations such as storing and preprocessing these large datasets were thus challenging. I developed a workflow that could easily scale to process several experiments effortlessly (**Figure 3.11**). After each experiment, the data were moved onto a storage server. To run the computationally intensive preprocessing step in parallel, I used the High Throughput Computing (HTC) system developed by Auguste Genovesio at the IBENS, based on 328 CPUs.

Image registration

The first step in the analysis of the calcium imaging data was to compensate for possible drifts in the X-Y plane. For this purpose, I registered the images by finding the maximum in the cross-correlation with a reference frame. The reference frame was a 10 s average of the calcium imaging data computed in the middle of the recording. The registered stacks were then manually inspected to evaluate the drift in the ventro-dorsal plane, a drift that could not be compensated. Experiments with such drifts were discarded. Movement artifacts were detected according to large deviations in the maximum of the cross-correlation between successive frames. All frames with large deviations were discarded, they mostly occurred during tail movements.

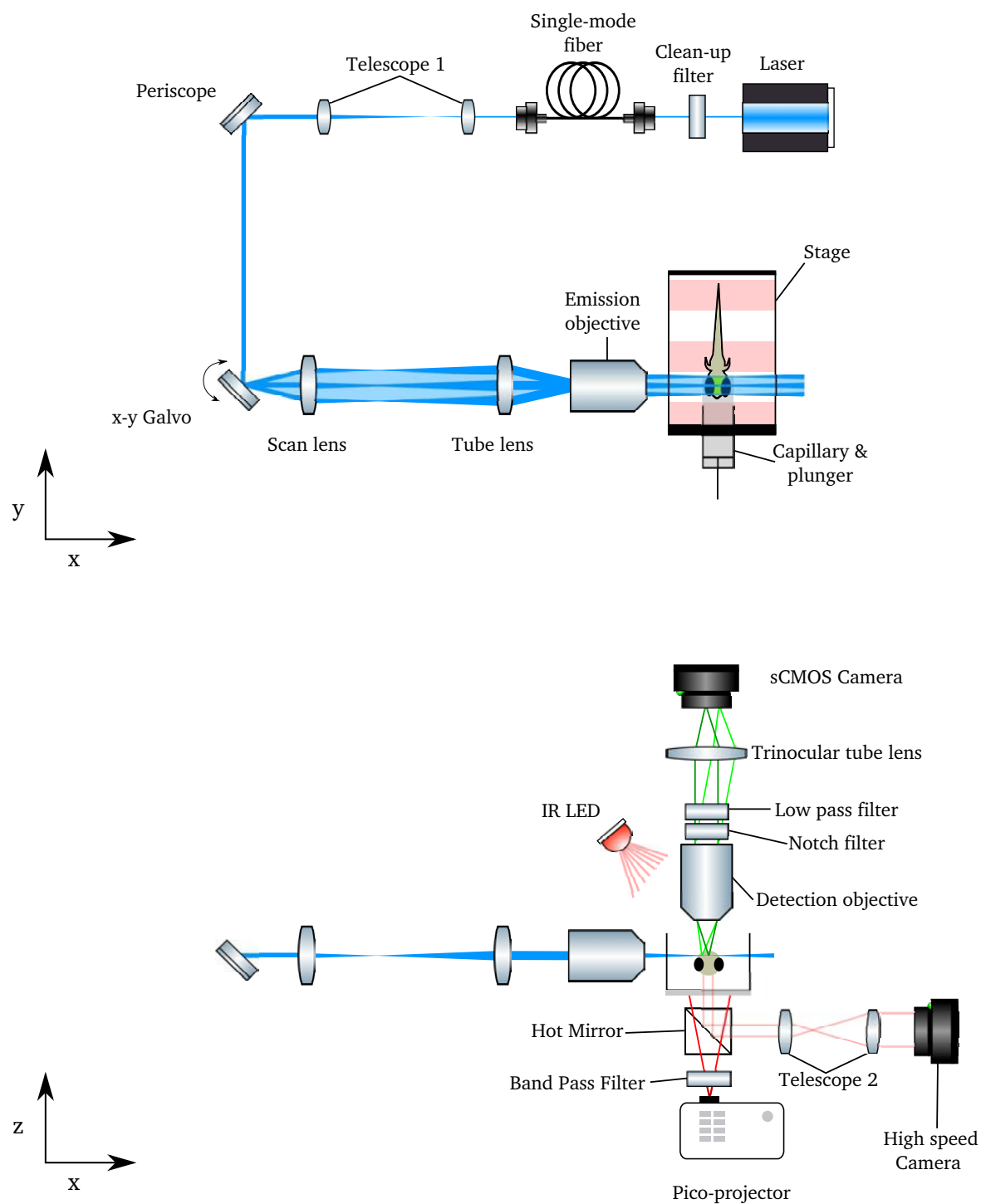


Fig. 3.10: **Scheme of the optical paths of the SPIM.** Up: top view, excitation path. A light sheet in the x-y plane allowed monitoring neuronal activity in a coronal section of the brain. Down: side view of the detection path. The tail movements were recorded and visual stimuli could be displayed below the larva. The control and data acquisition hardware are not shown. The components are listed in Supplementary Methods.

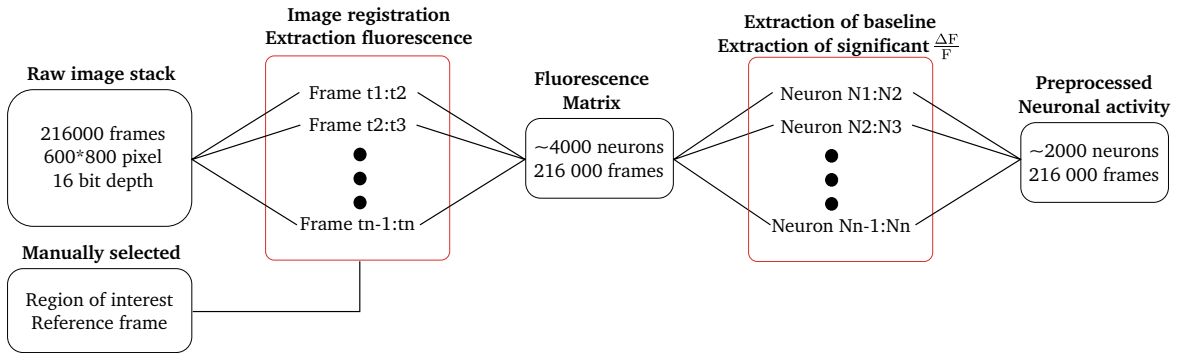


Fig. 3.11: **Workflow for image preprocessing.** The time series of significant fluorescent events for each hexagonal region was extracted from the original image stack. The first step was the registration of the images to compensate for potential slow drifts. The fluorescence of each region of interest (ROI) was computed on the registered images. In each ROI, the baseline fluorescence was then fitted and the significant increases in relative variation of fluorescence were computed. Parallelized operations on the Condor HTC are encircled in red.

Image segmentation

Individual regions of interest (ROIs) were defined as hexagons of side lengths equal to $6.3\mu m$, corresponding to an area roughly equal to a neuron's soma. The advantage of using hexagons was to maximize the area covered by the mapping while minimizing the contact between neighboring ROIs. I did not dissociate neuropil and neuronal somata in the analysis. To test whether individual ROIs contained relevant signals, in each ROI, I computed the average correlation between the fluorescence of each pixel and the average fluorescence of the ROI. **Figure 3.12.B** shows ROIs color-coded by this correlation. If the latter was lower than 0.3, the ROI was removed from the analysis.

Inference of fluorescence events

In each ROI, the fluorescence time signal was extracted by evaluating the average intensity across the pixels in each hexagon for each registered image. A smooth estimate of the fluorescence baseline for each ROI was calculated by computing the 30s-long causal running average of the 8th percentile of the raw data of the fluorescence signal (**Figure 3.12.C**). This estimate reflected slow fluctuations unrelated to the fast calcium transients associated with the neuronal activity. The resulting smooth curve baseline enabled computing the relative variation in fluorescence intensity $\frac{\Delta F}{F}$ computed as $\frac{\Delta F}{F} = \frac{F(t) - baseline(t)}{baseline(t)}$. A ROI's $\frac{\Delta F}{F}$ typically presented a positively skewed distribution, an example is showed in **Figure 3.12.D**. The latter peaked at a value μ ,

data points smaller than μ were unlikely to be related to neuronal firing. An estimate of the standard deviation (s.d.) of the baseline could be obtained by considering that the baseline is the result of a stochastic process. I thus fitted values of $\frac{\Delta F}{F}$ smaller than μ with a normal distribution of mean μ and s.d. σ_{noise} . For further analysis, I only considered fluorescence transients by imposing a threshold on each individual times series. Values of $\frac{\Delta F}{F}$ below $3\sigma_{noise}$ were set to 0. A typical trace obtained is shown in **Figure 3.12.E**. ROI with noise poorly fitted by a Gaussian ($R^2 < 0.9$), or with large-noise level $\sigma_{noise} > 0.014$ were discarded.

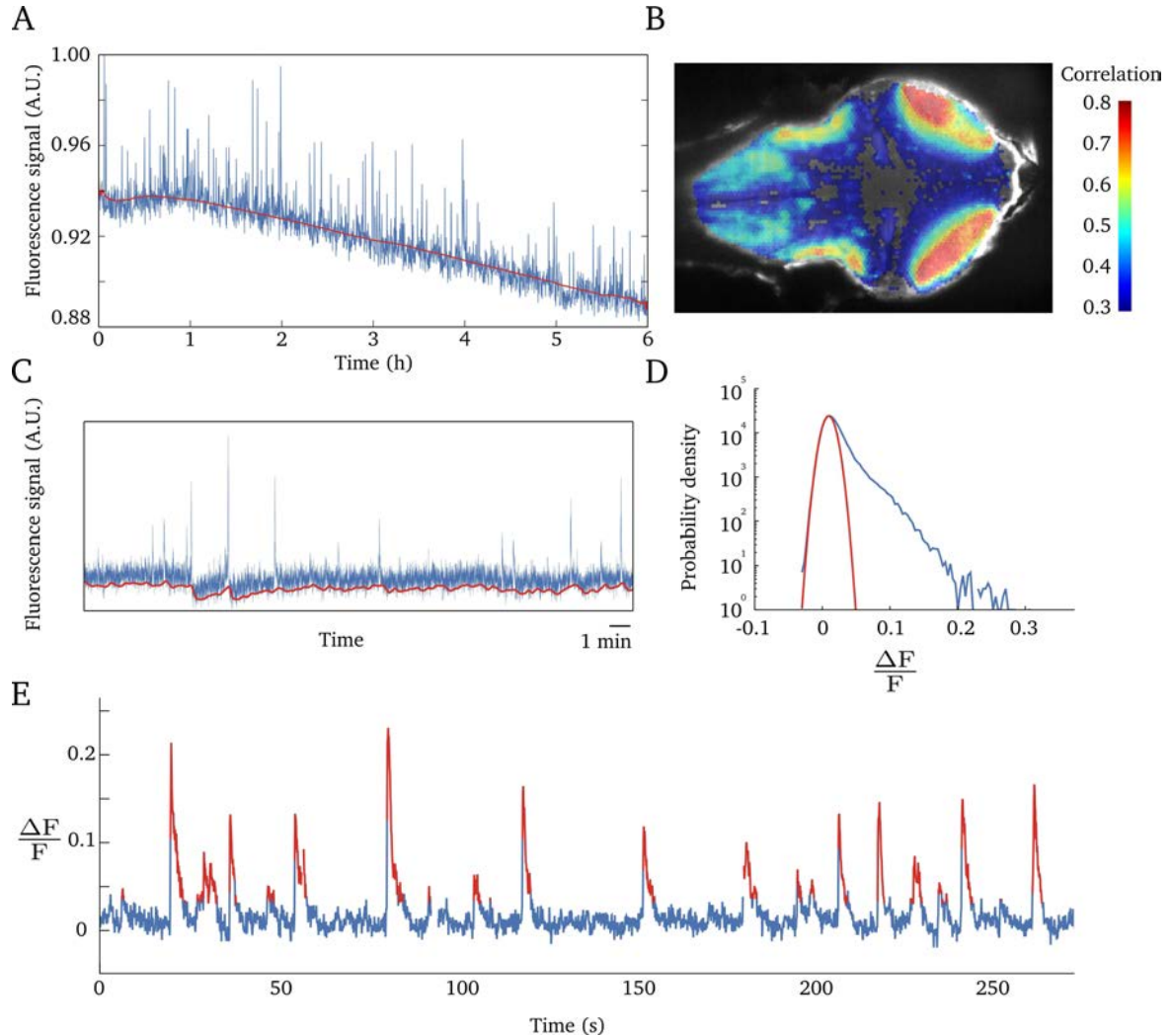


Fig. 3.12: **Preprocessing of the fluorescence signal.** (A) The fluorescence signal averaged across all ROIs during the 6h of recording (Blue). In red is a running average of the fluorescent signal. The relative decrease in baseline fluorescence was less than 6%. (B) Average pairwise correlation between pixels in each ROI, ROI with a correlation below 0.3 were discarded. (C) In blue, the fluorescence signal of a typical ROI. In red, baseline estimated from the ROI. (D) Probability density of the relative fluorescence changes $\frac{\Delta F}{F}$ of a typical ROI (blue) and the corresponding Gaussian fit to its value of $\frac{\Delta F}{F}$ smaller than μ (red). The s.d. of the Gaussian fit is σ_{noise} . (E) Example of a typical ROI $\frac{\Delta F}{F}$ (blue) along time, with significant fluorescence transients. The signal above $3\sigma_{noise}$ were highlighted in red.

3.4 Results

In this part, I will discuss the approach and some results, however, it should be noted that these results are still preliminary.

The neuronal basis of spontaneous movements was first characterized in humans by a macroscopic increase in activity measured in premotor regions before the onset of spontaneous movements (Shibasaki and Hallett, 2006). In order to test if a similar macroscopic effect existed in zebrafish larva, I computed the average activity pooled across ROIs before the onset of spontaneously generated movement. **Figure 3.13.A** shows a gradual build-up in activity starting ~ 1.5 s before the onset of movements, this time scale is similar to the readiness potential recorded in other species (see **Figure 1,5**). However, this macroscopic quantification was not sufficient to predict the onset of movements since spontaneous increase in the activity of a large portion of the neurons occurred in the absence of movement.

I then performed a mass univariate Mann-Whitney test on all ROIs to find neurons for which the median activity was significantly higher before the onset of a spontaneous tail movement. For each 100ms frame before the onset of movements, I tested whether the activity in each ROI was different from the inert regime. The inert regime was defined as frames recorded at least 8s away from any movement. **Figure 3.13.C** shows that the bilateral neuropil region 3 of the rhombencephalon displayed the strongest difference in activity between the preparation of spontaneous movements and the inert regime. The median activity in this region was statistically different from the inert regime 200ms as well as 1s before the onset of movement. The neurons capable of predicting the tail movements well in advance (1s before the movement's onset) were those showing the most significant increase just before the onset of movements (100ms, **Figure 3.13.B**).

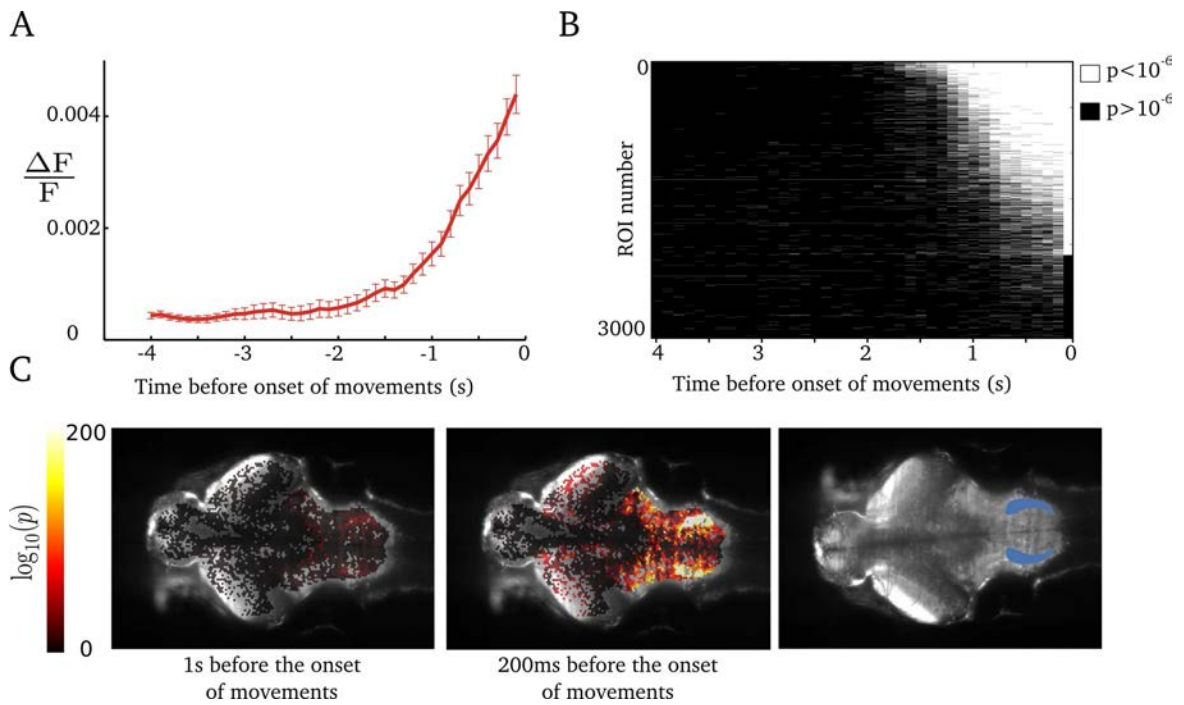


Fig. 3.13: Increase in activity prior to spontaneous movement. (A) Average activity pooled over ROIs before the onset of tail movements. (B) Raster plot of the results of the Mann-Whitney test for each ROI, and for each frame before the onset of the movements. White stripes (respectively black) indicate significant differences (respectively non significant) with respect to the median activity of the inert regime. The ROIs are ordered according to their significance 100 ms before the onset. The most significant ROIs just before the onset of movement are also those that display a significant difference the earliest before a movement onset. (C) Left, center : Map of the decimal logarithm of the p-value for each ROI 1s and 200ms before the onset of movements. Right : Location of the neuropil region 3 of the rhombencephalon. This position matches the location of the most significant ROIs. In (A), (B) and (C), only movements spaced by IBI larger than 8s were considered (N=199).

In order to study the influence of neuronal activity on the selection of movement, I performed a linear discrimination analysis (LDA) to find the projection of neuronal activity that would discriminate between the different categories of movement defined in **3.2.1**. Unlike principal component analysis that seeks to find the subspace with the maximal variance, LDA aims at finding a subspace that maximizes the separation of the different categories. Traditional LDA is infeasible in our configuration because of the high dimensionality of the data (~ 3000 neurons) compared to the number of samples in each movement class (~ 80 movements per category). Therefore, I used direct LDA (Xiao-Jun et al., 2004), a non-parametric variant of LDA aimed at finding maximal discriminative directions in high-dimensional configurations.

Figure 3.14.A shows the projections of neuronal activity 100ms before the onset of movement obtained by training a DLDA to discriminate the movement direction (positive or negative index of tail deflection) in each directional category of movement: asymmetrical scoot, routine turn and C bend. Rather than distinguishing the direction of asymmetrical movements independently of their category, the neuronal activity in the studied coronal section of the brain presented a sharp directional discrimination specific to routine turns. A section containing Mauthner cells might have performed a better separability of the C bend movements. The map of significant weights associated with each ROI is shown in **Figure 3.14.B**. It presents a bilateral anti-symmetric pattern in several brain regions: the migrated area of the pretectum (M1R and M1L), the neuropil of the optic tectum, the posterior mesencephalon and the posterior hind-brain. This pattern obtained using DLDA did not appear clearly when comparing the average neuronal activity between the onset of routine turns. Our inability to distinguish between the average pattern of activity for positive and negative routine turns was due to large variance independent of the direction of the turn that the DLDA method successfully discards.

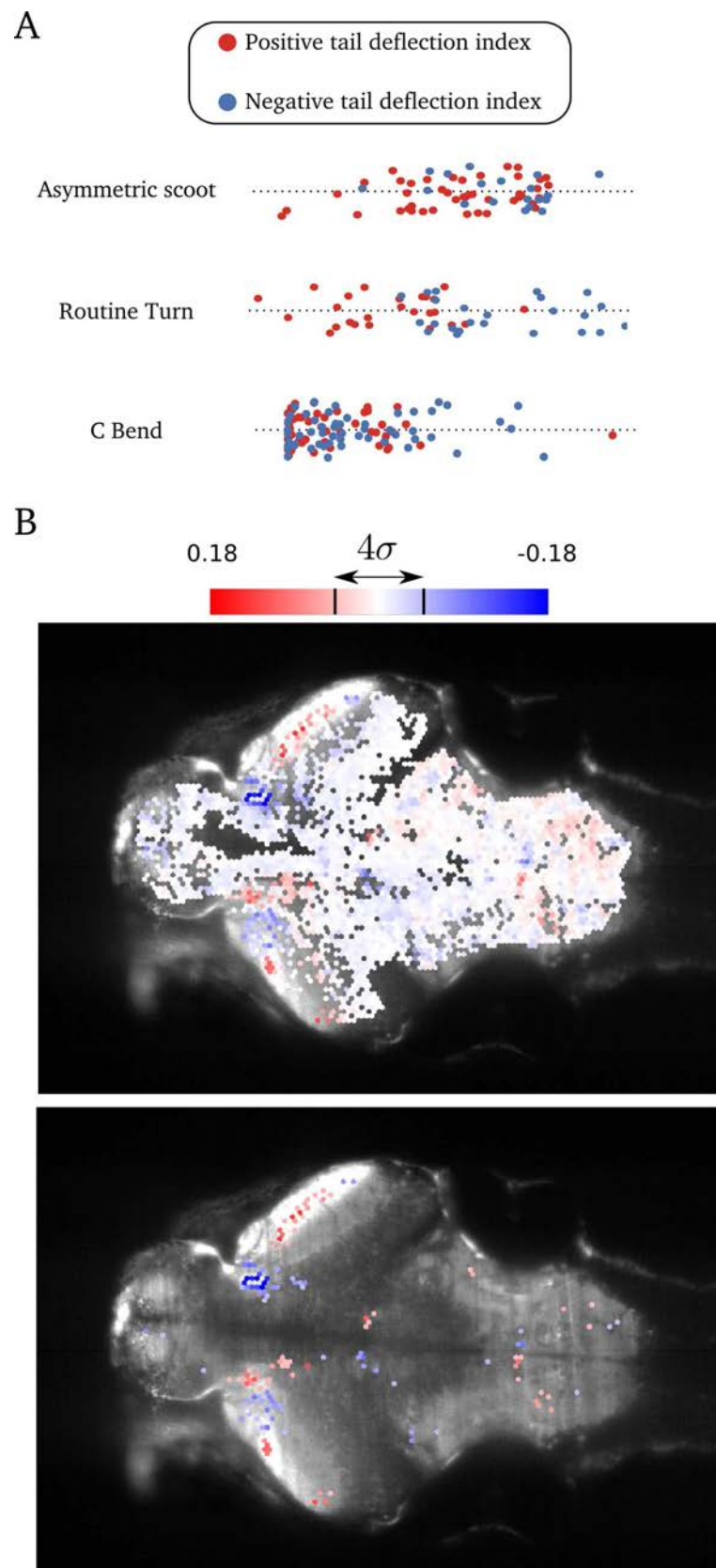


Fig. 3.14: Predicting movement direction using DLDA, legend next page

Fig. 3.14: (Previous page.) **(A)** The DLDA algorithm is applied separately on each category of movement in order to discriminate their direction (positive or negative) from the neuronal activity 100ms before the onset of movements. Each category of movement is associated with an axis (black dashed line). On each axis, the horizontal position of points represent the projection of the neuronal activity in 1D using DLDA to discriminate direction of movement. A random vertical jitter was added for visualization purposes. Blue dots (respectively red) represent movements with a positive (respectively negative) direction in the index of deflection. **(B)** Upper panel: the map of coefficients used in each ROI for the DLDA projection. Lower panel: only coefficients of absolute value larger than 2 standard deviations are shown. A bilateral antisymmetric pattern appears in several brain regions.

I then manually selected clusters of ROIs in the regions showing a bilateral antisymmetry in order to study independently the contribution of the different brain regions highlighted by DLDA (red and blue clusters in **Figure 3.15.A**). **Figure 3.15.B** shows typical time series associated with each cluster before the onset of spontaneous movements. The scatter plot in **Figure 3.15.C** displays the activity in each cluster 100ms before the onset of routine turn movements. The traces of the activity in the region 3 of the neuropil in the rhombocephalon displayed smaller fluctuations in the inert regime, explaining the difference in the median activity between the inert regime and just before the onset of a spontaneous tail movement (**Figure 3.15.B**). The bilateral clusters were correlated and did not exhibit differences between both directions of the routine turns (**Figure 3.15.C**). Activity in the bilateral clusters of the posterior mesencephalon and rhombencephalon displayed a phase opposition reminiscent of the hindbrain oscillators described by Ahrens et al. (2013b).

The phase of the oscillator before the onset of a routine turn was predictive of its direction (**Figure 3.15.C**). The group in the pretectum did not display phase opposition (**Figure 3.15.B**) but the relative level of activity in each group was also predictive of the direction of the turn. In all groups, there was no clear threshold in the activity prior to spontaneous movements.

A statistical test confirmed that the activity in the black clusters (corresponding to the neuropil region 3 of the rhombencephalon) was specific to the onset of the spontaneous movements but not to its direction. Alternatively, bilaterally anti-symmetrical clusters in the rhombencephalon, mesencephalon and pretectum displayed large fluctuations in the absence of movement but their activity before the onset of a movement was predictive of its direction (respectively negative) when the activity of the red(respectively blue) cluster was higher. The neuropil of the optic tectum were neither significantly predicting the direction of movements nor their onset.

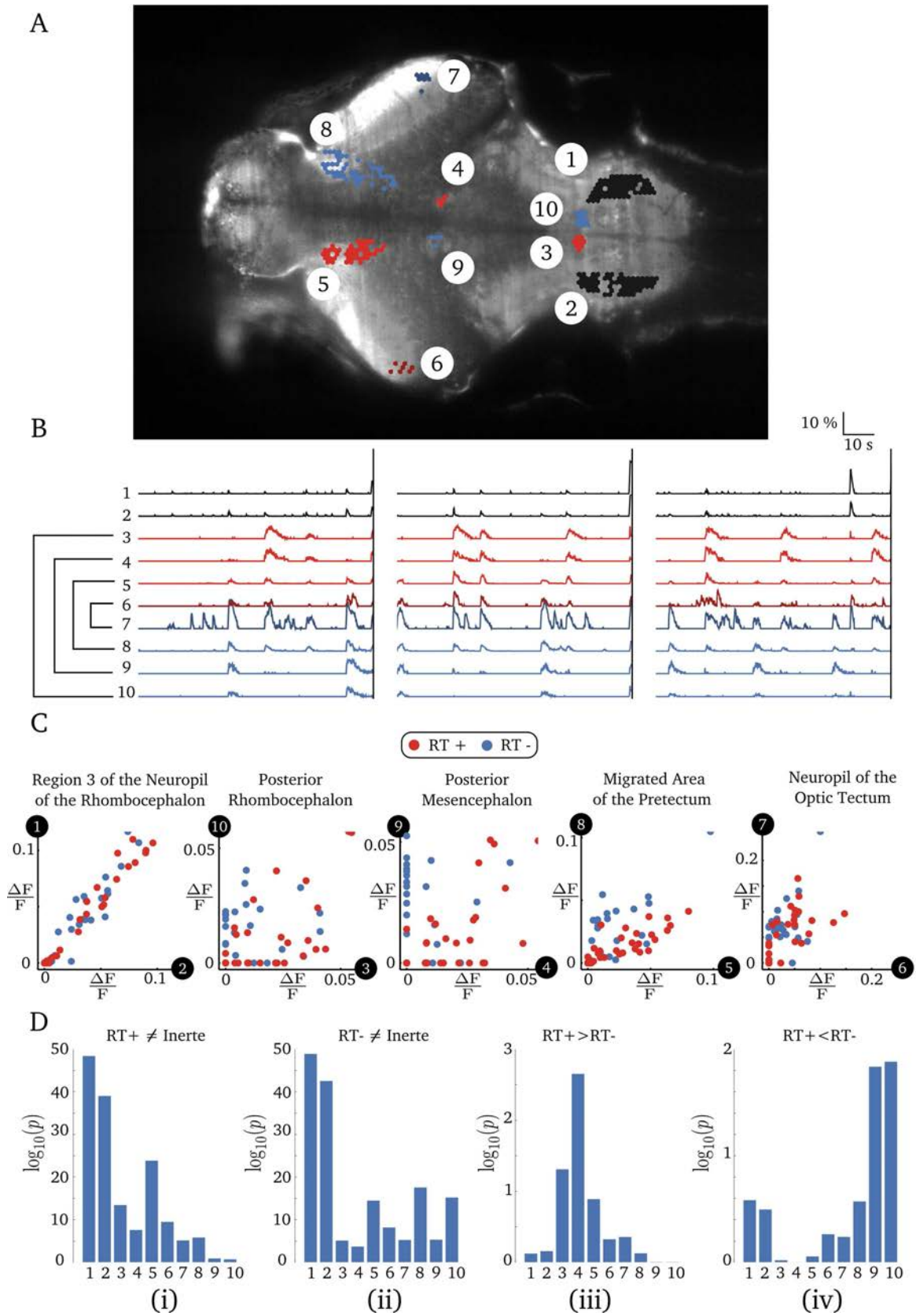


Fig. 3.15: Specificity for the directionality of routine turns, legend next page

Fig. 3.15: (Previous page.) **(A)** Manually labeled regions. Red and blue are the groups corresponding to the bilaterally antisymmetric regions found in (Figure 3.14.B), the red and blue colors correspond to the sign of the group in the DLDA map of coefficient (Figure 3.14.B). The black group corresponds to the region with the most significant increase in activity before movements (Figure 3.13.C). **(B)** Each of the three panels shows a 70s trace of the neuronal activity in the group indexed in (A), the vertical bars indicate the onset of a movement. The link between groups on the left indicate the bilaterally anti-symmetric structures. **(C)** Scatter plot for each bilateral cluster of neurons. In the scatter plot, the neuronal activity before a routine turn is represented by a dot, red (respectively blue) for positive routine turn (respectively negative). The neuronal activity in the region 3 of the neuropil of the rhombocephalon and in the optic tectum did not exhibit significant differences between positive and negative directions. For the posterior rhombocephalon, posterior mesencephalon and pretectum, if the red side was strongly active (respectively blue) corresponding to the group 3,4 and 5 (respectively 10,9 and 8), the tail movements were likely to be positive routine turns (respectively negative). **(D)** Each of the four bar plots shows the decimal logarithm of the p-value for each group of neurons (1-10), by testing the difference in the median neuronal activity across several conditions, using a Mann-Whitney test. **(i)** Test if the median activity was different before the onset of positive routine turns with respect to the inert regime. **(ii)** Test if the median activity was different before the onset of negative routine turns with respect to the inert regime. **(iii)** Test if the median of activity before the onset of positive routine turns was larger than before negative routine turn. **(iv)** Test if the median of activity before the onset of positive routine turns was smaller than before negative routine turns.

3.5 Supplementary Methods

Illumination path

The light-sheet was obtained by rapidly scanning a focused laser beam through the caudo-rostral axis of the larva's brain. The quality of the blue laser beam was improved by adding a clean-up filter (BP 5 nm, 488nm) and a single-mode fiber. A telescope was placed in the initial part of the path to enable adjustment of the beam's diameter. Then, the beam was projected onto a set of galvanometric mirrors driven by a triangular waveform at 400 Hz over an angular range of 6° . Oscillation of the mirrors around the z-axis generated the scanning of the beam in the x-y plane for, the other axis of rotation enabled controlling the vertical position of the light sheet. The association of the scanning ($f=75$ mm) and tube lenses (180 mm) extended the beam to a radius of 2.16 mm ($1/e^2$) at the entrance of the illumination objective. The beam intensity measured at the entrance of the illumination objective was $P=0.3$ mW. The low-NA illumination led to a $3.2 \mu\text{m}$ ($1/e^2$) beam waist (**Figure 3.16**).

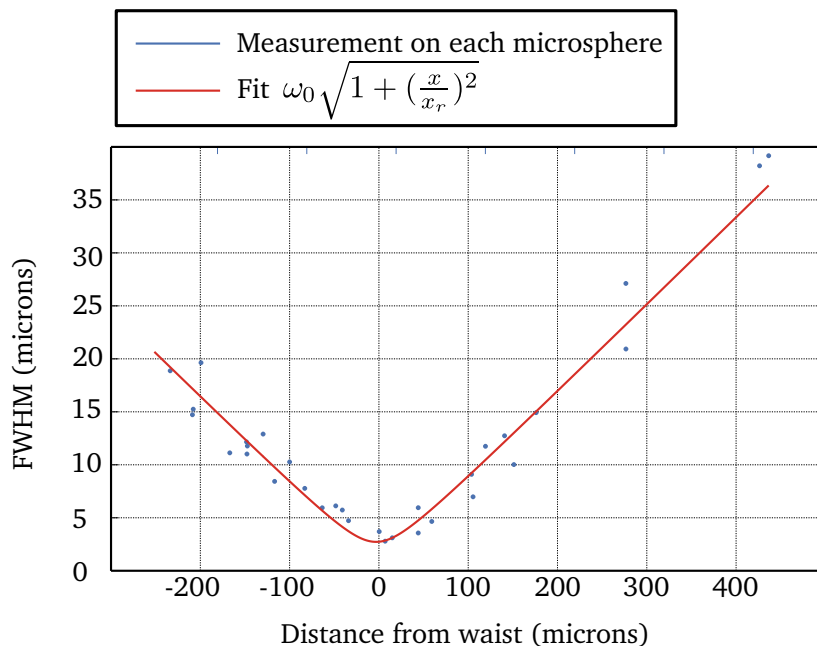


Fig. 3.16: **Axial profile of the light sheet.** Each blue dot corresponded to a fluorescent beads of $0.1 \mu\text{m}$. Its full width at half maximum (FWHM) was computed by scanning the light sheet in the vertical plane and measuring the vertical profile of the fluorescence intensity. The red line corresponds to a fit matching a Gaussian beam profile with $w_0 = 3.2 \mu\text{m}$. The optical sectioning is thus compatible with single-cell resolution (the typical soma has a diameter of $\sim 7 \mu\text{m}$).

Detection path

The detection path consisted of a water-dipping objective (16x, 0.8 NA, Nikon) mounted on a piezo objective positioner. An olympus trinocular tube lens allowed imaging the field of view. To record the neuronal activity, I used a sCMOS camera to record activity at 10 Hz with the external trigger mode and a binning of 2x2. A band-pass filter (525-50, Semrock) and low-pass filter (FF01-680, Semrock) filtered the infrared and laser light in order to image the green GcaMP5 fluorescence signal. The z-position of the detection objective was matched to the z-location of the light-sheet using a piezo in the detection arm. Taking into account the optical configuration and the binning chosen, the pixel area was $0.9 \mu m$. The binning of the camera was chosen to reduce the size of the datasets.

Optical Part

Table 3.1: Optical Part

Emission Path	
Laser	Phoxx 480-200, Omicron
Clean-up filter	XX.F488, Omicron
Single-mode fiber	Qioptiq, KineFlex
Telescope 1	LA1131-A-ML (f=50mm) + LA1433-A-ML (f=150mm), Thorlabs
Periscope	1x RS99, 2x Protected Silver Mirrors, Thorlabs
X-Y Galvo	Mounted XY 5mm galvo sets, Cambridge Technology
Scan lens	AC508-075-A-ML (f=75mm), Thorlabs
Tube lens	U-TLU (f=180mm), Olympus
Emission objective	UPlanSAPO 4x/0.16, Olympus
Source	
Stage	Custom-made
Capillary & plunger	701904 glass capillaries & 701932 plunger, Brand
Reception Path	
sCMOS Camera	Orca Flash 4, Hamamatsu
Trinocular tube lens	Olympus trinocular microscope
Low-pass filter	FF01-680 SP25, Semrock
Band-pass filter	525-50, Semrock
Detection objective	N16XLWD-PF, 16x/0.8, Nikon
Hot Mirror	FM201, Thorlabs
Band-Pass Filter	FF01 629/56, Sermrock
Pico-projector	PK320, Optoma
Telescope 2	DZ1/L1.5-10, ImagingSource
High-Speed Camera	Hxg20nir, Baumer
IR LED	NG50L (810nm), BDlaser

Chapter 4

Conclusions and perspectives

4.1 A visual virtual reality system for the zebrafish larva

In the first part of my thesis, I developed a method for studying the behavior of zebrafish larva within a visual virtual-reality (VR) system. While its head is immobile, the virtual environment allowed larvae to perform goal-directed behaviors. To determine the speed and orientation of the swimming larva from the tail kinematics, I used an autoregressive model fitted on a relatively small library of movements (~ 300 tail bouts). This model enabled me to associate tail movements of head-fixed larva with a visual feedback similar to what the larva would have encounter in freely swimming conditions.

Previous methods to record tail movements were developed to study specific behaviors such as unidirectional displacement triggered by a whole-field motion stimuli aligned with the larva (Portugues and Engert, 2011). Another method was tuned to provide a pre-determined feedback independent of the kinematics of the tail (Trivedi and Bollmann, 2013), in this case, the visual feedback matched the intended movement of the larva only occasionally. In contrast with these approaches, the proposed method allows navigating in two dimensions using different movement repertoires.

An alternative preparation proposed by Ahrens et al. (2013a) relies on "fictive swimming" where the trajectory of a paralyzed larva was extrapolated from extracellular recordings of nerves in the spinal cord. The method is technically advantageous because the paralyzer makes brain recordings more stable. Moreover, tail movements produced by head-fixed larva in agarose can cause unwanted mechanical constraints that are not present during free swim. On the other hand, by monitoring the real

kinematics of the tail, my approach is compatible with fine characterization and classification of the motor behaviors, and provides, in addition to the visual feedback, the proprioceptive feedback, absent in paralyzed larvae.

Using this method, I have reproduced goal-directed behaviors that are impossible to observe in open-loop settings. In a virtual environment presenting a whole-field motion, larvae were able to align and swim in the direction of motion using tail bouts of long durations ($\sim 300\text{ms}$). Larva presenting an initial deviation of 55° with the whole field motion were capable of aligning with a deviation of 20° after 3 tail bouts while maintaining an average speed of 1.5mm/s in the direction of motion. The same method allowed prey capture behavior in a different virtual environment. After detection of the prey, larvae were capable of producing a fine tail movement that aligned them with the moving prey. Then, using two other short duration bouts ($\sim 180\text{ms}$), larvae were capable of reaching the prey target for 16% of their attempts and up to 40% for the best larva. The behavior of the larva in the virtual environment reproduced characteristics monitored in free-swimming conditions (e.g. reduction of orientation change during successive bouts or the reduction of eye vergence as the larva approaches the prey (Trivedi and Bollmann, 2013)).

Moreover, the control of the visual environment allowed studying how larvae adapt to perturbations to the visual feedback. When the visual feedback was updated only at the end of a tail bout rather than being continuously provided in real time, the duration of bouts was longer (200ms instead of 180ms) and resulted in a 50% decrease of the prey-capture success rate. This indicates that larvae can integrate visual information in real time during a tail movement, in contrast to what was previously believed (Trivedi and Bollmann, 2013). Moreover, these results demonstrate that discrete tail bouts can be modulated during the short duration of a movement according to the visual feedback. Neurons whose activity sustained locomotion such as V2a cells in the hindbrain (Kimura et al., 2013) could contribute to the modulation of the duration of movements according to visual feedbacks.

In the future, this method can be used to study the neural mechanisms underlying fine goal-directed behaviors while large portions of the brain can be recorded in intact animals at high temporal and spatial resolution navigating in VR (Wolf et al., 2015). Since closed-loop systems generate unique trajectories for each trial, correlating behavior and the neuronal activity is a major challenge. A potential solution is

the analysis at the single-trial level of behavior and neuronal activity (Bonnen et al. (2015), Latimer et al. (2015)).

The flexibility of our method could be useful to understand how the same circuitry can be employed to generate multiple behaviors (Wyart and Knafo, 2015). Such circuits can include for example the Nucleus of the Medial Fasciculus (nMLF), a cluster of neurons involved in multiple flexible behaviors including the optomotor response and prey capture (Huang et al., 2013). The complexity of the neuronal dynamics is limited by the task complexity (Gao and Ganguli, 2015). Therefore, recording neuronal activity in large portion of the brain is especially advantageous when observing multiple behaviors.

Observation of motor actions in goal-driven navigation is limited by the level of locomotor activity in head-fixed larvae. Prey-capture behaviors could be triggered in only 14% of the trials similar to previous reports (Bianco and Engert (2015), Trivedi and Bollmann (2013)).

The behavioral paradigm could be improved by using multi-sensory stimulation (Candelier et al. (2015), Yokogawa et al. (2012)) or by combining the response of larvae with appropriate learning paradigms (Roberts et al., 2013). A similar methodology could also be applied in juvenile or adult fish in order to study more complex cognitive processes such as social behaviors or place conditioning in virtual-reality conditions.

4.2 Internally driven behaviors in zebrafish larva

I studied how zebrafish larva spontaneously generates actions. Since actions were not constrained by external stimuli, it was critical to perform a fine characterization of behavior in order to disassemble the variability observed in this configuration.

Therefore, I first developed a method for classifying tail bouts, using dynamic time warping for comparing tail movements, the repertoire of tail bouts recorded in head-fixed larvae appeared to form a continuum rather than a series of discrete group of movement types. Although previous studies have described discrete categories of movements (Budick and O'Malley, 2000), there are two reasons why some continuity is expected. The firing rate of reticulospinal neurons gradually influences the kinematic parameters of tail movements, such as the amount of turn for MiV1 neurons (Huang et al., 2013) or the tail-beat frequency for nMLF (Severi et al., 2014). Such populations of neurons are thought to modulate continuously the trajectories (Orger et al., 2008)

such as the gradation of trajectories observed in the virtual environment during prey capture essays (**Figure 2.5.D**).

In order to obtain a parsimonious representation of this continuum of locomotor actions, I trained a supervised classifier to identify 5 different categories of movements: scoot, asymmetrical scoot, routine turn, C bend and burst. Tail bouts were correctly classified with 82% chance while errors in the classification occurred mostly between similar categories. Although previous studies have performed categorization of behavior in free-swimming conditions, our method does not rely on the analysis of the generated trajectories and enabled me to analyze the behavior during functional imaging and to produce a fine description of the relation between neuronal activity and locomotion.

Using this movement classification tool, I studied the patterns of tail movements in the absence of sensory stimulation. Rather than a uniform stochastic process, the spontaneous behavior of head-restrained larvae was organized according to complex temporal patterns. The distribution of inter-bouts intervals (IBI) presented two deviations from a homogeneous Poissonian process: a heavy-tail regime with long periods of inactivity and rhythmic successions between movements at short times (~ 4 s). Movements chained in less than ~ 10 s were more likely to belong to similar categories and to have a similar directionality.

A good candidate model for describing the spontaneous ethogram of an individual larva was given by a semi-Markov model. A chain of events is a first order semi-Markov process if:

$$\mathbb{P}(\text{Mvt}_{i+1}, \text{IBI}_i = t | \text{Mvt}_i, \text{IBI}_{i-1}, \text{Mvt}_{i-1}, \dots) = \mathbb{P}(\text{Mvt}_{i+1}, \text{IBI}_i = t | \text{Mvt}_i) \quad (4.1)$$

Where Mvt_i represent the category of the movement i and IBI_i is the resting time preceding it. The duration of successive IBIs had a low correlation (0.04), thus, their independence in (4.1) is a valid hypothesis. However, in its non-parametric form, this model requires a large dataset of movements. Obtaining an ethogram averaged across larvae, by pooling the IBIs and movements of different fish would neglect the individual differences observed between larvae.

The ultimate goal would be to fit the semi-Markov chain for individual larvae. A similar approach in fly enabled finding idiosyncrasy in the transition rates that persisted over days and could identify uniquely individual fly (Kain et al., 2013). Using this approach for the zebrafish larva would provide a very useful tool to characterize the behavioral "personality" of individual larvae and study the neuronal mechanisms

underlying it.

It is unclear how similar the dynamics of spontaneous behaviors in head-fixed larva is with respect to that of natural conditions. Despite the lower rate of locomotor activity in head-restrained conditions, the burstiness of IBIs and the transition between categories of movements could still be similar to those in free-swimming conditions. Such findings would indicate that under head-restrained conditions, the larvae behave normally but they are in a less alert state.

Observations of freely swimming zebrafish could help to identify the role of internally driven behaviors. A first hypothesis would be that internally driven behaviors is required for sampling the environment efficiently during foraging (external motivation). Alternatively, spontaneously generated movements could help the larva to adapt to their continuously changing morphology and the associated change in flow dynamics (internal motivation). Moving only in response to imminent threat or attracting stimuli might not be the best strategy. The feedback resulting from internally driven behavior could help locomotor learning in the absence of imminent survival interests.

4.3 Neural basis of internal decisions

In order to understand the neuronal mechanisms underlying internal decisions, I recorded the spontaneous neuronal activity over long periods of time and from a large portion of the larva's brain, while simultaneously monitoring spontaneous tail movements.

On average, neurons displayed a build-up in activity ~ 1 s prior to the onset of spontaneous movements. This timing is consistent with what has been recorded in other species (**Figure 1.5**). In the recorded coronal section of the zebrafish's brain, I observed that the neuropil of the rhombencephalon presented a low baseline of activity but the latter increased before the onset of the spontaneous movement. Upstream neurons responsible for this accumulation of activity in the neuropil were not identified but they could exist in the non-monitored brain regions. Using dimensionality reduction algorithms, I could identify clusters of neurons predicting specifically the direction of routine turns (left or right). In the absence of spontaneous movements, different groups of neurons scattered within several brain regions presented spontaneous fluctuations with a bilateral anti-symmetric pattern over long time scales (~ 10 s). However, their activity prior to the onset of spontaneous movements was predictive of the direction of the imminent routine turn. The IBI within which successive movements

were similar (~ 10 s) roughly matched the typical duration of oscillations among the neurons within the cluster. Therefore, the spontaneous oscillations of this population could explain the similarity of successive movements.

These preliminary results validate the methodology by showing that highly informative neurons can be identified in the presence of large uninformative variance at the level of the large neuronal population. Given the timing of motor preparation in the order of seconds, brain-wide recordings at low-temporal sampling (typically a complete $200\ \mu\text{m}$ stack at 1 Hz) could accelerate the discovery of relevant anatomical structures involved in internal decisions. A potential pitfall could be that larvae do not move the tail spontaneously but as the result of the feedback of agarose resulting from an attempt to move the eye. This artifact could be avoided by freeing the eyes from agarose and monitoring their rotational kinematics. Finally, in the presence of whole-field motion in the caudo-rostral direction, 11% of the movements generated by the larva are routine turns (**Figure 3.6**). The cluster oscillations could account for the direction of these routine turns and would therefore account for spontaneous movements and for the variability observed in sensory evoked conditions.

It is possible that due to its relatively small number of neurons ($\sim 10^5$ vs $\sim 10^8$ in mice and $\sim 10^9$ in monkey), and their limited cognitive abilities, zebrafish is only suited to study simple stimulus/response associations. However, zebrafish gives the opportunity to simultaneously monitor large portions of the brain activity and the whole repertoire of natural movements. This is in sharp contrast to other animal models such as mice and monkeys where due to the constraints of the behavioral paradigms a limited number of behaviors can be monitored. This allows studying the rich interactions between the brain and its environment, namely, the role of action on sensory perception in virtual reality and the role of the brain's internal dynamics on spontaneous behaviors.

References

- Ahrens, M. B. and Engert, F. (2015). Large-scale imaging in small brains. *Current opinion in neurobiology*, 32:78–86.
- Ahrens, M. B., Huang, K. H., Narayan, S., Mensh, B. D., and Engert, F. (2013a). Two-photon calcium imaging during fictive navigation in virtual environments. *Frontiers in Neural Circuits*, 7(June).
- Ahrens, M. B., Li, J. M., Orger, M. B., Robson, D. N., Schier, A. F., Engert, F., and Portugues, R. (2012a). Brain-wide neuronal dynamics during motor adaptation in zebrafish. *Nature*, pages 1–34.
- Ahrens, M. B., Li, J. M., Orger, M. B., Robson, D. N., Schier, A. F., Engert, F., and Portugues, R. (2012b). Brain-wide neuronal dynamics during motor adaptation in zebrafish. *Nature*.
- Ahrens, M. B., Orger, M. B., Robson, D. N., Li, J. M., and Keller, P. J. (2013b). Whole-brain functional imaging at cellular resolution using light-sheet microscopy. *Nature methods*, 10(5):413–20.
- Akerboom, J., Chen, T.-W., Wardill, T. J., Tian, L., Marvin, J. S., Mutlu, S., Calderón, N. C., Esposti, F., Borghuis, B. G., Sun, X. R., et al. (2012). Optimization of a gcamp calcium indicator for neural activity imaging. *The Journal of Neuroscience*, 32(40):13819–13840.
- Aronov, D. and Tank, D. W. (2014). Engagement of Neural Circuits Underlying 2D Spatial Navigation in a Rodent Virtual Reality System. *Neuron*, 84(2):442–456.
- Ashe, J. and Georgopoulos, A. P. (1994). Movement parameters and neural activity in motor cortex and area 5. *Cerebral Cortex*, 4(6):590–600.
- Bardach, J. E., Ryther, J. H., McLarney, W. O., et al. (1972). *Aquaculture. The farming and husbandry of freshwater and marine organisms*. John Wiley & Sons, Inc.
- Bengio, Y. (2009). Learning deep architectures for ai. *Foundations and trends® in Machine Learning*, 2(1):1–127.
- Bergmann, M. and Iollo, A. (2011). Modeling and simulation of fish-like swimming. *Journal of Computational Physics*, 230(2):329–348.
- Bianco, I. H. and Engert, F. (2015). Visuomotor Transformations Underlying Hunting Behavior in Zebrafish. *Current Biology*, 25:831–846.

- Bianco, I. H., Kampff, A. R., and Engert, F. (2011a). Prey capture behavior evoked by simple visual stimuli in larval zebrafish. *Frontiers in systems neuroscience*, 5.
- Bianco, I. H., Kampff, A. R., and Engert, F. (2011b). Prey capture behavior evoked by simple visual stimuli in larval zebrafish. *Frontiers in systems neuroscience*, 5(December):101.
- Blanchard, T. C. and Hayden, B. Y. (2014). Neurons in dorsal anterior cingulate cortex signal postdecisional variables in a foraging task. *The Journal of Neuroscience*, 34(2):646–655.
- Bode, S., He, A. H., Soon, C. S., Trampel, R., Turner, R., and Haynes, J.-D. (2011). Tracking the unconscious generation of free decisions using ultra-high field fmri. *PloS one*, 6(6):e21612.
- Bonnen, K., Burge, J., Yates, J., Pillow, J., and Cormack, L. K. (2015). Continuous psychophysics: Target-tracking to measure visual sensitivity. *Journal of vision*, 15(3):14.
- Borla, M. A., Palecek, B., Budick, S., and O’Malley, D. M. (2002). Prey capture by larval zebrafish: evidence for fine axial motor control. *Brain, behavior and evolution*, 60(4):207–229.
- Budick, S. A. and O’Malley, D. M. (2000). Locomotor repertoire of the larval zebrafish: swimming, turning and prey capture. *Journal of Experimental Biology*, 203(17):2565–2579.
- Burgess, H. A. and Granato, M. (2007). Modulation of locomotor activity in larval zebrafish during light adaptation. *Journal of Experimental Biology*, 210(14):2526–2539.
- Burgess, H. A., Schoch, H., and Granato, M. (2010). Distinct retinal pathways drive spatial orientation behaviors in zebrafish navigation. *Current biology*, 20(4):381–386.
- Buss, R. R. and Drapeau, P. (2001). Synaptic drive to motoneurons during fictive swimming in the developing zebrafish. *Journal of Neurophysiology*, 86(1):197–210.
- Buzsáki, G., Peyrache, A., and Kubie, J. (2015). Emergence of Cognition from Action. *Cold Spring Harbor . . .*, LXXIX:1–11.
- Cadiou, C. F., Hong, H., Yamins, D. L., Pinto, N., Ardila, D., Solomon, E. A., Majaj, N. J., and DiCarlo, J. J. (2014). Deep neural networks rival the representation of primate it cortex for core visual object recognition. *PLoS computational biology*, 10(12):e1003963.
- Calhoun, A. J. and Hayden, B. Y. (2015). The foraging brain. *Current Opinion in Behavioral Sciences*, 5:24–31.
- Candelier, R., Sriti Murmu, M., Alejo Romano, S., Jouary, A., Debrégeas, G., and Sumbre, G. (2015). A microfluidic device to study neuronal and motor responses to acute chemical stimuli in zebrafish. *Scientific Reports*, 5:12196.

- Chen, X. and Engert, F. (2014). Navigational strategies underlying phototaxis in larval zebrafish. *Frontiers in systems neuroscience*, 8.
- Chiappe, M. E., Seelig, J. D., Reiser, M. B., and Jayaraman, V. (2010). Walking modulates speed sensitivity in drosophila motion vision. *Current Biology*, 20(16):1470–1475.
- Cisek, P. (2012). Making decisions through a distributed consensus. *Current opinion in neurobiology*, 22(6):927–936.
- Clark, D. a., Freifeld, L., and Clandinin, T. R. (2013). Mapping and cracking sensorimotor circuits in genetic model organisms. *Neuron*, 78(4):583–95.
- Collett, M., Chittka, L., and Collett, T. S. (2013). Spatial memory in insect navigation. *Current Biology*, 23(17):R789–R800.
- Cox, T. F. and Cox, M. A. (2000). *Multidimensional scaling*. CRC Press.
- Deo, R. C. and MacRae, C. A. (2011). The zebrafish: scalable in vivo modeling for systems biology. *Wiley Interdisciplinary Reviews: Systems Biology and Medicine*, 3(3):335–346.
- Derrac, J., García, S., and Herrera, F. (2014). Fuzzy nearest neighbor algorithms: Taxonomy, experimental analysis and prospects. *Information Sciences*, 260:98–119.
- Dombeck, D. a., Harvey, C. D., Tian, L., Looger, L. L., and Tank, D. W. (2010). Functional imaging of hippocampal place cells at cellular resolution during virtual navigation. *Nature neuroscience*, 13(11):1433–40.
- Dombeck, D. a. and Reiser, M. B. (2012). Real neuroscience in virtual worlds. *Current opinion in neurobiology*, 22(1):3–10.
- Edelman, S. (2015). The minority report: some common assumptions to reconsider in the modelling of the brain and behaviour. *Journal of Experimental & Theoretical Artificial Intelligence*, (ahead-of-print):1–26.
- Evinger, C., Kaneko, C., and Fuchs, A. F. (1982). Activity of omnipause neurons in alert cats during saccadic eye movements and visual stimuli. *Journal of Neurophysiology*, 47(5):827–844.
- Fajardo, O., Zhu, P., and Friedrich, R. W. (2013). Control of a specific motor program by a small brain area in zebrafish. *Frontiers in Neural Circuits*, 7(April):1–19.
- Fetcho, J. R. (2012). Neuroscience: crystal-clear brains. *Nature*, 485(7399):453–455.
- Fried, I., Mukamel, R., and Kreiman, G. (2011). Internally generated preactivation of single neurons in human medial frontal cortex predicts volition. *Neuron*, 69(3):548–562.
- Gabriel, J. P., Trivedi, C. A., Maurer, C. M., Ryu, S., and Bollmann, J. H. (2012). Layer-specific targeting of direction-selective neurons in the zebrafish optic tectum. *Neuron*, 76(6):1147–1160.

- Gahtan, E., Tanger, P., and Baier, H. (2005). Visual prey capture in larval zebrafish is controlled by identified reticulospinal neurons downstream of the tectum. *The Journal of neuroscience*, 25(40):9294–9303.
- Gao, P. and Ganguli, S. (2015). On simplicity and complexity in the brave new world of large-scale neuroscience. *Current opinion in neurobiology*, 32:148–155.
- Garey, J., Goodwillie, A., Frohlich, J., Morgan, M., Gustafsson, J.-A., Smithies, O., Korach, K., Ogawa, S., and Pfaff, D. (2003). Genetic contributions to generalized arousal of brain and behavior. *Proceedings of the National Academy of Sciences*, 100(19):11019–11022.
- Gavrila, D., Davis, L., et al. (1995). Towards 3-d model-based tracking and recognition of human movement: a multi-view approach. In *International workshop on automatic face-and gesture-recognition*, pages 272–277. Citeseer.
- Gibson, J. J. (1962). Observations on active touch. *Psychological review*, 69(6):477.
- Goh, K.-I. and Barabási, A.-L. (2008). Burstiness and memory in complex systems. *EPL (Europhysics Letters)*, 81(4):48002.
- Gottlieb, J., Oudeyer, P.-Y., Lopes, M., and Baranes, A. (2013). Information-seeking, curiosity, and attention: computational and neural mechanisms. *Trends in cognitive sciences*, 17(11):585–593.
- Gover, M. R. (1996). The embodied mind: Cognitive science and human experience (book). *Mind, Culture, and Activity*, 3(4):295–299.
- Hayden, B. Y., Pearson, J. M., and Platt, M. L. (2011). Neuronal basis of sequential foraging decisions in a patchy environment. *Nature neuroscience*, 14(7):933–939.
- Held, R. and Hein, A. (1963). Movement-produced stimulation in the development of visually guided behavior. *Journal of comparative and physiological psychology*, 56(5):872.
- Huang, K.-H., Ahrens, M. B., Dunn, T. W., and Engert, F. (2013). Spinal Projection Neurons Control Turning Behaviors in Zebrafish. *Current Biology*, pages 1–8.
- Hubel, D. H. and Wiesel, T. N. (1959). Receptive fields of single neurones in the cat’s striate cortex. *The Journal of physiology*, 148(3):574–591.
- Humphries, N. E., Queiroz, N., Dyer, J. R. M., Pade, N. G., Musyl, M. K., Schaefer, K. M., Fuller, D. W., Brunnschweiler, J. M., Doyle, T. K., Houghton, J. D. R., Hays, G. C., Jones, C. S., Noble, L. R., Wearmouth, V. J., Southall, E. J., and Sims, D. W. (2010). Environmental context explains Lévy and Brownian movement patterns of marine predators. *Nature*, 465(7301):1066–9.
- Juang, B.-H. and Rabiner, L. (1993). Fundamentals of speech recognition. *Signal Processing Series. Prentice Hall, Englewood Cliffs, NJ*.
- Jung, K., Jang, H., Kralik, J. D., and Jeong, J. (2014). Bursts and heavy tails in temporal and sequential dynamics of foraging decisions. *PLoS computational biology*, 10(8):e1003759.

- Jung, S. N., Borst, A., and Haag, J. (2011). Flight activity alters velocity tuning of fly motion-sensitive neurons. *The Journal of neuroscience*, 31(25):9231–9237.
- Kagaya, K. and Takahata, M. (2010). Readiness discharge for spontaneous initiation of walking in crayfish. *The Journal of neuroscience : the official journal of the Society for Neuroscience*, 30(4):1348–62.
- Kain, J., Stokes, C., Gaudry, Q., Song, X., Foley, J., Wilson, R., and de Bivort, B. (2013). Leg-tracking and automated behavioural classification in drosophila. *Nature communications*, 4:1910.
- Kalueff, A. V., Gebhardt, M., Stewart, A. M., Cachat, J. M., Brimmer, M., Chawla, J. S., Craddock, C., Kyzar, E. J., Roth, A., Landsman, S., et al. (2013). Towards a comprehensive catalog of zebrafish behavior 1.0 and beyond. *Zebrafish*, 10(1):70–86.
- Kaufman, M. T., Churchland, M. M., Ryu, S. I., and Shenoy, K. V. (2014). Cortical activity in the null space: permitting preparation without movement. *Nature Neuroscience*, (August 2013).
- Keller, J. M., Gray, M. R., and Givens, J. A. (1985). A fuzzy k-nearest neighbor algorithm. *Systems, Man and Cybernetics, IEEE Transactions on*, (4):580–585.
- Keogh, E. J. and Pazzani, M. J. (2000). Scaling up dynamic time warping for datamining applications. In *Proceedings of the sixth ACM SIGKDD international conference on Knowledge discovery and data mining*, pages 285–289. ACM.
- Kimura, Y., Satou, C., Fujioka, S., Shoji, W., Umeda, K., Ishizuka, T., Yawo, H., and Higashijima, S.-i. (2013). Hindbrain v2a neurons in the excitation of spinal locomotor circuits during zebrafish swimming. *Current Biology*, 23(10):843–849.
- Kroodsma, D. E. and Byers, B. E. (1991). The function (s) of bird song. *American Zoologist*, 31(2):318–328.
- Latimer, K. W., Yates, J. L., Meister, M. L., Huk, A. C., and Pillow, J. W. (2015). Single-trial spike trains in parietal cortex reveal discrete steps during decision-making. *Science*, 349(6244):184–187.
- Ljung, L. (1998). *System identification*. Springer.
- MacEvoy, S. P., Hanks, T. D., and Paradiso, M. A. (2008). Macaque v1 activity during natural vision: effects of natural scenes and saccades. *Journal of neurophysiology*, 99(2):460–472.
- McHenry, M. J. and Lauder, G. V. (2005). The mechanical scaling of coasting in zebrafish (*danio rerio*). *Journal of Experimental Biology*, 208(12):2289–2301.
- Menelaou, E. and McLean, D. L. (2012). A gradient in endogenous rhythmicity and oscillatory drive matches recruitment order in an axial motor pool. *The Journal of Neuroscience*, 32(32):10925–10939.
- Mirat, O., Sternberg, J. R., Severi, K. E., and Wyart, C. (2013). Zebrazoom: an automated program for high-throughput behavioral analysis and categorization. *Frontiers in neural circuits*, 7.

- Mu, Y., Li, X.-q., Zhang, B., and Du, J.-l. (2012). Visual input modulates audiomotor function via hypothalamic dopaminergic neurons through a cooperative mechanism. *Neuron*, 75(4):688–699.
- Murakami, M., Vicente, M. I., Costa, G. M., and Mainen, Z. F. (2014). Neural antecedents of self-initiated actions in secondary motor cortex. *Nature neuroscience*.
- Muto, A., Ohkura, M., Abe, G., Nakai, J., and Kawakami, K. (2013). Real-time visualization of neuronal activity during perception. *Current Biology*, 23(4):307–311.
- Muto, A., Orger, M. B., Wehman, A. M., Smear, M. C., Kay, J. N., Page-McCaw, P. S., Gahtan, E., Xiao, T., Nevin, L. M., Gosse, N. J., et al. (2005). Forward genetic analysis of visual behavior in zebrafish. *PLoS Genet*, 1(5):e66.
- Naumann, E. A., Kampff, A. R., Prober, D. A., Schier, A. F., and Engert, F. (2010). Monitoring neural activity with bioluminescence during natural behavior. *Nature neuroscience*, 13(4):513–520.
- Nishimoto, S., Vu, A. T., Naselaris, T., Benjamini, Y., Yu, B., and Gallant, J. L. (2011). Reconstructing visual experiences from brain activity evoked by natural movies. *Current Biology*, 21(19):1641–1646.
- Orger, M. B. and Baier, H. (2005). Channeling of red and green cone inputs to the zebrafish optomotor response. *Visual neuroscience*, 22(03):275–281.
- Orger, M. B., Kampff, A. R., Severi, K. E., Bollmann, J. H., and Engert, F. (2008). Control of visually guided behavior by distinct populations of spinal projection neurons. *Nature neuroscience*, 11(3):327–33.
- Panier, T., Romano, S. a., Olive, R., Pietri, T., Sumbre, G., Candelier, R., and Debrégeas, G. (2013). Fast functional imaging of multiple brain regions in intact zebrafish larvae using selective plane illumination microscopy. *Frontiers in neural circuits*, 7(April):65.
- Parichy, D. M. (2015). Advancing biology through a deeper understanding of zebrafish ecology and evolution. *eLife*, 4:e05635.
- Patterson, B. W., Abraham, A. O., MacIver, M. A., and McLean, D. L. (2013). Visually guided gradation of prey capture movements in larval zebrafish. *The Journal of experimental biology*, 216(16):3071–3083.
- Pfaff, D., Ribeiro, A., Matthews, J., and Kow, L.-M. (2008). Concepts and mechanisms of generalized central nervous system arousal. *Annals of the New York Academy of Sciences*, 1129(1):11–25.
- Piaget, J. (1972). Development and learning. *LAVATELLY, CS e STENDLER, F. Reading in child behavior and development. New York: Hartcourt Brace Janovich.*
- Portugues, R. and Engert, F. (2011). Adaptive Locomotor Behavior in Larval Zebrafish. *Frontiers in Systems Neuroscience*, 5(August):1–11.

- Portugues, R., Feierstein, C. E., Engert, F., and Orger, M. B. (2014). Whole-brain activity maps reveal stereotyped, distributed networks for visuomotor behavior. *Neuron*, 81(6):1328–1343.
- Proekt, A., Banavar, J. R., Maritan, A., and Pfaff, D. W. (2012). Scale invariance in the dynamics of spontaneous behavior. *Proceedings of the National Academy of Sciences*, 109(26):10564–10569.
- Raichle, M. E. (2006). The brain’s dark energy. *SCIENCE-NEW YORK THEN WASHINGTON-*, 314(5803):1249.
- Raichle, M. E. (2010). Two views of brain function. *Trends in cognitive sciences*, 14(4):180–190.
- Rinner, O., Rick, J. M., and Neuhauss, S. (2005). Contrast sensitivity, spatial and temporal tuning of the larval zebrafish optokinetic response. *Investigative ophthalmology & visual science*, 46(1):137–142.
- Riters, L. V. (2012). The role of motivation and reward neural systems in vocal communication in songbirds. *Frontiers in neuroendocrinology*, 33(2):194–209.
- Roberts, A. C., Bill, B. R., and Glanzman, D. L. (2013). Learning and memory in zebrafish larvae. *Frontiers in neural circuits*, 7.
- Rodriguez, A. and Laio, A. (2014). Clustering by fast search and find of density peaks. *Science*, 344(6191):1492–1496.
- Romano, S. A., Pietri, T., Pérez-Schuster, V., Jouary, A., Haudrechy, M., and Sumbre, G. (2015). Spontaneous neuronal network dynamics reveal circuit’s functional adaptations for behavior. *Neuron*, 85(5):1070–1085.
- Rosner, R., Egelhaaf, M., Grewe, J., and Warzecha, A.-K. (2009). Variability of blowfly head optomotor responses. *Journal of Experimental Biology*, 212(8):1170–1184.
- Roweis, S. T. and Saul, L. K. (2000). Nonlinear dimensionality reduction by locally linear embedding. *Science*, 290(5500):2323–2326.
- Schroeder, C. E., Wilson, D. A., Radman, T., Scharfman, H., and Lakatos, P. (2010). Dynamics of active sensing and perceptual selection. *Current opinion in neurobiology*, 20(2):172–176.
- Seelig, J. D. and Jayaraman, V. (2015). Neural dynamics for landmark orientation and angular path integration. *Nature*, 521(7551):186–191.
- Semmelhack, J. L., Donovan, J. C., Thiele, T. R., Kuehn, E., Laurell, E., and Baier, H. (2015). A dedicated visual pathway for prey detection in larval zebrafish. *eLife*, 3:e04878.
- Serrien, D. J. (2010). Decisions of voluntary action: what vs when. *Frontiers in neuroscience*, 4.

- Severi, K. E., Portugues, R., Marques, J. a. C., O'Malley, D. M., Orger, M. B., and Engert, F. (2014). Neural control and modulation of swimming speed in the larval zebrafish. *Neuron*, 83(3):692–707.
- Sherrington, C. (1906). *The integrative action of the nervous system*, volume 2. CUP Archive.
- Shettleworth, S. J. (2010). Cognition, communication, and behavior.
- Shibasaki, H. and Hallett, M. (2006). What is the Bereitschaftspotential? *Clinical neurophysiology : official journal of the International Federation of Clinical Neurophysiology*, 117(11):2341–56.
- Sims, D. W., Southall, E. J., Humphries, N. E., Hays, G. C., Bradshaw, C. J. a., Pitchford, J. W., James, A., Ahmed, M. Z., Brierley, A. S., Hindell, M. a., Morritt, D., Musyl, M. K., Righton, D., Shepard, E. L. C., Wearmouth, V. J., Wilson, R. P., Witt, M. J., and Metcalfe, J. D. (2008). Scaling laws of marine predator search behaviour. *Nature*, 451(7182):1098–102.
- Skinner, B. F. (1976). Particulars of my life. *Behaviorism*, 4(2):257–271.
- Sofroniew, N. J., Cohen, J. D., Lee, A. K., and Svoboda, K. (2014). Natural whisker-guided behavior by head-fixed mice in tactile virtual reality. *The Journal of Neuroscience*, 34(29):9537–9550.
- Sohal, V. S., Zhang, F., Yizhar, O., and Deisseroth, K. (2009). Parvalbumin neurons and gamma rhythms enhance cortical circuit performance. *Nature*, 459(7247):698–702.
- Sompolinsky, H. (2014). Computational neuroscience: beyond the local circuit. *Current opinion in neurobiology*, 25:xiii–xviii.
- Soon, C. S., Brass, M., Heinze, H.-J., and Haynes, J.-D. (2008). Unconscious determinants of free decisions in the human brain. *Nature neuroscience*, 11(5):543–545.
- Sorribes, A., Armendariz, B. G., Lopez-Pigozzi, D., Murga, C., and de Polavieja, G. G. (2011). The origin of behavioral bursts in decision-making circuitry.
- Trivedi, C. A. and Bollmann, J. H. (2013). Visually driven chaining of elementary swim patterns into a goal-directed motor sequence : a virtual reality study of zebrafish prey capture Article type : Received on : Accepted on : Frontiers website link : Citation : Running Title : Virtual prey captur.
- Van der Maaten, L. and Hinton, G. (2008). Visualizing data using t-sne. *Journal of Machine Learning Research*, 9(2579-2605):85.
- Viswanathan, G. M. (2010). Ecology: Fish in lévy-flight foraging. *Nature*, 465(7301):1018–1019.
- Vladimirov, N., Mu, Y., Kawashima, T., Bennett, D. V., Yang, C.-T., Looger, L. L., Keller, P. J., Freeman, J., and Ahrens, M. B. (2014). Light-sheet functional imaging in fictively behaving zebrafish. *Nature methods*, 11(9):883–4.

- Wellock, C. (2012). Variability in singing and in song in the zebra finch.
- Wessberg, J., Stambaugh, C. R., Kralik, J. D., Beck, P. D., Laubach, M., Chapin, J. K., Kim, J., Biggs, S. J., Srinivasan, M. A., and Nicolelis, M. A. (2000). Real-time prediction of hand trajectory by ensembles of cortical neurons in primates. *Nature*, 408(6810):361–365.
- Wolf, S., Supatto, W., Debrégeas, G., Mahou, P., Kruglik, S. G., Sintès, J.-M., Beaurepaire, E., and Candelier, R. (2015). Whole-brain functional imaging with two-photon light-sheet microscopy. *Nature methods*, 12(5):379–380.
- Woods, I. G., Schoppik, D., Shi, V. J., Zimmerman, S., Coleman, H. a., Greenwood, J., Soucy, E. R., and Schier, A. F. (2014). Neuropeptidergic signaling partitions arousal behaviors in zebrafish. *The Journal of neuroscience : the official journal of the Society for Neuroscience*, 34(9):3142–60.
- Wu, L.-Q. and Dickman, J. D. (2012). Neural correlates of a magnetic sense. *science*, 336(6084):1054–1057.
- Wyart, C., Del Bene, F., Warp, E., Scott, E. K., Trauner, D., Baier, H., and Isacoff, E. Y. (2009). Optogenetic dissection of a behavioural module in the vertebrate spinal cord. *Nature*, 461(7262):407–410.
- Wyart, C. and Knafo, S. (2015). Sensorimotor integration in the spinal cord, from behaviors to circuits: New tools to close the loop? In *New Techniques in Systems Neuroscience*, pages 197–234. Springer.
- Xiao-Jun, W., Kittler, J., Jing-Yu, Y., Messer, K., and Shitong, W. (2004). A new direct lda (d-lda) algorithm for feature extraction in face recognition. In *null*, pages 545–548. IEEE.
- Yokogawa, T., Hannan, M. C., and Burgess, H. A. (2012). The dorsal raphe modulates sensory responsiveness during arousal in zebrafish. *The Journal of Neuroscience*, 32(43):15205–15215.

